A STUDY ON THE ELECTRIC DIPOLE MOMENT OF ATOMS

A thesis

Submitted For The Degree of

Doctor of Philosophy In the Faculty of Science

Bangalore University

By

ANGOM DILIP KUMAR SINGH

Indian Institute of Astrophysics

Bangalore

India

1998

Declaration

I hereby declare that the matter contained in this thesis is the result of the investigations carried out by me at the Indian Institute of Astrophysics, Bangalore, under the supervision of Professor Bhanu Pratap Das. This work has not been submitted for the award of any degree, diploma, associateship, fellowship, etc. of any university or institute.

Angom Dilip Kumar Singh
(Candidate)

Bangalore 560034
1998 August

Certificate

This is to certify that the thesis entitled 'A Study on Eelectric Dipole Moment in Atoms submitted to the Bangalore University by Mr. Angom Dilip Kumar Singh for the award of the degree of Doctor of Philosophy in the faculty of Science, is based on the results of the investigations carried out by him under my supervision and guidance, at the Indian Institute of Astrophysics. This thesis has not been submitted for the award of any degree. diploma, associateship, fellowship, etc. of any university or institute.

Prof. Bhanu Pratap Das
(Supervisor)

Bangalore 560034
1998 August

Dedicated to my grandfather

Angom Indra Singh

Contents

List of Figures

List of Tables

Chapter 1

Introduction

1.1　An Overview

The forms of symmetries exhibited by physical systems can be classified as continuous and discrete. With each symmetry there is an associated transformation and these obey characteristic group structures. The continuous symmetries are associated with transformations which has the concept of infinitesimal transformation and a finite transformation can be achieved by applying a sequence of infinitesimal transformations. Whereas in discrete symmetries, there is no concept of infinitesimal transformations, instead the transformation takes the physical system from one state to another. The state of the system before and after the transformation can be same or different. If the system remains the same after the transformation then it is invariant under the particular symmetry, if the state is different after the transformation then the symmetry is said to be violated by the system[3]. In classical physics the discrete symmetries figure less prominently than they do in quantum physics[2].

The three important discrete symmetries of interest in physical studies are charge conjugation(C), space-inversion/parity (P) and time-reversal(T). According to the CPT theorem[3] all physical systems described in local field theories are invariant under the combined CPT transformation. A physical system/process can violate each of these symmetries individually such that it is compensated by another of the symmetry but when combined the CPT-theorem is still valid. It has been now established that the weak interaction violates parity but to date no concrete evidence of T violation has been observed

apart from the decay of kaons. Symmetry violations can be observed in laboratory by looking for their signatures in physical systems. For a single particle or a composite system the intrinsic Electric Dipole Moment(EDM) in a non-degenerate state is the signature of P and T violation. The significance of observing such an EDM is that it could lead to a better understanding of the origin of T or CP violation.

Neutral Atomic systems are good candidates to search for EDM as it is a composite system of leptons and hadrons. The collective many-body effects can enhance the EDM arising from interaction in a certain sector or due to intrinsic EDM of the constituent particles either constructively or destructively. The effect of a particular interaction(property) can be studied by an appropriate choice of atomic system. The enhancement factor is proportional to the atomic number Z and hence heavier atoms are preferred. Once an atom is chosen based on the physical effect of interest, the intrinsic EDM can be measured by subjecting the atom to a constant external electric field $\vec{E}$. The interaction Hamiltonian between $\vec{E}$ and $\vec{D}_a$ is $-\vec{D}_a \cdot \vec{E}$. Experimentally $\vec{D}_a$ is measured as the linear response to a constant external electric field. Though all the theoretical descriptions are applicable to both atomic systems as well as ionic systems, ions cannot be used in experiments as the external field gives rise to a net force acting on it. From now on only atomic systems will be considered.

The atomic Hamiltonian is the sum of kinetic energy part of the electrons, electron-nucleus coulomb interaction, electron-electron coulomb interaction and the PT-violating interaction Hamiltonian H_{PTV}. The presence of H_{PTV} implies that the eigen states of the atomic Hamiltonian are no more eigen-states of parity operator $\hat{P}$. The theoretical computation is done by treating H_{PTV} as the perturbation which mixes opposite parity eigen states of the unperturbed Hamiltonian H_{atom}, which has the kinetic energy of the electrons, electron-electron coulomb interaction and electron-nucleus coulomb interaction. This gives a mixed parity ground state of the atom, from which the intrinsic atomic EDM $\vec{D}_a$ is computed as linear response to the external field.

1.2   Historical Background on Atomic EDM

The history of atomic EDM spans not too long in time but the events and their implications are fascinating. It has held great minds together and has had its moments of triumph and share of critics as well , which in natural science tends to push the subject more into introspection. Having survived many such moments of introspection the quest for atomic EDM now stands exposed to deeper introspection: the experimental confirmation of a finite atomic EDM.

The articles by Prof. P. G. H. Sandars and Prof. Norman F. Ramsey [4, 5] are the basic references that have been used in writing this section, more emphasis is given to experiments than theory as they have been the driving force of this subject."If one is about to be attacked he should counter attack" therein lies the genesis to the whole history of atomic EDM[5]. And Ramsey did indeed attack the issue of experimental evidence for non-existence of nuclear electric dipole moment, based on the assumption that partiy is conserved, which he thought would be a possible subject of query from Prof. Ed Purcell. This was in 1950, Ramsey was then teaching a course on molecular beams in Harvard which was attended by Prof. Ed Purcell. Later, they proposed an experiment to measure the neutron EDM[6]. This was the precursor to several events that unfolded and ultimately lead to the search for an atomic EDM.

Finding no satisfactory experiments to look for parity nonconservation Ramsey and Purcell started one to measure neutron EDM with their graduate student Jim Smith[7]. The use of atoms was considered and discarded as external electric field would be shielded by the electrons. This set the path to the Schiff cancellation/theorem[8], that appeared in 1963. There were moments of amusement and bets[9], the time Feynman had bet with Ramsey on the futility of an experiment on parity-nonconservation. This elucidate the sacrosanct attitude towards parity conservation that prevailed among the theorists. Further impetus was given when the ongoing tau-theta paradox was attributed to parity-nonconservation in weak interaction by Lee and Yang [10]. Parity-nonconservation in weak interaction was experimentally confirmed by C. S. Wu and her collaborators[11] in 1957.

The year 1957 was the year of parity-nonconservation. The investigation on using

atoms was set into motion by Salpeter[12], with his work on the atomic effects of an electronic electric dipole moment. In another development in 1959, Zel'dovich[13] put forward the idea of neutral current interaction between the electrons and nucleus in an atom, which could introduce optical rotation if the predictions of neutral currents were true. This was the first proposal to detect discrete symmetry violations in atomic systems, though Wu had used cobalt atoms, it was the radioactive decay of the nucleus that was used as the signature and not the atomic properties.

Though the search for parity-nonconservation was vindicated, the search for the neutron EDM was yet to face another onslaught from theorists. It was shown by Landau[14] that nonzero neutron EDM require time-reversal violation too. Ramsey continued his experiments but this time with a different goal; to look for "time-reversal violation". The time-reversal violation was indirectly observed in neutral-kaon decay experiment by Cronin and co-workers[15] in 1964.

Serious efforts to measure atomic EDM which arises due to the electronic EDM were impeded by the demon of Schiff cancellation. A new route was set forth with the path breaking work of Sandars[16], where he investigated the relativistic aspect of Schiff cancellation and derived the atomic EDM that arises due to the electron EDM. This set a stage for many atomic EDM experiments that were to be conducted. As established by Schiff[8] an atom can still have EDM due to finite nucleus effects too. The first atomic EDM was carried at Brandeis[17] using atomic caesium in 1964. Atomic caesium is a system which is sensitive to electronic EDM and not to those that originate from the nuclear sector. The next important proposal in atomic EDM was the use of polar molecules by Sandars[18], this set the into motion the use of molecules.

Other important milestones in the atomic EDM experiments are: the experiment with molecules[19], the cell experiments by Fortson[20, 21], use of optical pumping instead of an external magnetic field[22] and more advanced and complicated beam experiments[23]. With these experiments the atomic EDM is now firm on its pedestal. The techniques and methods associated with these are described in brief along the thesis.

1.3   Discrete Symmetries

In quantum mechanics the Hamiltonian is the starting point of any computation. The Hamiltonian H is invariant under a transformation $\hat{O}$ if

$$\left[H, \hat{O}\right] = 0,$$

that is it commutes with the transformation operator. Otherwise H is not invariant under $\hat{O}$. Other terminologies used for this are symmetry violation and odd under the particular symmetry. But in case of P it is referred to as P-nonconservation also.

Though the CPT theorem has three discrete symmetries as components, only P and T are the subject of this study. A brief discussion of these symmetries are given in the following sections.

1.3.1   Parity or Space Inversion Symmetry

The parity transformation is the change in sign of all the spatial-coordinate axes. It is a unitary transformation and has eigen-value ± 1. If $\hat{P}$ is the parity transformation operator and $\mathcal{B}(x, y, z)$ a function, its parity transformation is

$$\hat{P}\mathcal{B}(x, y, z) = \mathcal{B}(-x, -y, -z). \tag{1.1}$$

Similarly, let $\hat{O}$ be an operator and $\hat{O}'$ be its parity transformed expression then they are related as

$$\hat{O}' = \hat{P}\hat{O}\hat{P}^{-1} = \hat{P}\hat{O}\hat{P}^{\dagger}$$

The reflection symmetry also flips the sign of the coordinate but in three dimensions it is quite different from parity. The parity transformation is a composite symmetry in three dimension, it involves one reflection and one rotation each. But a sequence of rotations nor a sequence of reflections cannot constitute parity transformation. More precisely, in cartesian coordinate system in three dimension parity transformation is reflection about one coordinate and rotation about this axis by 180^0, the sequence of the reflection and rotation commutes. The expressions can be derived for other coordinate systems too.

Consider the electric dipole operator $\vec{D}$, it is odd under parity transformation as it is a vector operator

$$\hat{P}\vec{D}\hat{P}^{-1} = -\vec{D}.$$

From which it follows that dipole expectation for a system is nonzero only when the Hamiltonian of the system is odd under parity transformation. That is, if H is the Hamiltonian of the system, then $\langle\vec{D}\rangle$ is nonzero for the system only when

$$\left[H, \hat{P}\right] \neq 0.$$

Hence $\langle\vec{D}\rangle$ is a signature of parity violation in the system.

1.3.2   Time Reversal or Motion Reversal Symmetry

Time-reversal or motion reversal symmetry transformation is reversing the sign of time coordinate. The time-reversal transformation operator is antiunitary[24] and unlike in parity transformation its eigenvalues are dependent on the system considered[2, 25]. In operator form it is a combination of a complex conjugation operator and unitary part which reverses the sign of time coordinate. It is represented by $\hat{\theta}$ and given by

$$\hat{\theta} = \hat{U}\hat{K},$$

$\hat{K}$ is complex conjugation operator and $\hat{U}$ is a unitary operator which reverses the sign of time coordinate. Then the transformation of a function or an operator given in the parity symmetry can be extended to time-reversal too.

The dipole operator transforms under time-reversal as

$$\hat{\theta}\vec{D}\hat{\theta}^{-1} = \vec{D},$$

that is $\vec{D}$ is invariant under time-reversal. For an atom in the hyperfine state $|FM\rangle$, the expectation value of dipole operator is

$$\langle\vec{D}\rangle = \langle FM|\vec{D}|FM\rangle.$$

According to the projection theorem the expectation value of a vector operator with respect to angular momentum eigenstates is proportional to the angular momentum of the system.

Using this the expectation value of dipole operator for an atom in the state $|FM\rangle$ is

$$\langle FM|\vec{D}|FM\rangle = c\langle FM|\vec{F}|FM\rangle, \qquad (1.2)$$

where c is the constant of proportionality. Applying time-reversal transformation, the above relation takes the form

$$\langle FM|\hat{\theta}^\dagger\hat{\theta}\vec{D}\hat{\theta}^{-1}\hat{\theta}|FM\rangle = c\langle FM|\hat{\theta}^\dagger\hat{\theta}\vec{F}\hat{\theta}^{-1}\hat{\theta}|FM\rangle.$$

Using the relations $\hat{\theta}\vec{F}\hat{\theta}^{-1} = -\vec{F}$ and $\hat{\theta}|FM\rangle = (-1)^{(F-M)}|F-M\rangle$, we get

$$\langle FM|\vec{D}|FM\rangle = -c\langle FM|\vec{F}|FM\rangle. \qquad (1.3)$$

Comparing (1.2) and (1.3), the time-reversal symmetry is not violated if $\langle \vec{D}\rangle = 0$ and if $\langle \vec{D}\rangle \neq 0$ then the time-reversal symmetry is violated. Hence EDM is a signature of time-reversal symmetry violation. The difference from parity-nonconservation is that, in time-reversal it is the form of the expectation–which in experiments translates to measurement of dynamic variables–that manifests the time-reversal violation. Whereas intrinsic atomic EDM is a signature of parity-nonconservation as it doesn't commute with the parity operator.

1.4   Outline of the Chapters

All the chapters in the thesis has a common thread–atomic EDM–linking them from the last line of one to the first line of the next. Yet, exceptions there must be as is the rule, as an exception to the thread but overwhelmingly within the scope of the thesis is the penultimate chapter. If the other chapters are on the atomic EDM then the last chapter makes a contact with the Parity-nonconservation in atoms through the many-body physics route. An attempt has been made to make the chapters compact, closely related and continuous, if otherwise, the vital thread-link must have flared and broke along the journey.

There are four chapters excluding the present one, each of them has been divided based on its role with respect to the intrinsic EDM of atoms. The second chapter "Intrinsic Electric Dipole Moment in Atoms" gives an account of the mechanism that can contribute

to the origin of EDM in atoms. A more detailed presentation is given for the mechanisms chosen for the present study, namely the electron-nucleus tensor-pseudotensor interaction and Schiff moment. For each of these, the form of the effective Hamiltonian and expression of the matrix elements required are derived. Along with it the approach for computation of the atomic EDM is also elucidated. Since no physical theory is complete without experimental verification, in the last part of the chapter a brief sketch of the sophisticated experiments for measuring atomic EDM is attempted. Due liberty has been taken to give more importance to the basic principles of the experiments than the fine details which is really the heart of any experiment. The last section of the chapter is the experimental proposal to use the modern techniques of laser cooling and trapping to measure the EDM of atomic Yb. To make a ground work for this proposal, the techniques and principles of laser cooling and trapping are explored in the preceding few sections.

The third chapter "The configuration interaction and many-body perturbation theory Based Atomic-Body Theories" pertains to the atomic many-body theories and methods that used in the computation of atomic EDM. Starting from Configuration Interaction(CI) method a slow and step-by-step transition is made towards an almost-coupled-cluster formalism. In the process of transition different methods having features of the two are also studied. All the methods use the configuration state approach instead of the generally preferred single-particle approach. This approach has both advantages and disadvantages, these are described in the chapter. The first few sections are devoted to CI and improvement on the performance using different formalism but with the same physical effects. It is followed by sections on many-body perturbation theory(MBPT) based on Bloch-equation and formalisms to compute atomic EDM, where equations required are derived and discussed. Later, an analysis on the size-consistency of these theories is done and remedies are considered. The size-consistent methods based on modifications to Bloch-equation are the subject of sections that follows. In these, the equations for coupled electron pair approximation(CEPA)-0 and CEPA-2 for computing the atomic EDM are derived, both the formalisms are size-consistent theories.

The fourth chapter "Computation of electric dipole moment with Different Many-Body Methods and Comparison" is on the application of the many-body theories considered

in Chapter3. But it is also a direct descendant of Chapter2 as the different effective Hamiltonians used in this chapter were the material for Chapter2. In essence this chapter is the computational implementation and study of the theories presented in Chapter2-3 in specific atomic systems. The whole study is limited to atomic Yb. First part is on the configuration space used and its construction. Next the details of the different perturbations used in the study are scrutinized at length. With these information in hand a lowest order computation of the Yb EDM is attempted next. After gathering certain trends and behaviors of the perturbation Hamiltonians the many-body theories explored in Chapter:3 are put to test. First part of the test confirms the agreement of the results between different CI implementations and matrix based Bloch-equation method. This validates some of the issues on size-consistency that were brought out in Chapter:3. Along the way the wave-operators used in Bloch-equation are subjected to a fairly deep exposition and their computational implementations are also presented. Once through with CI and matrix-based Bloch-equation, the spot-light shifts to the size-consistent methods. Here the CEPA-0 and CEPA-2 equations are torn apart term by term and the effect of a collection of terms brought to minute examination.

The fifth chapter "Parity Non-Conservation in Atomic Yb" adds to variety and maybe a bit of nostalgia too. But the real aim is to explore the complexity of the structure computations in a rare Earth atom like Yb. In the process, unintentional and without malice, yet another atomic many-body structure computation method is pulled out from among the plethora of many-body theories in physics. Nostalgic, as the very quest of intrinsic EDM of single particle or a composite system of particles was set in motion to detect parity-nonconservation in physical systems. The first section of this chapter is on the spin-dependent parity-nonconservation effective Hamiltonian. The form of matrix elements required are almost identical to those used in the computation of atomic EDM. The only difference is that here the quantity of interest is not an expectation value as in EDM but a transition moment. A brief outline of the computational method used is given and is followed by an analysis on the modification. Where the modification is in the two-body potential and the tools of analysis are the topics covered in earlier chapters. The chapter is rounded of by the last section which has the results. A finishing touch is

given with the reference that follows giving the preceding works.

The last chapter of the thesis is "Conclusion and Future Directions" which gives an analysis of the results from various chapters. And presents ways in which the present computation can be improved. It also gives the improvement required for the methods used in this computation to make it applicable to other systems of interest.

1.5   Notations and Units Used

This section will in few words put down the notations used in mathematical expressions, conventions followed and the like. Anything appearing here after that does not conform to these are mistakes. Not all the equations are labeled, only those referenced are labeled and the label has the chapter number and the sequence of equation separated by a <u>dot</u>. The figures and tables on the other hand are all labeled, if not, it is unintended. Vectors are represented by either Latin or Greek alphabet with an arrow stuck to the invisible apple on its head e.g. $\vec{A}$. The usual bold-faced capitals are reserved for matrices, so **A** means a matrix and not a vector under any circumstances. The single particle orbitals are in general represented by $|\psi\rangle$, particular cases are represented by specifying the principle quantum number and symmetry like in $|6s\rangle$. For orbitals other than s symmetry $j = l - s$ orbital is tagged by a suffix '*' like in $p*$. A general configuration state function(CSF) is represented by $|\Phi\rangle$ and a particular CSF by specifying the valence/core orbitals and their occupation number like $|6s^2\rangle$. An atomic state function(ASF) is represented by $|\Psi\rangle$. The definitions of these are given where they first appear. In all the equations and mathematical expressions parentheses are used liberally for clarity. A constant which itself is a product of physical constants is identified by a calligraphic capital letter e.g. $\mathcal{A} = \sqrt{2}C_T\sigma_N G_F$. Calligraphic letters are also used to denote other constants like CI coefficients too. The dummy indices in tensors are superscripted with due respect and the dummy indices in matrix elements as subscripts but not with less respect. Other than these no conventions binds further in putting additional superscripts/subscripts, it is all a matter of real estate available from then on.

Throughout the thesis 'with respect to' is abbreviated as *wrt*. Frequently used termin-

ologies are also abbreviated after their first occurrence other than in the chapter heading. The diagrams given are more of a representation to understand the physical effects and the Goldstone rules are not applicable. This is because the energy denominator is different from the one required in Goldstone rules.

In the entire thesis without any exception the unit of physical quantities are in atomic units[26]. Atomic unit is the system of units where the fundamental constants: $\hbar$ Planck's constant divided by 2π, c the velocity of light and e the charge of electron are set to unity. For the electromagnetic fields $4\pi\epsilon_0 = 1$, where ϵ_0 is the permittivity of vacuum. In this system of unit the length is measured in Bohr radius a_0 and energy in hartrees, where $1\,a_0 = \hbar^2/m_e e^2 = 0.5291\ 77 \times 10^{-10} m$ and $1\,\text{hartree} = (m_e c^2 \alpha^2)/eh = e^2/a_0 = 4.3597\ 50$ joules,which is equal to $27.2113\ 96$ eV. Another useful quantity is the fine structure constant $\alpha = e^2/m_e c$. In atomic units the velocity of light $c = \alpha^{-1} a.u.$, where one atomic unit of velocity is $\alpha c = 2.1876\ 91 \times 10^6 m/s$. In atomic units the unit of EDM is ea_0.

References

[1] Alok Shukla *Theory of Electric Dipole Moment of Atomic Rubidium due to Parity and Time Reversal Violation*, Ph.D Thesis submitted to Utah State University(1991).

[2] J. J. Sakurai, *Modern Quantum Mechanics*(Addison-Wesley Company Inc, 1985).

[3] W. Pauli, *Neils Bohr and the Development of Physics* (McGraw-Hill, New York, 1955).

[4] P. G. H. Sandars, *Time Reversal–The Arthur Rich Memorial Symposium* Ed. by Mark Skalsky, Phillip H. Bucksbaum, Ralph S. Conti and David W. Gidley, 5 (American Institute of Physics, New york, 1991)

[5] Norman F. Ramsey, *Time Reversal–The Arthur Rich Memorial Symposium* Ed. by Mark Skalsky, Phillip H. Bucksbaum, Ralph S. Conti and David W. Gidley, 179 (American Institute of Physics, New York, 1991)

[6] E. M. Purcell and N. F. Ramsey, Phys. Rev. **78**, 807(1950).

[7] J. H. Smith, E. M. Purcell and N. F. Ramsey, Phys. Rev. **108**, 120(1957).

[8] L. I. Schiff, Phys Rev **132**, 2194(1963).

[9] Ralph Leighton, *Surely You are Joking Mr. Feynman*, Ed by Edward Hutchings, pp-248(W. W. Norton and Company, New York, 1985).

[10] T. D. Lee and C. N. Yang, Phys. Rev. **104**, 254(1956).

[11] C. S. Wu, E. Ambler, R. N. Hayward, D. D. Hoppes and R. P. Hudson, Phys. Rev. **105**, 1413(1957).

[12] E. E. Salpeter, Phys. Rev. **112**, 1642(1958).

[13] Ya. B. Zel'dovich, Zh. Eksp. Teor. Fiz **36**, 964(1959).

[14] L. D. Landau, Nucl. Phys. **3**, 127(1957).

[15] J. H. Christenson, J. W. Cronin, V. L. Fitch and R. Turlay, Phys. Rev. Lett. **13**, 138(1964).

[16] P. G. H. Sandars, Phys. Rev. **14**, 194(1965).

[17] P. G. H. Sandars and E. Lipworth, Phys. Rev. Lett. **13**, 718,(1964).

[18] P. G. H. Sandars, Phys. Rev. Lett. **19**, 1396(1967).

[19] G. E. Harrison, P. G. H. Sandars and S. J. Wright, Phys. Rev. Lett. **22**, 1263(1969).

[20] T. C. Vold, F. J. Raab, B. R. Hackel and E. N. Fortson, Phys. Rev. Lett.**52**, 2229(1984).

[21] S. K. Lamoreux, J. P. Jacobs, B. R. Heckel, F. J. Raab and E. N. Fortson, Phys. Rev. Lett. **59**, 2275(1987).

[22] S. A. Murthy, D. Krause, Z. L. Li and L. R. Hunter, Phys. Rev. Lett. **63**, 965(1989).

[23] K. Abdullah, C. Carlsberg, E. D. Commins, H. Gould and S. R. Ross, Phys. Rev. Lett. **65**, 2347(1990).

[24] E. P. Wigner, Jour. of Math. Phys. **1**, 409(1960).

[25] E. P. Wigner, Jour. of Math. Phys. **1**, 414(1960).

[26] W. E. Baylis and G. W. E. Drake *Atomic, Molecular and Optical Physics Handbook*, Chapter 1, edited by W. K. Gordon, (American Institute of Physics, Wood bury, New York, 1995).

Chapter 2

Intrinsic Electric Dipole Moment in Atomic Systems

2.1 Possible Sources for Electric Dipole Moment in an Atom

An atom being a composite system there are many physical phenomena which can lead to an intrinsic atomic EDM. It can arise due to the following:

- The sub-atomic particles have intrinsic EDM. That is either electrons or protons or neutrons have an intrinsic EDM.

- The interaction between the sub-atomic particles violates P and T symmetries. The possible interactions are electron-electron, electron-nucleon and nucleon-nucleon.

The first case is due to the intrinsic property of the sub-atomic particles. Among all, the most important one is the intrinsic EDM of the electron. An effective intrinsic atomic EDM hamiltonian can be obtained by considering the various interaction terms in the presence of an external electric field $H_{\mathrm{PTV}}^{\mathrm{eff}}$. According to Schiff theorem a composite system of charged particles each with an intrinsic EDM has no intrinsic atomic EDM as a whole when treated non-relativistically. This is due to the cancellation of terms that contribute to $H_{\mathrm{PTV}}^{\mathrm{eff}}$. The cancellation is incomplete if the atomic system is treated relativistically. The P and T violating interaction Hamiltonian due to intrinsic EDM of electrons for an

atom with N electrons is

$$H_{\text{PTV}} = -d_e \sum_{i=1}^{N} \beta_i \vec{\sigma}_i \cdot \vec{E}_i^{\text{int}}, \tag{2.1}$$

where d_e is the intrinsic EDM of the electrons, β_i and $\vec{\sigma}_i$ are the Dirac matrix and spin-operator for the ith electron. $\vec{E}_i^{\text{int}}$ is the electric field experienced by the ith electron due to the other electrons. The electron spin contributes to the Hamiltonian as it is the only vector quantity associated with the electron, hence it decides the direction of quantization and only the component of electron EDM oriented along this direction is observable. The summation over the electron spin in (2.1) implies major cancellations for closed-shell atoms. To study the atomic EDM due to the intrinsic EDM of the electrons open-shell atoms should be chosen so that this cancellation is incomplete. An effective Hamiltonian can be derived from this Hamiltonian as

$$H_{\text{PTV}}^{\text{eff}} = \sum_{i=1}^{N} 2id_e \beta_i \gamma_{5i} \vec{p}_i^2.$$

Where $\vec{p}_i$ and γ_{5i} are the linear momentum and Dirac matrix for the ith electron. Though the closed-shell atoms are not a good choice for studying the contribution from the electron EDM they are good for studying effects which has contributions from nucleus. In this thesis only the latter effects will be studied.

In current-current interaction formalism one form of interaction that violates P and T simultaneously is the electron-nucleus tensor-pseudo-tensor interaction [1]. The electron-electron tensor-pseudo-tensor(TPT) contribution is expected to be negligible as the electron-electron interaction dominated by Coulomb repulsion. An important feature is that this form of interaction is not allowed in the Standard Model(SM) of particle physics. The effect of PT-violating nucleon-nucleon interaction can manifest as Schiff moment. Which further interact with the electrons to give a finite intrinsic atomic EDM. These are discussed further in the following sections.

2.2   Atomic EDM due to Electron-Nucleus TPT-Interaction

2.2.1   Effective Hamiltonian for the Electron-Nucleus TPT-Interaction

From current algebra, the interaction Hamiltonian corresponding to the electron-nucleus TPT current-current interaction is

$$H_{\text{PTV}} = \frac{iC_T G_F}{\sqrt{2}} \left(\overline{\psi}_n \sigma^{\mu\nu} \psi_n\right) \left(\overline{\psi}_e \gamma^5 \sigma^{\mu\nu} \psi_e\right),$$

where C_T is the tensor-pseudo-tensor coupling constant, G_F is the Fermi coupling constant, ψ_n and ψ_e are the nucleon and electron fields, γ^5 is the Dirac matrix and $\sigma^{\mu\nu}$ is a tensor got from the Dirac matrices as

$$\sigma^{\mu\nu} = \frac{i}{2}\left(\gamma^\mu\gamma^\nu - \gamma^\nu\gamma^\mu\right).$$

$\sigma^{\mu\nu}$ is an antisymmetric tensor of rank two, when combined with the Dirac matrix γ^5 it has the properties of a pseudo-tensor. The constant phase factor i is included in the interaction Hamiltonian is to ensure that the matrix element of H_{PTV} is real. In all the expressions used so far the Einstein-Wigner convention has been used, according to which summation is implied over the repeated indices.

In the SM of particle physics the TPT current-current interaction is not allowed. Which means within SM the value of the coupling constant C_T is zero. If in an atomic system a finite intrinsic EDM is observed and can be attributed to the tensor-pseudo-tensor current-current interaction then it is a clear indication of nonzero C_T. Which is a signature of physics beyond the SM.

Using the definition of $\sigma^{\mu\nu}$ and treating the nuclear part non-relativistically H_{PTV} can be simplified to

$$H_{\text{PTV}} = i2\sqrt{2}\Big(C_T G_F\Big)\Big(\vec{I}\cdot\beta\vec{\alpha}\Big)\rho_N(r) = i2\sqrt{2}\Big(C_T G_F\Big)\begin{pmatrix} 0 & \vec{\sigma}_N\cdot\vec{\sigma} \\ \vec{\sigma}_N\cdot\vec{\sigma} & 0 \end{pmatrix}\rho_N(r), \quad (2.2)$$

where $\vec{I}$ is the nuclear spin, $\vec{\alpha}$ is the Dirac matrix and $\rho_N(r)$ is the nuclear density at r. The presence of the nuclear density implies that H_{PTV} is effective within the nuclear

region alone. Among the orbitals only s and $p*$ have non-zero amplitude in the nuclear region and orbital amplitudes of other symmetries is almost zero in the nuclear region. The PT-violating property of H_{PTV} can be checked by applying the P and T transformations separately. The effective Hamiltonian H_{PTV} is odd under parity transformation as $\vec{\alpha}$ transforms like a vector and using Heisenberg equation of motion it can be shown that in relativistic formalism it represents the velocity. Similarly, since the T-reversal transformation has a complex conjugation part it is also odd under T-reversal transformation.

The motivation for studying this form of interaction in an atom is that there are non-standard models in particle physics which allows this form of electron-nucleus interaction. An estimate of C_T can be made when the theoretical computation is combined with the experimental results. Based on which constraints can be put on the validity of the possible non-standard particle physics models. Another important feature of this study is the close connection with the experiments, where each compliments the other. For study on the atomic EDM due to electron-nucleus TPT-interaction as mentioned earlier a closed-shell atom is the right choice. This avoids the contribution from the electron EDM, which dominates in the case of open-shell atoms. Here atomic Yb has been chosen as it is a closed-shell atom and has high Z. In addition, it has interesting many-body effects as it is a rare earth element.

2.2.2   Matrix Element of Electron-Nucleus TPT-Interaction Hamiltonian

To compute the intrinsic EDM of an atom arising from the electron-nucleus TPT-interaction the $sp*$ approximation will be used. In this approximation only the matrix elements between orbitals of s and $p*$ symmetries are computed. This follows from the physical condition that only these orbitals are non-zero within the nuclear region. From now on atomic EDM will be used instead of referring explicitly as the intrinsic EDM of an atom. While computing the matrix elements the relativistic notation of the two component orbitals will be used. In this notation a orbital $|\psi\rangle$ in central approximation identified by the principal quantum number n, angular momentum quantum numbers κ and m in spherical

polar coordinates is represented as

$$|\psi\rangle = \frac{1}{r}\begin{pmatrix} P_{n\kappa}(r) & \chi_{\kappa m}(\theta,\phi) \\ iQ_{n\kappa}(r) & \chi_{-\kappa m}(\theta,\phi) \end{pmatrix}. \tag{2.3}$$

Where $P(r)$ is the large-component, $Q(r)$ is the small component, $\chi_{\kappa m}(\theta,\phi)$ and $\chi_{-\kappa m}(\theta,\varphi)$ are the corresponding angular parts. The angular part $\chi_{\kappa m}$ in terms of spinors can be expressed as

$$\chi_{\kappa m}(\theta,\phi) = \sum_{\sigma=\pm\frac{1}{2}} C(l1/2j; m-\sigma,\sigma)Y^l_{m-\sigma}(\theta,\phi)|\phi_\sigma\rangle,$$

where j is the total angular momentum of the orbital, $C(l1/2j; m-\sigma,\sigma)$ is Clebsch-Gordan co-efficient, $Y^l_{m-\sigma}$ is spherical harmonics and $|\phi_\sigma\rangle$ is spin part of the orbital. The spin part $|\phi_\sigma\rangle$ can either be the spin-up state $|\alpha\rangle$ or the spin-down state $|\beta\rangle$. In this form of notation the orbital $|ns\rangle$ assumes the form

$$|ns\rangle = \frac{1}{r}\begin{pmatrix} P_{n-1}(r) & \chi_{-1m}(\theta,\phi) \\ iQ_{n-1}(r) & \chi_{1m}(\theta,\phi) \end{pmatrix}.$$

The orbital $|np*\rangle$ can also be expressed in a similar form. Then in $sp*$-approximation the required matrix element of H_{PTV} is either $\langle ns|H_{\text{PTV}}|n'p*\rangle$ or $\langle n'p*|H_{\text{PTV}}|ns\rangle$. As an example consider the matrix element $\langle ns|H_{\text{PTV}}|n'p*\rangle$. Using the definitions of the orbitals and the effective interaction Hamiltonian H_{PTV}, this matrix element can be written as

$$\langle ns|H_{\text{PTV}}|n'p*\rangle = i\sqrt{2}\left(C_T G_F\right)\int_0^\infty\int_\Omega dr d\Omega \left(P_{n-1}(r)\chi^\dagger_{-1m}(\theta,\phi) \quad -iQ_{n-1}(r)\chi^\dagger_{1m}(\theta,\phi)\right) \times$$
$$\begin{pmatrix} 0 & \vec{\sigma}_N\cdot\vec{\sigma} \\ \vec{\sigma}_N\cdot\vec{\sigma} & 0 \end{pmatrix}\begin{pmatrix} P_{n'1}(r) & \chi_{1m}(\theta,\phi) \\ iQ_{n'1}(r) & \chi_{-1m}(\theta,\phi) \end{pmatrix}\rho_N(r).$$

Where $d\Omega$ denotes the integration over the angular coordinates. While computing the matrix element only the z-component is considered as it is the only observable component. After the angular integration the matrix element takes the form

$$\langle ns|H_{\text{PTV}}|n'p*\rangle = -\sqrt{2}\left(C_T G_F \sigma_{Nz}\right)\int_0^\infty dr \left(P_{n-1}(r)Q_{n'1}(r) - \frac{1}{3}Q_{n-1}(r)P_{n'1}(r)\right)\rho_N(r). \tag{2.4}$$

That is the angular integrations introduces constant multiplication factors. The angular factors were computed with the convention(coupling sequence) in J.J. Sakurai[2]. The

difference in the convention can introduce phase factors which can lead to s sign difference. A similar expression for other matrix elements can also be derived. Though the radial integration has limits from 0 to ∞, it is required only within the nuclear region as $\rho_N(r)$ beyond it is zero. While computing the matrix elements it is important to get accurate radial part of the orbitals and the nuclear density. A fairly accurate model of the nuclear density which agrees quite well with the experimental results is the Fermi-nucleus. In this model the nuclear density is given by

$$\rho_N(r) = \frac{\rho_0}{1 + \exp\frac{(r-b)}{a}},$$

where ρ_0 is a constant, b is the half density radius as $\rho_N(r) = \rho_0/2$ ans a is related to the skin thickness t as $t/a = 4\ln 3$.

The radial component of the orbitals can be computed using suitable methods, this will be discussed in detail in the later chapters.

2.2.3 The Atomic EDM as an Expectation Value of Dipole Operator

The electron-nucleus TPT-interaction Hamiltonian is introduced as a perturbation to the atomic Hamiltonian. At the single particle level let $|ns\rangle$ be the outer most occupied orbital in the ground state configuration. When the interaction Hamiltonian H_{PTV} is introduced as a perturbation $|ns\rangle$ will have admixture from orbitals of other symmetries opposite is parity. As mentioned earlier the only the virtual orbitals $n'p*$ will contribute to the admixture. In case of atomic Yb which is a closed-shell atom with $6s$ as the outermost occupied shell $n = 6$ and as $p*$ orbitals are occupied till $n = 5$ the virtual $p*$ symmetry orbitals are $(n' > 5)p*$.

The new orbitals are no longer parity eigen-states as they are of mixed parity. Represent the mixed parity orbital by $|\widetilde{6s}\rangle$, using perturbation theory this can be written as

$$|\widetilde{6s}\rangle = |6s\rangle + |6s^{\text{corr}}\rangle = |6s\rangle + \sum_{n'=6}^{\infty} |n'p*\rangle \frac{\langle n'p* | H_{\text{PTV}} | 6s\rangle}{\epsilon_{6s} - \epsilon_{n'p*}},$$

where ϵ_{6s} and $\epsilon_{n'p*}$ are the orbital energies of $|6s\rangle$ and $|n'p*\rangle$ respectively. This is the lowest order effect, other higher order effects from the residual coloumb interaction can

also contribute to it. Computation at the many-body level can be done in many ways depending on the many-body effects included, a few methods will be used and discussed in later chapters.

The atomic EDM $\vec{D}_a$ is the expectation value of the dipole operator $\vec{D} = -r$ with respect to the mixed parity states [3]

$$\vec{D}_a = \left\langle \widetilde{6s} \middle| \vec{D} \middle| \widetilde{6s} \right\rangle = 2 \sum_{n'=6}^{\infty} \frac{\left\langle 6s \middle| \vec{D} \middle| n'p* \right\rangle \left\langle n'p* \middle| H_{\text{PTV}} \middle| 6s \right\rangle}{\epsilon_{6s} - \epsilon_{n'p*}}. \tag{2.5}$$

Where the multiplication factor 2 is to include the complex conjugate term which is identical to the normal term due to the following: first, the dipole operator is hermitian, diagonal and its matrix elements are real hence $\langle ns| \vec{D} |n'p* \rangle = \langle n'p*| \vec{D} |ns \rangle$ and second, H_{PTV} is anti-hermitian, from (2.4) its matrix elements are real and hence $\langle na| H_{\text{PTV}}^{\dagger} |n'p* \rangle = \langle n'p* | H_{\text{PTV}} |ns \rangle$. Another method of computing which gives the same result is the method of linear response to an external electric field. This formulation is more appealing as it has direct bearing on experiments to detect the atomic EDM. When an external constant electric field $\vec{E}$ is applied the atomic EDM $\vec{D}_a$ interacts with it. The interaction Hamiltonian between the dipole moment of the atom and $\vec{E}$ is $-\vec{E} \cdot \vec{d}$.

2.3 The Schiff Moment

2.3.1 The Effective Schiff Moment Hamiltonian

In an atomic system even if the nucleus has a finite EDM, it cannot be detected by applying an external electric field as the screening due to the electrons will make the electric field inside the nucleus zero. The nuclear EDM can manifest itself in the atom through interactions with the electrons [4, 5, 6]. A finite EDM of the nucleus introduces an interaction term in the electron sector of the atom which leads to mixing of opposite parity states and can be observe by measuring the EDM of the atom.

Let $\rho_q(r)$ and $\rho_d(r)$ represent the normalized electric charge and dipole moment density of the nucleus. Though the charge distribution of the nucleus is solely decided by the protons at the nucleon level, the dipole distribution can have contributions from the neutrons

too. The electrons being point particles the electron-nucleus interaction can be written as

$$\int d^3r' \left[-\frac{\rho_q(r')}{|\vec{r} - \vec{r}'|} + \vec{\mu}_N \rho_d(r') \cdot \vec{\nabla}' \left(\frac{1}{|\vec{r} - \vec{r}'|} \right) \right],$$

where the $\vec{\mu}_N$ is the nuclear electric dipole moment. In this form of the nucleus-electron interaction we have neglected the interaction of the intrinsic electric dipole moment of the electrons with the nuclear electric field. This is valid if the atom under consideration is a closed-shell, where the net contribution from the electron EDM cancel out. For a many electron system these interaction terms can be written as

$$-\sum_i \int d^3r' \left[\frac{\rho_q(r)}{|\vec{r}_i - \vec{r}'|} + \vec{\mu}_N \rho_d(r') \cdot \vec{\nabla}' \left(\frac{1}{|\vec{r}_i - \vec{r}'|} \right) \right].$$

Thus the atomic Hamiltonian is

$$H = H_{\text{atom}} - \sum_i \vec{\mu}_N \rho_d(r') \cdot \vec{\nabla}' \left(\frac{1}{|\vec{r}_i - \vec{r}'|} \right),$$

where

$$H_{\text{atom}} = \sum_i \left\{ t_i - Z \int d^3r' \frac{\rho_q(r')}{|\vec{r}_i - \vec{r}'|} + \sum_{j>i} \frac{1}{r_{ij}} \right\}$$

The infinitesimal displacement operator Q with respect to the electrons can be written as

$$Q = \frac{-i}{Z} \vec{\mu}_N \cdot \sum_i \vec{\nabla}'_i$$

The commutation of the displacement operator with the atomic Hamiltonian gives

$$[Q, H_{\text{atom}}] = i\vec{\mu}_N \cdot \sum_i \int d^3r' \rho_q(r') \vec{\nabla}' \left(\frac{1}{|\vec{r}_i - \vec{r}'|} \right).$$

The atomic Hamiltonian can be written using the displacement operator as

$$H = H_{\text{atom}} + i[Q, H_{\text{atom}}] - \sum_i \int d^3r' \left(\rho_d(r') - \rho_q(r') \right) \vec{\mu}_N \cdot \vec{\nabla}'_i \left(\frac{1}{|\vec{r}_i - \vec{r}'|} \right).$$

In the above expression if the charge distribution is the same as the dipole distribution then the third term does not contribute. The total Hamiltonian H can be written in terms of the finite displacement operator $e^{(iQ)}$ by subtracting the higher order terms as

$$H = e^{iQ} H e^{-iQ} + \frac{1}{2} [Q, [Q, H_{\text{atom}}]] + \cdots.$$

Consider the interaction term linear in μ_N with further simplifications it assumes the form

$$H_S = \sum_i \frac{\vec{S}}{I(I+1)} \cdot \vec{\nabla}\Big(4\pi\delta(\vec{r}_i)\Big),$$

where the vector coefficient $\vec{S}$ in the above expression is the Schiff moment which is purely a nuclear property and the remaining part are in the electron co-ordinate. For computing the atomic EDM within the electron sector the contribution from the nuclear sector can be treated as a parameter which can be estimated from the experimental results. The above expression is the effective Schiff moment interaction Hamiltonian in the electron co-ordinate.

2.3.2   The Schiff Moment Matrix Element

The delta function in the expression for the effective Schiff moment Hamiltonian implies that the contribution from the electron sector will be non-zero if the electronic wavefunction is finite within the nucleus. With this condition only the s and $p*$ orbitals need to be considered in the electronic matrix elements as these are the only orbitals which are finite within the nucleus. To get the general form of the matrix element consider the two orbitals $n'p*$ and ns, the matrix element between these orbitals is

$$\Big\langle n'p* \Big| H_S \Big| ns \Big\rangle = \frac{S}{I(I+1)}\vec{I}\cdot\int d^3r\psi^*(n'p*)\psi(ns)\vec{\nabla}(4\pi\delta(\vec{r})).$$

Let the direction of quantization be the z-axis, then only those dynamic variables along this axis are the observables. Taking the z-component alone in terms of spherical polar coordinate system

$$\delta(\vec{r}) = \left(\frac{1}{r^2}\right)\delta(r)\delta(\phi)\delta(\cos\theta) \quad\text{and}\quad \frac{\partial}{\partial z} = \cos\theta\frac{\partial}{\partial r} - \left(\frac{1}{r\sin\theta}\right)\frac{\partial}{\partial\theta}$$

Taking stretched orbitals *ie* the orbitals with $m = 1/2$. After the integration over spin component, the orbital component of the integrand in relativistic form is

$$\frac{-1}{r^2\sqrt{3}}\Big[P^*_{n'1}(r)P_{n-1}(r)Y^*_{10}(\theta,\phi)Y_{00}(\theta,\phi) + Q^*_{n'1}(r)Q_{n-1}(r)Y^*_{00}(\theta,\phi)Y_{10}(\theta,\phi)\Big]$$

In the above expression the radial parts are real and using the properties of the spherical harmonics can be simplified to the form

$$\frac{-1}{4\pi r^2}\cos\theta\Big[P^*_{n'1}(r)P_{n-1}(r) + Q^*_{n'1}(r)Q_{n-1}(r)\Big] = \frac{-1}{4\pi r^2}f(r,\theta).$$

The whole of the integrand being independent of ϕ the integration over ϕ is quite trivial. After integration by parts and combining all the expressions, the form of the required integration over the electron coordinate is

$$
\frac{S}{I(I+1)}I_z \int\int dr d\Omega \delta(\vec{r})\frac{\partial}{\partial z}\Big(f(r,\theta)\Big)
$$
$$
= \frac{S}{I(I+1)}I_z \int\int dr d(\cos\theta)\frac{1}{r^2}\delta(r)\delta(\cos\theta)\left(\cos\theta\frac{\partial}{\partial r} - \left(\frac{1}{r\sin\theta}\right)\frac{\partial}{\partial\theta}\right)f(r,\theta)
$$

The first term does not contribute to the integration as it is proportional to $\cos^2\theta$ and integration over $\cos\theta$ in presence of $\delta(\cos\theta)$ makes it zero. The second term in the integrand is independent of $\cos\theta$ and hence the integration over $\cos\theta$ gives unity and only the integration over the radial coordinate remains.

$$
\langle n'p* |H_S| ns\rangle = \frac{S}{I(I+1)}I_z \int dr\frac{\delta(r)}{r^3}\Big[P_{n'1}(r)P_{n-1}(r) + Q_{n'1}(r)Q_{n-1}(r)\Big]
$$
$$
= \frac{S}{I(I+1)}I_z \left[\frac{1}{r^3}\Big(P_{n'1}(r)P_{n-1}(r) + Q_{n'1}(r)Q_{n-1}(r)\Big)\right]_{r=0} \qquad (2.6)
$$

This is required expression for the matrix element of the effective Schiff moment operator with $s \leftrightarrow p*$ approximation.

2.3.3 Computation of Schiff Moment

Consider the matrix element (2.6), the contribution from the electronic part alone is

$$
\mathcal{B} = \left[\frac{1}{r^3}\Big(P_{n'1}(r)P_{n-1}(r) + Q_{n'1}(r)Q_{n-1}(r)\Big)\right]_{r=0}. \qquad (2.7)
$$

Since $\mathcal{B}$ is evaluated at the origin, its evaluation requires the value of $(P_{n'1}(r)Q_{n-1}(r) + Q_{n'1}P_{n-1}(r))$ at the first few grid points near the origin. In the final expression no components should be proportional to negative power in r, if not the expression when evaluated at $r=0$ will diverge.

Using the orbital in the form given in (2.3), near the origin a power series expansion of the radial part can be done[7]. Similarly, the r dependent part in (2.6) can also be expressed in power series and the most general form of expansion is

$$
\Big(P_{n'1}(r)P_{n-1}(r) + Q_{n'1}(r)Q_{n-1}(r)\Big) = \sum_{i=1}^{N} a_i r^i. \qquad (2.8)
$$

Where N is the order to which the power series is to be taken and a_i is the coefficient of the ith order term in the expansion. Since the orbitals satisfy the boundary conditions $|\psi\rangle = 0$ at $r = 0, \infty$ the constant term that is $i = 0$ has been avoided in the expansion. The disadvantage of using this form of expansion is that if the terms with $i < 3$ contributes then the Schiff moment diverges as (2.8) has to be divided by r^3 and evaluated at $r = 0$. On the other hand if the power series starts from $i = 3$ then the coefficient of r^3 is the required electronic component contribution to the atomic EDM arising from the Schiff moment.

Given the values of $(P_{n'1}(r)P_{n-1}(r) + Q_{n'1}(r)Q_{n-1}(r))$ at the first few grid points, the coefficients a_i can be evaluated by using generalized least square fit algorithms. The power series expansion is appropriate only in the region close to the origin, beyond the first few grid points the exponential parts in the orbital starts to dominate and this no longer holds. As a check, the terms $a_1 r$ and $a_2 r^2$ are also included in the least square fit, these terms can be neglected if the coefficients a_1 and a_2 are very small compared to a_3. This was found true for the matrix element involving orbitals $6s$ and $6p*$ for atomic Yb. As in the case of electron-nucleus TPT-interaction, the outermost orbital $6s$ in Yb with the admixture introduced by H_S can be written as

$$\left|\widetilde{6s}\right\rangle = \left|6s\right\rangle + \left|6s^{\text{corr}}\right\rangle = \left|6s\right\rangle + \sum_{n'=6}^{\infty} \left|n'p*\right\rangle \frac{\left\langle n'p* \left|H_S\right|6s\right\rangle}{\epsilon_{6s} - \epsilon_{n'p*}},$$

The next step in the computation of the atomic EDM due to the Schiff moment is to compute the expectation value of the dipole operator. That is, the expression for the atomic EDM arising from the Schiff moment involving only the most important orbitals in atomic Yb is

$$\vec{D}_a = \left\langle \widetilde{6s} \left|\vec{d}\right| \widetilde{6s}\right\rangle = 2 \sum_{n'=6}^{\infty} \frac{\left\langle 6s \left|\vec{d}\right| n'p*\right\rangle \left\langle n'p* \left|H_S\right|6s\right\rangle}{\epsilon_{6s} - \epsilon_{n'p*}}.$$

This expression is similar to (2.5) except for the replacement of H_{PTV} by H_S. A major difference in the form of the atomic EDM induced due to H_{PTV} and H_S is; the matrix element of H_S is evaluated within the nuclear region but for the first few points from the origin, whereas for H_{PTV} all the points within the nuclear region are considered.

2.4 Experiments to Measure Atomic EDM

Norman F. Ramsey's experiments on neutron EDM measurement was the first effort in measuring the intrinsic EDM of a system[8]. Though the initial quest of neutron EDM was as a signature of P-nonconservation it was later proved that it is also a signature of T-reversal violation[9]. This was followed by experiments in atomic systems. The first experiment in atomic system to measure EDM was on atomic caesium[10]. Atomic caesium was chosen as it is sensitive to electron EDM due to its open-shell structure. Later, experiments were carried out with closed-shell atoms to probe the contribution from the nuclear sector to the atomic EDM. As the present study is limited to atomic EDM which involves the nucleus the description of the experiments will be limited to closed-shell atomic systems.

2.4.1 General Principle

Let $\vec{D}_a$ and $\vec{\mu}$ be the intrinsic EDM and magnetic dipole moment of a closed-shell atom and $\vec{I}$ be the nuclear spin of the atom. Since $\vec{I}$ is the only the vector quantity associated with the atom it is also the direction of quantization. The EDM of the atom can be rewritten as $D_a \vec{I}$. In the presence of a constant external electric field $\vec{E}$ and a magnetic field $\vec{B}$, the interaction Hamiltonian is

$$H = \frac{-1}{I}\left(D_a \vec{I}\cdot\vec{E} + \mu\vec{I}\cdot\vec{B} \right).$$

Due to which the atom precess about the direction of the fields. The precession frequency ω_0 is different for different relative orientations of $\vec{E}$ and $\vec{B}$. In addition to the term linear in external electric field, there is Stark shift which has quadratic dependence on the external electric field. The quadratic Stark shift is a weak field effect. Whereas the shift due to the atomic EDM is independent of the electric field strength. The required measure of atomic EDM is the signal that is linearly dependent on the external electric field.

Reversing the direction of $\vec{E}$ flips the sign of its contribution to the interaction Hamiltonian but the term due to $\vec{B}$ remains unaltered. The difference in the Larmor precession frequency when the alignment of $\vec{E}$ and $\vec{B}$ is switched from parallel to antiparallel is $\delta\omega_0 = 2D_a E/I\hbar$. Various other spurious signals in the experimental setup can also be

detected and accounted for by doing the experiment in various relative field alignments. Once the Larmor frequency shift is measured the atomic EDM can be extracted as

$$D_a = \frac{I\hbar\delta\omega_0}{E}.$$

Though Larmor frequency by origin refer to the frequency of precession of a particle with magnetic moment in a constant magnetic field, here it is used for the precession of a particle with electric dipole moment in a constant external electric field. The principle of the experiment is fairly straightforward but it is a deception. As the quantity of measurement D_a is extremely small it is one among the most challenging physics experiments. Some of the experimental setups has the best precision and accuracy in the present day physics experiments.

2.4.2   Experimental Setup

The importance of these atomic experiments lies in its contribution to the understanding of the theory of particle physics and challenge lies in removing all the unwanted signals and extracting the true signal of atomic EDM plus the accuracy and precision required. The heart of the experimental setup is the atoms used for the measurement and the external electric and magnetic fields. Using the traditional techniques this can be done in two ways: first the atoms are confined within a cell sandwiched between electric field plates along one axis and magnetic field poles along another axis[11] and second use a vertical beam of atoms and apply the external fields along the path[12]. The accuracy of these techniques are limited by the motional magnetic field $\vec{B}_{mot}$ and other associated systematic errors; since the atoms are moving with a velocity $\vec{v}$ it experiences a magnetic field $\vec{B}_{mot} = \vec{E} \times \vec{v}/c$, which can mimic the EDM signal.

The atomic cell experiments are resonant flourescence experiments. It has two atomic cells sandwiching an electric field plate between them. Two more electric plates are fixed on the parallel faces to the first plate. This configuration of the electric plates make it easier to maintain the required voltages and the electric field in the two cells are opposite in sign. The cells are filled with a mixture of the atoms of interest and a buffer gas. The buffer gas prevents the atoms from sticking on the cell walls. The magnetic field poles are

then added. Though the atoms precess due to the combined effect of $\vec{E}$ and $\vec{B}$, it can be considered as a collection of classical magnetic dipoles precessing with a Larmor frequency ω_L in an effective magnetic field. The precession frequency of the atoms is measured by shining a circularly polarized laser beam, where the polarization is modulated with a frequency ω. Resonance occurs when ω is equal to ω_L and the required signal is the transmitted intensity which is circularly polarized with the polarization modulated at the frequency 2ω.

The atomic beam experiments uses a vertical beam of atoms, vertical beams are used to avoid the curved trajectory due to Earths gravity. Once the atoms comes out from the atomic oven they pass through a state selection chamber. The state selection chamber maximizes the population of the atoms in a particular state and are then passed through an evacuated chamber where a constant electric field $\vec{E}$ and magnetic field $\vec{B}$ are applied. Within the $\vec{E}$ and $\vec{B}$ chamber the atomic states gets remixed due to the interaction of the electromagnetic-magnetic fields with the atomic EDM. The degree of remixing is a function of the atomic EDM, so once this is measured the atomic EDM can be extracted. The degree of remixing is measured by shining a probe laser beam. To compensate for any effect due to velocity gradient of the atoms due to gravity, the experiment is done with two atomic beams; one downgoing atomic beam and another upgoing. This cancels the effect of velocity dependence.

Both the experimental schemes has certain common drawbacks, they are as listed below:

- In both the schemes the atoms of interest are spread across a large region. It is difficult to keep the electromagnetic-magnetic fields uniform when the region is large but it is essential for the experiment. When the electromagnetic-magnetic fields are not uniform there can be signals which are similar to the atomic EDM signal.

- Both the experiments involve atoms having a velocity distribution, which cannot be neglected. This contributes to the velocity dependent motional magnetic field $\vec{B}_{mot}$, which is an unwanted effect as it can mimic the atomic EDM signal.

A part of the first problem can be avoided by polarizing the atoms using laser beams of

appropriate frequency[13] and do away with the need for external magnetic field. Whereas the electric field is still required, a solution to this problem is to confine the atoms to a small region in space. For the second problem the solution is to make the atoms static, which if done in a collection of atoms will cause condensation. As the atoms are required in a gas phase the required solution is to maintain the atoms in gas phase with minimum possible velocity distribution. As the velocity distribution is defined by the temperature of the atoms, this can be done by lowering the temperature of the atoms.

Among the recent techniques developed in atomic physics the method of "laser cooling and trapping of atoms" when used can improve the accuracy of the experiments in terms of the contamination from the motional magnetic field and the spread of the atomic cloud. This will be topic of the following sections.

2.5 Laser Cooling of Atoms

The basic idea of laser cooling is to slow down atoms using radiation pressure due to incoherent resonance scattering [14, 15]. The resonant frequency of an atom in motion undergoes Doppler shift and when it encounters a photon of appropriate frequency, the photon is absorbed and imparts its momentum to the atom. There is a net loss of momentum along its original direction of motion when the atom re-emits the photon by spontaneous decay. This is because the photon emitted by spontaneous decay mechanism has no preferential direction where as it absorbs photons coming from a definite direction. Steps of resonant absorption followed by spontaneous emission is called one flourescence cycle. After one such cycle the velocity of the atom changes, if the source of the photons is monochromatic then they are no longer resonant with the atoms. Hence further slowing down of the atom by flourescence cycle stops. This can be overcome in the following ways:

- Use a chirped laser, where the frequency of the photons emitted is not monochromatic but within a range and varies from the lower frequency to the higher over a suitable time period. The atoms then remain resonant till the highest component in the range and the diffusion heating due to spontaneous emission sets the limit on the cooling effect.

- If the atomic levels employed are appropriate vary the magnetic field within the cooling region such that as the atom slows down the resonant frequency reduces. This technique is called as Zeeman cooling.

Both techniques have been successfully used in cooling atoms[16, 17]. The drawback of a single laser method is: the atoms are decelerated along one direction–the direction of the laser beam. The effect of spontaneous decay induces a diffusion heating perpendicular to the direction of the laser beam and puts a lower limit on the cooling effect achieved. But this can be avoided and atoms can be further cooled using counterpropagating red-detuned laser beams along x, y and z axes. In this laser configuration an atom experiences a damping force independent of its direction of motion and only a static atom experiences no damping force. The diffusion heating due to recoil from spontaneous emission still exists but unlike in the unidirectional cooling, it is in equilibrium with the cooling force. The lower temperature limit to which the atoms can cooled is called the Doppler cooling limit.

Let ω_0 and ω_L be the resonant frequency of the atom and the laser frequency. The optimum conditions are achieved when the life-time of the excited state τ satisfies the condition $(\omega_0 - \omega_L) = 1/2\tau$. The minimum temperature T the atoms can be cooled is

$$T = \frac{\hbar}{2k_{\mathrm{B}}\tau},$$

where k_{B} is the Boltzmann constant. Using the appropriate quantities the Doppler cooling limit is 125 μK for caesium and 240μK for sodium. When experiments were carried out, it was found that atoms were at much lower temperatures than the Doppler cooling limit. This has been explained with other cooling mechanisms–polarization gradient cooling–other than the Doppler cooling present in the setup. In these setups the atoms are slowed down due to dissipative force arising from incoherent resonant scattering and atoms are not confined by a potential.

2.6   Laser Trapping of Atoms

Trapping an atom is: confining it to a limited region by creating a potential such that to escape from it requires a certain amount of kinetic energy. This is relatively easy for

charged particles where an electric field configuration can confine it. But for electrically neutral systems like atoms it is not so straight forward as the force exerted on it by an electromagnetic-magnetic field is very small. Other than the static electric field, the other forms of potentials that can be employed are the magnetic field and strong laser fields that can induce a dipole moment in the atom. Depending on the form of the field used there are different kinds of atom traps. The most important for the present study is the magneto-optical trap(MOT), with which an experimental measurement of EDM of atomic Yb has been proposed. The trapping techniques are briefly described in the following sections to give a starting point for the Yb EDM experiment. Though MOT is the technique used, for completeness the other methods of atom traps are also described.

2.6.1   Magneto-Optical Traps(MOT)

This method can be applied to atoms which has a magnetic dipole moment, which arises from the nuclear spin $\vec{I}$. The magnetic dipole moment makes the atom sensitive to an external magnetic field. If $\vec{\mu}$ is the magnetic dipole moment of the atom and $\vec{B}$ the external magnetic field then the interaction Hamiltonian is

$$H_{\text{int}} = -\vec{\mu} \cdot \vec{B} = g\mu_{\text{B}} I_Z |B|,$$

where g is the Lande g-value, μ_{B} is the Bohr magneton and I_z is the magnetic quantum number of the atom. The product of these three quantities give the magnetic dipole moment component along the direction of the external magnetic field.

The depth of the potential created using magnetic fields is very shallow, for atoms with a magnetic dipole moment of 1 Bohr magneton a magnetic field of 1 tesla can create potential with trap depth of 1K. It was first applied successfully to ultracold neutrons [18].

As the trap depth is small the atoms are cooled before injecting them into the trap region. The trap region is a quadrupole magnetic field created by two coaxial coils. The magnetic field created by the coils has low field region at the center and increases radially away from the center. An atom with its magnetic dipole moment antiparallel to the magnetic field has minimum potential energy in the central region and increases as it is displaced to the outer regions of stronger field. Thus for the antiparallely aligned atoms

the magnetic field forms a potential well. For the antiparallel atoms it form a potential hill. But the depth of the potential well is too small to be effective in trapping a sizable number of atoms. This is about the magnetic part of the trapping field configuration.

The optical field is created by counter-propagating red-detuned lasers crossing the center of the magnetic field. The gradient in the magnetic field with distance from the center creates a gradient in the zeeman level separations. This arrangement generates a dissipative force on an atom: as the atom moves away from the center at some point the zeeman level separation is resonant with the Doppler shifted laser photon. When this occurs there is a resonant absorption of the laser photon by the atom. Since the laser beams are red-detuned the resonance happens only with the laser propagating opposite to the atomic velocity. The net effect is that, under ideal conditions the motion of an atoms execute a damped harmonic oscillator till it settles down at the center of the field.

2.6.2 Laser Traps

In MOT the trapping potential was created by the magnetic field and the Zeeman splitting combined with the red-detuned laser beams provided a dissipative force. That is MOT has two components one is the trapping potential and the other mechanism which continually drive atoms to the bottom of the potential well. An atom trap with these components but purely with laser fields can be created. Where the force is created due to intensity gradient and radiative in origin. It is given by the relation

$$F_{\text{dipole}} = \chi |\nabla(I)|,$$

where χ is the atomic polarizability and I is the laser field intensity. The force arises from the in-phase interaction between the induced atomic dipole moment and the laser field.

When an atom is subjected to a very intense laser field, it induces an oscillating electric dipole in the atom. This interacts with the laser field itself. If electric field of the laser field has a gradient due to intensity inhomogeneity, then it exerts a force on the atom. This force is called as dipole force. The nature of the dipole force is such that with red-detuned laser fields the atoms in ground state are driven towards the strong field region–high laser intensity region. With blue-detuned laser field, the atoms are driven towards low intensity

region. Thus with proper fine-tuning a suitable trap potential can be created. As in MOT
the trap potential is still not substantial and other mechanisms can heat up the atoms.

In practice the required intensity profile of the laser field is produced by strong focusing
of a laser beam with gaussian profile. As in MOT to counteract the heating mechanisms,
counter propagating laser beams are used to cool the atoms. The disadvantage of the trap
is the high laser intensity required which complicates the heating and cooling procedures
and the small size of the trap area. The later can be a boon for collective systems like
molecules, where a tightly focused laser beam can be used to manipulate them—optical
tweezers.

2.6.3   Magnetic Traps

The simplest atomic trap with magnetic fields alone is the quadrupole magnetic field
created with two co-axial coils. Though there is a region of low magnetic field no static
magnetic field has minima. This can be remedied by introducing a time variation to
the magnetic field such that the time-averaged potential assumes the form of a harmonic
potential. The trap potential created is called as time-averaged orbiting potential(TOP).
This has been successfully used by Wieman and co-workers to observe Bose-Einstein
condensation for the first time using Rb vapour[19].

Another magnetic field configuration that can be used for neutral atom trapping is a
combination of the dipole field created by a coil and quadrupole field created by four wires.
This uses Earths gravitational force of attraction on the atom. The magnetic coil is placed
with its plane parallel to the ground, such that the force on an atom from the magnetic
field balances the gravitational pull on it. This creates a potential energy gradient along
the vertical direction—along the axis of the coil, but has no horizontal confinement.

The horizontal confinement is created by using four vertical wires which are arranged
along the vertices of a rectangle. Each wire carry currents in a direction opposite to its
neighbors. This creates a quadrupole field which has minimum field intensity at the central
region.

2.7 The Yb Experimental Setup Using Laser Cooling and Trapping Techniques

The Doppler-cooling technique [20] combined with the method of polarization-gradient cooling[21] can cool atoms to sub–Doppler temperatures of around one micro–Kelvin. These cold atoms can be confined in space by a dipole–force trap with a far-off-resonant laser light[22]. Laser-manipulated atoms have many advantages for the search of permanent atomic EDMs. First, the motional magnetic field $\vec{v} \times \vec{E}$ is small, where $\vec{v}$ is the velocity of an atom and $\vec{E}$ is the static electric field applied for EDM measurement. Second, long observation of cold atoms with virtually no perturbation can be realized by a blue–detuned–dipole–force trap. In fact, the measurement of hyperfine coherence time as long as 4 seconds has been performed for sodium atoms [22]. A blue–detuned trap is better for our purpose than a red–detuned one because the atoms are located in the region without the laser light in the former trap whereas in the latter trap atoms are always subject to a strong trap beam. In addition, since the atoms are well localized, the spatial inhomogeneities of the external electric and magnetic fields are small over the sample region. Third, the application of large electric field is possible in the high-vacuum chamber used in laser cooling experiment unlike in vapour cells. The imperfect reversal of the electric field and the current leakage , which are limiting systematics in the vapour cell EDM measurement[13], can also be overcome in the laser trap configuration.

Thus, the key to the atomic EDM search is to find an atom which can enjoy the advantages of the laser cooling technique as well as sensitivity enhancement. Groups at Stanford[22, 23] and Texas[24] have proposed EDM searches with laser cooled alkali atoms. The enhanced sensitivity to an intrinsic electron EDM makes atomic caesium important. The paramagnetism of the ground-state, however, causes serious problems of cold atom collisions [24], which limits the accuracy of an EDM experiment. Therefore, if one searches for an atomic EDM arising from hadron-related interactions, it would be appropriate to use closed–shell atoms. From an experimental viewpoint, the diamagnetism of the ground state of closed–shell atoms overcomes the difficulty due to cold collisions, and it also indicates that one can measure nuclear contribution without the disadvantage of having to

deal with a large electron magnetic moment. From theoretical point of view, apart from being sensitive to the Schiff moment and other T–violating hadron interactions, its large sensitivity to the tensor–pseudotensor(T-PT) electron-nucleon interaction as shown for a Yb atom by our calculation in this paper makes it a good choice for probing the atomic EDM from the lepton–hadron interaction sector. Atomic Yb is an excellent candidate for applying the laser cooling technique. The ground-state $^1S_0(0 \text{ cm}^{-1})$ and the excited state $^1P_1(25068.222 \text{ cm}^{-1})$ can be considered as a closed two–state system, when the transition between them for cooling. There is, therefore, no need of an additional laser for re-pumping which is required in the case of alkali atoms. Also, high-power and narrow-bandwidth 398.8nm light source for laser cooling, which tunes the $^1S_0 - ^1P_1$ transition, is obtained by resonant frequency-doubling of Ti:sapphire laser. A short radiative lifetime of 5.5ns[25] of $^1P_1$ state would enable one to rapidly repeat the absorption–spontaneous emission cycle, which means that a large force can be exerted on Yb atoms. For example, the distance required for slowing a fast atomic beam from an oven of 700 K could be shorter than 20cm with cooling laser of saturated intensity. Thus, a large solid angle from the Yb oven is utilized, which permits the use of a large number of atoms for the experiment. We have recently succeeded in laser cooling and trapping of Yb atoms using this transition[26, 27]. This singlet transition would be also useful for optical pumping and dipole-force–trapping. In addition, the intercombination transition $^1S_0 - ^3P_1(17992.007 \text{ cm}^{-1})$ is complementary to the singlet transition in that the radiative lifetime of $^3P_1$ state is as long as 827ns[25]. Although this transition cannot be used for slowing a fast atom, it may be useful for a second cooling because it makes the Doppler-cooling temperature as low as 4μ K[28].

The procedure of the atomic EDM measurement with laser cooled Yb atoms will be as follows(see Fig. 1): First, a fast atomic beam from a hot oven will be slowed down by the Zeeman–tuning method. After this pre–cooling stage, the atoms will be trapped and cooled by the magneto–optical trap(MOT)[29]. A high density and large number of atoms would be loaded into the MOT within several seconds. Then the atomic beam and magnetic field for MOT will be turned off. At the same time the detunings of the trapping laser beams will be changed and it's intensity reduced to produce moving optical mollasses in the

EDM measurement

magnetic shield

**lasers for dipole-force trap,
optical pumping,
probing**

electric field plates

MOT **Zeeman Slower** **Yb oven**
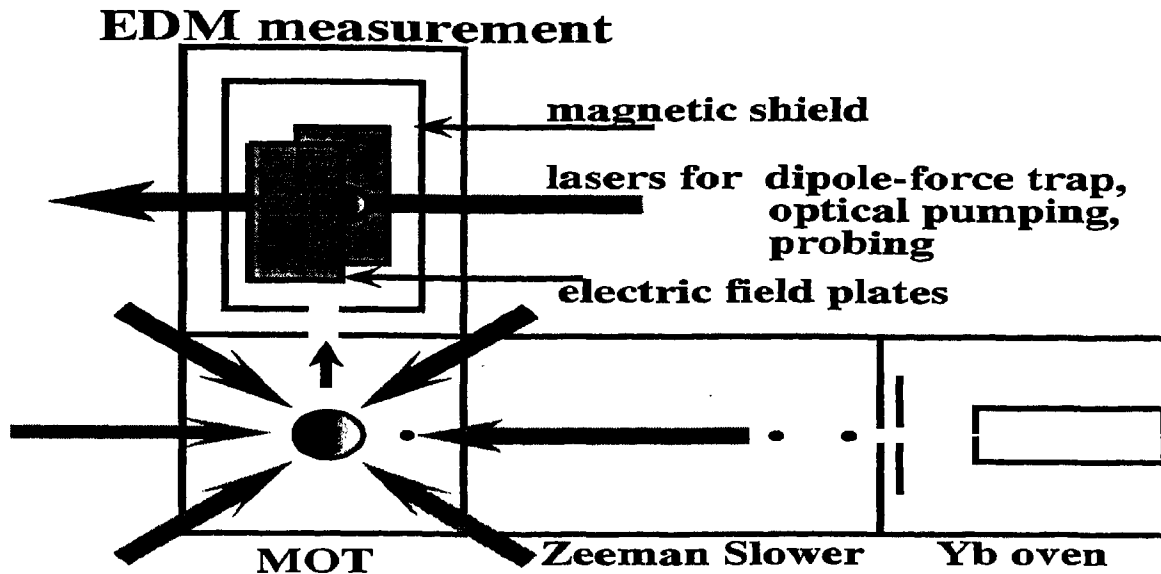
Figure 2.1: *Proposed experimental setup. A fast atomic beam from a hot oven will be slowed down by the Zeeman–tuning method, and then the atoms will be magneto–optically trapped. The atoms are launched to the EDM measurement region by changing the detunings of the trapping laser beams. A high power laser beam will trap the atoms by far–blue–detuned dipole force. After polarizing the spin by optical pumping, a probe laser will monitor the Larmor precession frequency.*

micro Kelvin region by the polarization–gradient cooling method. When the atoms reach the EDM measurement region where a high static electric field is applied, a high power laser for a far–blue–detuned dipole force trap[30] will be turned on. Optical pumping will be also performed to polarize the nuclear spin by the application of a circularly polarized resonant light pulse[31]. Finally an additional laser beam will probe the Larmor precession frequency. The loading and measurement procedure will be repeated many times to reduce the statistical uncertainty.

Our proposal [32] has other advantages. As pointed out earlier in this paper, the electron-spin-exchange collisions between cold Cs atoms cause shift and dephasing of Zeeman sublevel resonance[24]. In the case of Yb atoms, however, the cold collisions have negligible effect because the Yb atom has no electron spin in the ground-state. Among

seven isotopes, ^{171}Yb and ^{173}Yb have nuclear spins $I = 1/2$ and $I = 5/2$, respectively, and so are useful for EDM search. The comparison of results of these two isotopes would be helpful in eliminating some systematic errors in the experiments. The existence of nuclear quadrupole moment of ^{173}Yb will not cause significant problems because of the good homogeneity of electric field over the small sample region and absence of wall collision in our experiment.

We also propose the use of the polarization technique to measure the EDM. In the conventional cell experiments[11, 13], a particular component of spin polarization, S_z for example, is detected through absorption of a circularly-polarized probe light traversing in the z direction. Since the laser cooled atoms have quite narrow optical linewidth, the absorption signals would suffer large random variations due to the frequency-jitter of the probe laser. Also, the optical thickness of dense cold atoms is so high at resonance that the probe light is significantly attenuated and will not be so sensitive to the change of S_z. In the polarization technique, on the other hand, S_z is detected through paramagnetic Faraday effect[31] where rotation of polarization is induced by S_z for linearly polarized off-resonant light traversing in the z direction. At sufficiently large off-resonance, a probe light is not attenuated, and also the signals are less sensitive to the frequency-jitter.

References

[1] S.M. Barr, Int. J. Mod. Phys. A **8**,209,(1993).

[2] J. J. Sakurai, *Modern Quantum Mechanics*(Addison-Wesley Company Inc, 1985).

[3] Ann-Marie Martensson-Pendrill, *Methods in Computational Chemistry, Volume 5: Atomic and Molecular Properties*, Ed by Stephen Wilson, 99(Plenum Press, New York, 1992).

[4] L. I. Schiff, Phys Rev **132**, 2194(1963).

[5] P. V. Coveny and P. G. H. Sandars, J. Phys. B **16**, 3727(1983).

[6] I. B. Khriplovich, *Parity Nonconservation in Atomic Phenomena*(Gordon and Breach, Philadelphia, 1991).

[7] Harry M. Quiney, Jon K. Laerdahl, Knut Fægri Jr. and Trond Saue, Phys Rev A **57**,920(1998).

[8] J. H. Smith, E. M. Purcell and N. F. Ramsey, Phys. Rev. **108**, 120(1957).

[9] L. Landau, Nucl. Phys. **3**, 127(1957).

[10] P. G. H. Sandars and E. Lipworth, Phys. Rev. Lett. **13**, 718,(1964).

[11] J. P. Jacobs, W. M. Klipstein, S. K. Lamoreaux, B. R. Hackel and E. N. Fortson, Phys. Rev. A **52**, 3521 (1995).

[12] D. Commins, Stephen B. Ross, David De Mille and B. C. Regan, Phys. Rev. A **50**, 2960(1994).

[13] S. A. Murthy, D. Krause Jr., L. Li and L. R. Hunter, Phys. Rev. Lett. **63**, 965 (1989).

[14] William D. Phillips, Phillip L. Gould and Paul D. Lett, Science **239**, 877(1988).

[15] Steven Chu, Science **253**, 861(1991).

[16] W. Ertmer, R. Blatt, J. L. Hall and M. Zhu, Phys. Rev. Lett. **54**, 996(1985).

[17] J. Prodan, A. Migdall, W. D. Phillips, I. So, H. J. Metcalf, and J. Dalibard, Phys. Rev. Lett **54**, 992(1985).

[18] K. J. Kugler, W. Paul and U. Trinks, Phys. Lett. **72B**,422(1978).

[19] M. H. Anderson, J. R. Ensher, M. R. Matthews, C. E. Wieman and E. A. Cornell, Science **269**, 198(1995).

[20] see, for example, W. D. Phillips, *Laser Manipulation of Atoms and Ions*, (Elsevier, Amsterdam, 1992) p289,

[21] see, for example, C. Cohen-Tannoudji, *Laser Manipulation of Atoms and Ions*, (Elsevier, Amsterdam,1992) p99

[22] N. Davidson,H. J. Lee, C. S. Adams, M. Kasevich and S. Chu , Phys. Rev. Lett., **74**, 1311(1995)

[23] M. A. Kasevich, E. Riis, S. Chu and R. G. DeVoe Phys. Rev. Lett.**63**, 612(1989)

[24] M. Bijlsma, B. J. Verhaar, and D. J. Heinzen, Phys. Rev.A **49** R4285(1994).

[25] M. Bauman and G. Wandel, Phys. Lett. **28A** 200(1968)

[26] M. Fujimito *et al.*, unpublished.

[27] The first laser cooling of Yb atomic beam with a broad-bandwidth laser was performed by M. Watanabe *et al.* , J. Opt. Soc. Am. **B 13**,2377(1996).

[28] The unique features of Yb laser-cooling was first pointed out by J. Hall, M. Zhu and P. Buch ., J. Opt. Soc. Am. **B 6**, 2194(1989).

[29] E. L. Raab, M. Prentiss, A. Cable, S. Chu and D. E. Pritchard, Phys. Rev. Lett. **59** 2631(1987)

[30] M. Watanabe, R. Ohmukai, K. Hayasaka, H. Imajo, and S. Urabe, Opt. Lett. **19**, 637 (1994).

[31] W. Happer, Rev. Mod. Phys. **44**, 169(1972).

[32] Y. Takahashi, M. Fujimoto, T. Yabuzaki,Angom Dilip Singh, Manoj K. Samal and B. P. Das, *Not published.*

Chapter 3

Configuration Interaction and Many-Body Perturbation Theory Based Atomic Many-Body Theories

3.1 Description of the Atomic States

The Dirac-coulomb Hamiltonian of an atom is

$$H_{\text{atom}} = \sum_i \left(c\alpha_i \cdot p_i + (\beta - 1)c^2 - \frac{Z}{r_i} \right) + \sum_{i>j} \frac{1}{r_{ij}}. \tag{3.1}$$

Define U_{DF} as the independent particle central field Dirac-Fock potential then the atomic Hamiltonian can be redefined as

$$H_{\text{atom}} = \sum_i \left(t_i + U_{\text{DF}} \right) + V_{\text{es}} = \sum_i h_i + V_{\text{es}} = H_0 + V_{\text{es}}, \tag{3.2}$$

$$V_{\text{es}} = \sum_{i>j} \frac{1}{r_{ij}} - U_{\text{DF}} \text{ and } t_i = c\alpha_i \cdot p_i + (\beta_i - 1)c^2 - \frac{Z}{r_i},$$

then single electron Hamiltonian h_i satisfies the Schrodinger equation

$$h|\psi_i\rangle = \epsilon_i|\psi_i\rangle.$$

Where $|\psi_i\rangle$ is orbital and ϵ_i is the single particle energy. A set of orbitals $\{|\psi_i\rangle\}$ can be got from the above eigenvalue equation and from it a set of configuration state functions(CSFs) $\{|\Phi_i\rangle\}$ can be constructed.

A CSF is a linear combination of determinants identified by the quantum numbers γ, total angular momentum J and total magnetic quantum number M. Where γ is

39

an additional quantum number required to define the CSF uniquely. The atomic state function(ASF) can then be got as a linear combination of these CSFs. An ASF is defined by the same J and M but with a different additional quantum number Γ to identify each of the ASF uniquely

$$\left|\Psi(\Gamma_i JM)\right\rangle = \sum_j \mathcal{C}_{ij}\left|\Phi(\gamma_j JM)\right\rangle.$$

ASFs are eigen-functions of the atomic Hamiltonian and satisfies the Schrodinger equation

$$H_{\text{atom}}\left|\Psi(\Gamma_i JM)\right\rangle = E_i\left|\Psi(\Gamma_i JM)\right\rangle,$$

where E_i is the energy eigenvalue of the ASF. While computing matrix elements of operators it is summed over M and effectively it is the quantum numbers Γ and J that identifies an ASF. In addition as H_{atom} commute with the parity operator P the CSFs and ASF are parity eigenstates. Using the orbitals a single particle computation can be done by introducing H_{PTV} and V_{es} as perturbations [1]. Here only the Configuration based methods CI and modified CI, and Bloch equation based MBPT methods are discussed.

3.2   CI Method Based Computations

3.2.1   Computation of EDM with CI Wave-Functions

From definition an ASF $|\Psi_i(\Gamma_i JM)\rangle$ within a CSF space $\{|\Phi_j(\gamma_j JM)\rangle\}$ is

$$\left|\Psi(\Gamma_i JM)\right\rangle = \sum_j \mathcal{C}_{ij}\left|\Phi(\gamma_j JM)\right\rangle.$$

In the CI method the CSF co-efficients $\mathcal{C}_{ij}$ are got after diagonalizing the atomic Hamiltonian within the CSF space[4]. Since the atomic Hamiltonian commutes with the parity operator the ASFs are eigen-states of parity. Let $\{|\Phi_i(\gamma_i JM)\rangle\}$ and $\{|\overline{\Phi}_i(\gamma_i J'M')\rangle\}$ be CSF spaces of opposite parities. Diagonalizing the atomic Hamiltonian within these CSF spaces give two sets of ASFs $\{|\Psi_i(\Gamma_i JM)\rangle\}$ and $\{|\overline{\Psi}_i(\Gamma_i' J'M')\rangle\}$, which are opposite in

Dropping the quantum numbers in general $|\Psi_i\rangle$ represents an ASF in $\{|\Psi_i(\Gamma_i JM)\rangle\}$ with quantum numbers Γ_i, J and M, similarly $|\overline{\Psi}_i\rangle$ represents the corresponding ASF in opposite parity space with quantum numbers Γ_i', J' and M'

Let $|\Psi_0\rangle \in \{|\Psi_i(\Gamma_i JM)\rangle\}$ be the ground state ASF. The PT-violating interactions within the atom introduce opposite parity corrections to the ASFs. It is *wrt* the mixed parity ground state the expectation value of the dipole operator is to be computed. Let $|\widetilde{\Psi}_0\rangle$ be the mixed parity ground state, using perturbation theory it can be written in terms of the CI wavefunctions as

$$\left|\widetilde{\Psi}_0\right\rangle = \left|\Psi_0\right\rangle + \sum_I \frac{\left|\overline{\Psi}_I\right\rangle\left\langle\overline{\Psi}_I\left|H_{\text{PTV}}\right|\Psi_0\right\rangle}{E_0 - \overline{E}_I}.$$

Where $\overline{E}_I$ and E_0 are the energies of the opposite parity ASFs and the ground state ASF. The atomic EDM is then

$$\vec{D}_a = \left\langle\widetilde{\Psi}_0\left|\vec{D}\right|\widetilde{\Psi}_0\right\rangle = 2\sum_I \frac{\left\langle\Psi_0\left|\vec{D}\right|\overline{\Psi}_I\right\rangle\left\langle\overline{\Psi}_I\left|H_{\text{PTV}}\right|\Psi_0\right\rangle}{E_0 - \overline{E}_I},$$

which in terms of CSF with CI coefficients can be written as

$$\vec{D}_a = 2\sum_{Iijkl} \mathcal{C}_{0i}\overline{\mathcal{C}}_{Ij}\overline{\mathcal{C}}_{Ik}\mathcal{C}_{0l}\frac{\left\langle\Phi_i\left|\vec{D}\right|\overline{\Phi}_j\right\rangle\left\langle\overline{\Phi}_k\left|H_{\text{PTV}}\right|\Phi_l\right\rangle}{E_0 - \overline{E}_I}.$$

This is the required expression of the atomic EDM in terms of the CSFs. This approach requires two diagonalizations, one each in the two opposite parity CSF subspaces. When the number of the CSFs in these subspaces are large the diagonalization approach is less desirable in terms of computational efficiency.

3.2.2   Computation of EDM Using Perturbed CI Method

Let the ground state configuration of the atom be $|\Phi_0\rangle$ and $\{|\Phi_i\rangle\}$ be a set of CSFs which has same parity and total angular momentum as $|\Phi_0\rangle$. The CSF $|\Phi_0\rangle$ does not have any dynamic electron-correlation effects but an ASF $|\Psi_0\rangle$ which includes all the electron-correlation effects within $\{|\Phi_i\rangle\}$ can be constructed by doing a configuration interaction(CI) calculation with H_{atom} in $\{|\Phi_i\rangle\}$. The ground state ASF $|\Psi_0\rangle$ satisfy the Schrodinger equation

$$H_{\text{atom}}\left|\Psi_0\right\rangle = E_0\left|\Psi_0\right\rangle. \tag{3.3}$$

Where $|\Psi_0\rangle = \sum_i \mathcal{C}_{0i}|\Phi_i\rangle$, $\mathcal{C}_{0i}$ are the CI coefficients got by diagonalizing the H_{atom} matrix within $\{|\Phi_i\rangle\}$. Introduce the parity and time-reversal(PT) violating interaction Hamilto-

nian H_{PTV} as a perturbation, the total atomic Hamiltonian assumes the form

$$H = H_{\text{atom}} + H_{\text{PTV}}.$$

As H_{PTV} does not commute with the parity operator the eigenfunctions of H are no longer parity eigenstates. It introduces an opposite parity correction to the wave-function and since H_{PTV} scales as G_F it should be included to first order only. The Schrodinger equation assumes the form

$$H\big|\tilde{\Psi}_0\big\rangle = E_0\big|\tilde{\Psi}_0\big\rangle, \quad \text{where} \quad \big|\tilde{\Psi}_0\big\rangle = \big|\Psi_0\big\rangle + \big|\Psi_0^1\big\rangle.$$

The perturbation H_{PTV} introduces no energy correction as it is odd in parity. Let $\{|\overline{\Phi}_i\rangle\}$ represent the opposite parity configuration space. Expressing $|\Psi_0^1\rangle$ as a linear combination of opposite parity configurations, the ground state ASF of H is

$$\big|\tilde{\Psi}_0\big\rangle = \big|\Psi_0\big\rangle + \big|\Psi_0^1\big\rangle = \sum_i \mathcal{C}_{0i}\big|\Phi_i\big\rangle + \sum_m \overline{C}_{0m}\big|\overline{\Phi}_m\big\rangle, \qquad (3.4)$$

where $\overline{C}_{0m}$ are the correction coefficients first order in H_{PTV} but all order in V_{es} in a restricted configuration subspace. Introduce perturbation parameter λ, the Schrodinger equation becomes

$$\left(H_{\text{atom}} + \lambda H_{\text{PTV}} \right)\left(\sum_i \mathcal{C}_{0i}\big|\Phi_i\big\rangle + \lambda \sum_m \overline{C}_{0m}\big|\overline{\Phi}_m\big\rangle \right) = E_0\left(\sum_i \mathcal{C}_{0i}\big|\Phi_i\big\rangle + \lambda \sum_m \overline{C}_{0m}\big|\overline{\Phi}_m\big\rangle \right). \tag{3.5}$$

Project the equation onto $|\Psi_0^1\rangle$ and retain the first order terms in λ. This gives the matrix equation.

$$\left(\mathbf{E}_0 - \mathbf{H}_0^{--} \right)\overline{\mathcal{C}} = \mathbf{H}_{\text{PTV}}^{-+}\mathcal{C}, \qquad (3.6)$$

solving this matrix equation will give the required coefficients of the opposite parity CSFs $\overline{C}_{0m}$. The expectation value of the atomic EDM can then be computed using the perturbed ASFs as

$$\vec{D}_a = \big\langle \tilde{\Psi}_0\big|\vec{D}\big|\tilde{\Psi}_0\big\rangle = 2\sum_{ij} \mathcal{C}_{0i}\overline{C}_{0j}\big\langle \Phi_i\big|\vec{D}\big|\overline{\Phi}_j\big\rangle.$$

Where $\vec{D}$ is the dipole operator. Unlike the earlier approach, in this approach only the ground state CSF space needs to be diagonalized. Using the Bloch equation based formulations the diagonalization can be avoided altogether. Another advantage of using the Bloch equation based formulation is that it requires less memory.

3.3 The Computation of EDM using MBPT

MBPT at the single particle level was used in atomic structure calculation by Kelly[5, 6, 7] for the first time to compute correlation energies. Here the computations are at the level of configurations. The V_{es} part in equation(3.2) can be treated perturbatively by partitioning the configuration space into model and complementary spaces $\{|\Phi_i\rangle_P\}$ and $\{|\Phi_i\rangle_Q\}$ respectively[2]. The model space has configurations which mix strongly with the ground state configuration and the rest of the configurations are included in the complementary space. The projection operators for these CSF spaces are

$$P = \sum_i |\Phi_i\rangle_{P\,P}\langle\Phi_i|, \quad Q = \sum_i |\Phi_i\rangle_{Q\,Q}\langle\Phi_i| \quad \text{and} \quad P + Q = 1.$$

The mixing from the complementary space is computed using Rayleigh-Schrodinger perturbation theory. The essence of Rayleigh-Schrodinger perturbation theory is the Bloch equation [8]

$$\left[\Omega_{es}, H_0\right]P = QV_{es}\Omega_{es}P - \chi_{es}PV_{es}\Omega_{es}P, \tag{3.7}$$

where $\chi_{es} = \sum_{n=1}^{\infty} \Omega_{es}^{(n)}$ and can be written in recursive form as

$$\left[\Omega_{es}^{(n)}, H_0\right]P = QV_{es}\Omega_{es}^{(n-1)}P - \sum_{m=1}^{(n-1)} \Omega_{es}^{(m)}PV_{es}\Omega_{es}^{(n-m-1)}P. \tag{3.8}$$

To compute the intrinsic EDM of an atom, two more perturbations H_{PTV} and H_{dip} are to be introduced. Including H_{PTV} as a perturbation the total atomic Hamiltonian assumes the form

$$H = H_0 + V_{es} + \lambda H_{PTV},$$

where λ is the perturbation parameter. These perturbations introduce corrections to the configurations in P-space, corrections from V_{es} are of same parity as the unperturbed CSF but the corrections from H_{PTV} are opposite in parity. The residual coulomb interaction V_{es} is to be treated to all order but H_{PTV} should be treated to first order only. The exact Schrodinger equation is

$$H|\tilde{\Psi}\rangle = E_0|\tilde{\Psi}\rangle, \tag{3.9}$$

where

$$|\tilde{\Psi}\rangle = |\Phi_0\rangle_P + \sum_j \mathcal{C}_j |\Phi_j\rangle_Q + \sum_k \overline{\mathcal{C}}_k |\overline{\Phi}_k\rangle_Q = \left(\Omega_{es} + \lambda\Omega_{es,edm}\right)|\Phi_0\rangle_P.$$

The value of the atomic EDM is then

$$\vec{D}_a = \frac{\langle \tilde{\Psi} | \vec{D} | \tilde{\Psi} \rangle}{\langle \tilde{\Psi} | \tilde{\Psi} \rangle}.$$

$\vec{D}$ being an odd parity operator connects CSFs of opposite parities, so only those terms linear in λ need to be retained, we get

$$\vec{D}_a = \langle \Phi_0 | \Omega_{es}^\dagger \vec{D} \Omega_{es,edm} | \Psi_0 \rangle + \langle \Psi_0 | \Omega_{es,edm}^\dagger \vec{D} \Omega_{es} | \Phi_0 \rangle = \langle \Phi_0 | \left(\vec{D}_a \right)_{eff} | \Phi_0 \rangle. \qquad (3.10)$$

Where $(\vec{D}_a)_{eff} = P(\Omega_{es}^\dagger \vec{D} \Omega_{es,edm} + \Omega_{es,edm}^\dagger \vec{D} \Omega_{es})P$ is the effective intrinsic atomic EDM operator and is different from the usual effective dipole operator. The usual effective dipole operator $\vec{D}_{eff}$ used in computing dipole transition amplitude connects two CSFs of different parities. The effective intrinsic atomic EDM operator is an expectation value operator and the wave-operators in it has H_{PTV} and residual coulomb operators as perturbations where as in $\vec{D}_{eff}$ it is only H_{es}. The wave operators $\Omega_{es,edm}$ and Ω_{es} are computed from the modified Bloch equation

$$\left[\Omega^{(n)}, H_0 \right] P = Q H' \Omega^{(n-1)} P - \sum_{m=1}^{(n-1)} \Omega^{(m)} P H' \Omega^{(n-m-1)} P. \qquad (3.11)$$

Where $H' = V_{es} + \lambda H_{PTV}$. Out of all terms only those which has residual coulomb interaction alone and those that have one order of H_{PTV} are required. Define $\Omega^{(n)}(edm)$ as the nth order wave-operator required for the EDM computation. This can be got from (3.11) as

$$\Omega^{(n)}(edm) = \Omega_{es}^{(n)} + \lambda \left(\frac{\partial}{\partial \lambda} \left(\Omega^{(n)} \right) \Big|_{\lambda=0} \right) = \Omega_{es}^{(n)} + \lambda \Omega_{es,edm}^{(n-1)}. \qquad (3.12)$$

The total wave-operator $\Omega(edm)$ is defined by the total order of the perturbations but while writing out the components Ω_{es} and $\Omega_{es,edm}$ the superscript denote the order of residual coulomb interaction and the additional subscript 'edm' denote the presence of H_{PTV} as perturbation. With these perturbations the first order wave-operator can be written as

$$\left[\Omega^{(1)}, H_0 \right] P = Q \left(V_{es} - \lambda H_{PTV} \right) P.$$

Which using the resolvent operator

$$R = \sum_i \frac{| \Phi_i \rangle_Q \langle \Phi_i |}{(E_0 - H_0)}, \quad \text{gives} \quad \Omega^{(1)} P = R \left(V_{es} + \lambda H_{PTV} \right) P. \qquad (3.13)$$

As the two perturbations are opposite in parity, it is appropriate that the model space and the complementary space be separated into subspaces of opposite parities. Then the model space projection operator can be divided into P_+ and P_-. Doing the same with complementary space projection operator and the resolvent operator we can write

$$P = P_+ + P_- \ ; \ Q = Q_+ + Q_- \ ; \ R = R_+ + R_-.$$

With these definitions (3.13) can be rewritten as

$$\Omega^{(1)}P = \left(R_+V_{es} + \lambda R_-H_{PTV}\right)P_+ + \left(R_-V_{es} + \lambda R_+H_{PTV}\right)P_-. \tag{3.14}$$

To make the derivation less cumbersome assume that, the model space has configurations of only one parity i.e. $P = P_+$, then

$$\Omega^{(1)}P = \left(R_+V_{es} + \lambda R_-H_{PTV}\right)P_+ = \left(\Omega^{(1)}_{es} + \lambda\Omega^{(0)}_{es,edm}\right)P_+.$$

The expression for the wave-operator has been splitted according to the definition given earlier, according to which indicing of wave-operator $\Omega_{es,edm}$ is based on the order of V_{es} e.g. $\Omega^{(0)}_{es,edm}$ has one order of H_{PTV} but no V_{es} at all. Similarly the expression for the second order wave-operator is

$$\left[\Omega^{(2)}, H_0\right]P_+ = Q\left(V_{es} + \lambda H_{PTV}\right)\Omega^{(1)}P_+ - Q\Omega^{(1)}P_+\left(V_{es} + \lambda H_{PTV}\right)P_+.$$

Using the definition of (3.12)

$$
\begin{aligned}
\Omega^{(2)}(edm)P_+ &= \left(R_+V_{es}R_+V_{es} - R_+(R_+V_{es}P_+)V_{es}\right)P_+ + \lambda\Big(R_-V_{es}R_-H_{PTV} + R_-H_{PTV}R_+V_{es} \\
&\quad - R_-(R_-H_{PTV}P_+)V_{es}\Big)P_+, \\
&= \left(\Omega^{(2)}_{es} + \lambda\Omega^{(1)}_{es,edm}\right)P_+ \tag{3.15}
\end{aligned}
$$

The other higher order wave-operators can be evaluated in the same way. In general the wave-operator $\Omega^{(n)}_{es,edm}$ can be got from the modified Bloch equation

$$\left[\Omega^{(n)}_{es,edm}, H_0\right]P_+ = \left(Q_-H_{PTV}\Omega^{(n)}_{es} + Q_-V_{es}\Omega^{(n-1)}_{es,edm} - \sum_{m=0}^{n-1}\Omega^{(m)}_{es,edm}P_+V_{es}\Omega^{(n-m-1)}_{es}\right)P_+.$$

In writing the above equation $\Omega^{(-1)}_{es,edm} = 0$ has been used and the renormalization term start contributing from $n = 1$ onwards. The above equation is valid starting from $n = 0$.

3.4 Computation of the wave-operator

3.4.1 Wave-Operator Computed in terms of order of Perturbation

The derivations in the previous section is general and the atomic Hamiltonian can be partitioned into any convenient form . For computation Epstein-Nesbet(EN) partitioning[9] will be used. With EN-partitioning the unperturbed Hamiltonian is defined as

$$H_0 = \sum_i \left|\Phi_i\right\rangle\left\langle\Phi_i\left|H_{\text{atom}}\right|\Phi_i\right\rangle\left\langle\Phi_i\right| = \sum_i \left\langle\Phi_i\left|H_{\text{atom}}\right|\Phi_i\right\rangle\left|\Phi_i\right\rangle\left\langle\Phi_i\right|. \tag{3.16}$$

To distinguish the residual coulomb interaction from V_{es} defined earlier, it will be denoted by H_{es} and connects different CSFs. It is given by

$$H_{\text{es}} = \sum_{i,j} \left|\Phi_i\right\rangle\left\langle\Phi_i\left|H_{\text{atom}}\right|\Phi_j\right\rangle\left\langle\Phi_j\right| = \sum_{i,j,i\neq j} \left\langle\Phi_i\left|H_{\text{atom}}\right|\Phi_j\right\rangle\left|\Phi_i\right\rangle\left\langle\Phi_j\right|. \tag{3.17}$$

In EN-partitioning the effect of diagonal ladder diagrams is taken to all orders in first order wave-function and second order for energy. The energy of CSF $\left|\Phi_i\right\rangle$ in EN-partitioning is the expectation value of H_{atom} and the Schrodinger equation for the unperturbed atomic Hamiltonian H_0 is

$$H_0\left|\Phi_i\right\rangle = E_i\left|\Phi_i\right\rangle \quad \text{where} \quad E_i = \left\langle\Phi_i\left|H_{\text{atom}}\right|\Phi_i\right\rangle.$$

The definitions of P and Q do not change, but the energy denominator changes. In the following derivations the indices i and j cover all the CSFs within the configuration space considered. Similarly, H_{PTV} assumes the form

$$H_{\text{PTV}} = \sum_{i,j} \left|\overline{\Phi}_i\right\rangle\left\langle\overline{\Phi}_i\left|H_{\text{PTV}}\right|\Phi_j\right\rangle\left\langle\Phi_j\right| = \sum_{i,j} \left\langle\overline{\Phi}_i\left|H_{\text{PTV}}\right|\Phi_j\right\rangle\left|\overline{\Phi}_i\right\rangle\left\langle\Phi_j\right|, \tag{3.18}$$

That is the unperturbed Hamiltonian and the perturbations are cast in operator form within the configuration space considered. Consider the expression for $\Omega_{\text{es}}^{(1)}$, in terms of these definitions it can be written as

$$\Omega_{\text{es}}^{(1)}P_+ = \sum_{i,j} \frac{\left|\Phi_j\right\rangle_Q \,_Q\left\langle\Phi_j\left|H_{\text{atom}}\right|\Phi_i\right\rangle_P \,_P\left\langle\Phi_i\right|}{(E_i - E_j)} = \left(\sum_{i,j} \frac{_Q\left\langle\Phi_j\left|H_{\text{atom}}\right|\Phi_i\right\rangle_P}{(E_i - E_j)}\right) \left|\Phi_j\right\rangle_Q \,_P\left\langle\Phi_i\right|,$$

where $i \in P$, $j \in Q$ and $E_i = \left\langle\Phi_i\right|H_{\text{atom}}\left|\Phi_i\right\rangle$, the term within parentheses in the expression on the right hand side is just a number. The expression can be rewritten as

$$\Omega_{\text{es}}^{(1)}P_+ = \sum_{i,j} C_{ji}^{(1)}(\text{es})\left|\Phi_j\right\rangle_Q \,_P\left\langle\Phi_i\right| \quad \text{where} \quad C_{ji}^{(1)}(\text{es}) = \frac{_Q\left\langle\Phi_j\left|H_{\text{atom}}\right|\Phi_i\right\rangle_P}{(E_i - E_j)}.$$

The second order wave-operator in terms of matrix elements is

$$\Omega_{\mathrm{es}}^{(2)} P_+ = \sum_{i,j} \frac{\left|\Phi_j\right\rangle_{QQ}\left\langle\Phi_j\right|}{E_i - E_j}\left(H_{\mathrm{es}}\Omega_{\mathrm{es}}^{(1)} - \Omega_{\mathrm{es}}^{(1)}\sum_k \left|\Phi_k\right\rangle_{PP}\left\langle\Phi_k\right|H_{\mathrm{es}}\right)\left|\Phi_i\right\rangle_{PP}\left\langle\Phi_i\right|,$$

where $k \in P_+$. Substituting the expressions for H_{es} and $\Omega_{\mathrm{es}}^{(1)}$ in terms of the matrix elements we get

$$\Omega_{\mathrm{es}}^{(2)} P_+ = \sum_{i,j}\left[\left(\sum_l {}_Q\left\langle\Phi_j\middle|H_{\mathrm{atom}}\middle|\Phi_l\right\rangle_Q \mathcal{C}_{li}^{(1)}(\mathrm{es}) + \sum_k \mathcal{C}_{jk}^{(1)}(\mathrm{es})_P\left\langle\Phi_k\middle|H_{\mathrm{atom}}\middle|\Phi_i\right\rangle_P\right)\right]\frac{\left|\Phi_j\right\rangle_{QP}\left\langle\Phi_i\right|}{E_i - E_j},$$

where $l \in Q$, the whole expression within the square brackets is just a number, the wave-operator second order in residual coulomb interaction can be written as

$$\Omega_{\mathrm{es}}^{(2)} = \sum_{ij}\mathcal{C}_{ji}^{(2)}(\mathrm{es})\left|\Phi_j\right\rangle_{QP}\left\langle\Phi_i\right|.$$

This can be extended to higher orders and summing all orders the full wave-operator can be defined as

$$\Omega_{\mathrm{es}} = \sum_{nij}\mathcal{C}_{ji}^{(n)}\left|\Phi_j\right\rangle_{QP}\left\langle\Phi_i\right|. \tag{3.19}$$

A similar expression for the wave-operator $\Omega_{\mathrm{es,edm}}^{(n)}$ can also be obtained. Consider the expression for $\Omega_{\mathrm{es,edm}}^{(0)}$, in terms of the operators defined earlier it can be written as

$$\begin{aligned}\Omega_{\mathrm{es,edm}}^{(0)} P_+ &= \sum_{i,j}\frac{\left|\overline{\Phi}_j\right\rangle_{QQ}\left\langle\overline{\Phi}_j\middle|H_{\mathrm{PTV}}\middle|\Phi_i\right\rangle_{PP}\left\langle\Phi_i\right|}{(E_i - E_j)} = \sum_{i,j}\frac{{}_Q\left\langle\overline{\Phi}_j\middle|H_{\mathrm{PTV}}\middle|\Phi_i\right\rangle_P}{(E_i - E_j)}\left|\overline{\Phi}_j\right\rangle_{QP}\left\langle\Phi_i\right|\\ &= \sum_{i,j}\mathcal{C}_{ji}^{(0)}(\mathrm{es,edm})\left|\overline{\Phi}_j\right\rangle_{QP}\left\langle\Phi_i\right|.\end{aligned}$$

Like in the case of Ω_{es}, the above expression can be generalized to any order n by using the Bloch equation and summed to get the full wave-operator

$$\Omega_{\mathrm{es,edm}} = \sum_{nij}\mathcal{C}_{ji}^{(n)}(\mathrm{es,edm})\left|\overline{\Phi}_j\right\rangle_{QP}\left\langle\Phi_i\right|. \tag{3.20}$$

Using the expression for Ω_{es} and $\Omega_{\mathrm{es,edm}}$ the wave-operators $\Omega_{\mathrm{es}}^{\dagger}$ and $\Omega_{\mathrm{es,edm}}^{\dagger}$ can also be derived. Let these be represented as

$$\Omega^{\dagger(n)}(es) = \sum_{ij}\overline{\mathcal{C}}_{ji}^{(n)}(\mathrm{es})\left|\Phi_j\right\rangle_{PQ}\left\langle\Phi_i\right|, \quad \Omega^{\dagger(n)}(es,edm) = \sum_{ij}\overline{\mathcal{C}}_{ji}^{(n)}(\mathrm{es,edm})\left|\Phi_j\right\rangle_{PQ}\left\langle\overline{\Phi}_i\right|,$$

The wave-operators Ω_{es} and $\Omega_{\mathrm{es,edm}}$ has the following properties:

- The co-efficients in Ω_{es} and $\Omega_{es,edm}$ are real as these are product of real matrix elements, hence $\overline{C}_{ji}^{(n)}(es) = C_{ij}^{(n)}(es)$ and $\overline{C}_{ji}^{(n)}(es, edm) = C_{ij}^{(n)}(es, edm)$.

- These wave-operators are non-hermitian *ie* $\Omega_{es}^{\dagger} \neq \Omega_{es}$ and $\Omega_{es,edm}^{\dagger} \neq \Omega_{es,edm}$. This is evident from the form of the projection operator part in the expression of the wave-operators.

- The wave-operators are state specific, $\Omega_{es}^{\dagger}$ and $\Omega_{es,edm}^{\dagger}$ can act only on the bra CSF $\langle\Phi_0|$ and not on any other ket nor bra. Similarly, Ω_{es} and $\Omega_{es,edm}$ can act only on the ket CSF $|\Phi_0\rangle$.

The atomic EDM in terms of the wave-operators can be computed using the expression (3.10) as

$$\vec{D}_a = 2\langle\Phi_0|\Omega_{es}^{\dagger}\vec{D}\Omega_{es,edm}|\Phi_0\rangle \tag{3.21}$$

This is the required value of D_a. The factor of two takes care of the hermitian conjugate term in the expectation value.

3.4.2 Wave-Operator Computed in terms of Order of Iteration

The wave-operator computed using the Bloch equation (3.8) is an order by order approach. Since the computation of the wave-operator is a blanket matrix multiplication the Bloch equation can be recast in an iterative form

$$\left[\Omega_{es}^{(n)}, H_0\right] P = Q H_{es}\Omega_{es}^{(n-1)} P - \Omega_{es}^{(n-1)} \Delta E^{(n)} P. \tag{3.22}$$

Where $\Delta E^{(n)} = P H_{es}\Omega_{es}^{(n-1)} P$ is the energy correction from the wave-operator computed in the previous iteration. The zeroth order iteration gives $\Omega_{es}^{(0)} = I$ and the first iteration gives

$$\left[\Omega_{es}^{(1)}, H_0\right] P = Q V_{es}\Omega_{es}^{(0)} P = Q H_{es} P.$$

This has the same form as the equation for the first order wave-operator in the order by order approach. Consider the second iteration, the expression for the wave-operator is

$$\left[\Omega_{es}^{(2)}, H_0\right] P = Q H_{es}\Omega_{es}^{(1)} P - \Omega_{es}^{(1)} \Delta E^{(2)} P$$

The wave-operator of higher iterations can also be derived in a sequence. The advantage of using the iterative approach over the order by order approach is the amount of the memory space saved. In the order by order approach wave-operators of all orders need to be stored to compute the renormalization term, where as in the iterative approach only $\Omega_{\text{es}}^{(n-1)}$ and $\Omega_{\text{es}}^{(n)}$ need to be saved and for closed shell systems $\Delta E^{(n)}$ is just a number and hence a scalar. In addition as there is no summation in the renormalization term the number of operations required is also reduced significantly.

To compute atomic EDM the PT-violating Hamiltonian H_{PTV} should also be included as a perturbation. Since H_{PTV} should be treated to first order only it does not contribute to ΔE. The Bloch equation for the wave-operator $\Omega_{\text{es,edm}}^{(n)}$ is

$$\left[\Omega_{\text{es,edm}}^{(n)}, H_0\right] P = Q\left[H_{\text{es}}\Omega_{\text{es,edm}}^{(n)} + H_{\text{PTV}}\Omega_{\text{es}}^{(n-1)} - \Omega_{\text{es,edm}}^{(n-1)}\Delta E^{(n)}\right] P$$

Since the equation is cast in iterative form and not in order of perturbation using the converged wave-operator Ω_{es} and the corresponding energy correction ΔE the above equation assumes the form

$$\left[\Omega_{\text{es,edm}}^{(n)}, H_0\right] P = Q\left[H_{\text{es}}\Omega_{\text{es,edm}}^{(n)} + H_{\text{PTV}}\Omega_{\text{es}} - \Omega_{\text{es,edm}}^{(n-1)}\Delta E\right] P \qquad (3.23)$$

From the wave-operators given by (3.22) and (3.23) the expression for the atomic EDM assumes the form

$$\vec{D}_a = 2\left\langle\Phi_0\left|\Omega_{\text{es}}^{\dagger}\vec{D}\Omega_{\text{es,edm}}\right|\Phi_0\right\rangle$$

3.5 Computation of $E1_{\text{PNC}}$–the parity non-conserving transition amplitude–using MBPT formalism

Unlike the case of EDM, for the computation of $E1_{\text{PNC}}$ the dipole matrix element is to be computed between two different mixed parity states. Define $|\Psi_i\rangle$ and $|\Psi_f\rangle$ as the initial and final states which are eigen-states of the atomic Hamiltonian without the odd-parity Hamiltonian. With the parity odd Hamiltonian H_{pnc} included the atomic Hamiltonian assumes the form

$$H = H_0 + V_{\text{es}} + \lambda H_{\text{pnc}}.$$

In operator form H_{pnc} can be defined within the configuration space–which include configurations of both parities–as

$$H_{pnc} = \sum_{ij} \left(\left\langle \Phi_i \middle| H_{pnc} \middle| \Phi_j \right\rangle \right) \middle| \Phi_j \right\rangle \left\langle \Phi_i \middle|$$

Since H_{pnc} connects configurations opposite in parity, in the above expression $|\Phi_i\rangle$ and $|\Phi_j\rangle$ should be of opposite parities. With the opposite parity corrections the eigen-states $|\Psi_i\rangle$ and $|\Psi_f\rangle$ assumes the form

$$\left| \Psi_i \right\rangle \rightarrow \left| \tilde{\Psi}_i \right\rangle = \left| \Psi_i \right\rangle + \left| \Psi_i^{corr} \right\rangle \text{ and } \left| \Psi_f \right\rangle \rightarrow \left| \tilde{\Psi}_f \right\rangle = \left| \Psi_f \right\rangle + \left| \Psi_f^{corr} \right\rangle$$

Then the required $E1_{PNC}$ transition amplitude is

$$E1_{PNC} = \frac{\left\langle \tilde{\Psi}_f \middle| \vec{D} \middle| \tilde{\Psi}_i \right\rangle}{\sqrt{\left\langle \tilde{\Psi}_i \middle| \tilde{\Psi}_i \right\rangle \left\langle \tilde{\Psi}_f \middle| \tilde{\Psi}_f \right\rangle}}.$$

The aim of using MBPT is to get eigen-states $|\tilde{\Psi}_i\rangle$ and $|\tilde{\Psi}_f\rangle$. To get these eigen-states we once more partition the configuration space into model and complementary space. In single reference case the parity mixed eigen-states can be written similar to EDM case as:

$$\left| \tilde{\Psi}_i \right\rangle = \left(\Omega_{es}(i) + \lambda \Omega_{es,pnc}(i) \right) \left| \Phi_i \right\rangle_P \text{ and } \left| \tilde{\Psi}_f \right\rangle = \left(\Omega_{es}(f) + \lambda \Omega_{es,pnc}(f) \right) \left| \Phi_f \right\rangle_P$$

The indices i and f within parentheses denotes the state dependence of the wave-operator and λ is the perturbation parameter. Using the above expressions for mixed parity states $E1_{PNC}$ can be written as

$$E1_{PNC} = \frac{{}_P\!\left\langle \Phi_f \middle| \left(\Omega_{es}^\dagger(f) + \lambda \Omega_{es,pnc}^\dagger(f) \right) \vec{D} \left(\Omega_{es}(i) + \lambda \Omega_{es,pnc}(i) \right) \middle| \Phi_i \right\rangle_P}{\sqrt{\left\langle \tilde{\Psi}_f \middle| \tilde{\Psi}_f \right\rangle \left\langle \tilde{\Psi}_i \middle| \tilde{\Psi}_i \right\rangle}}$$

Terms that contribute to $E1_{PNC}$ are those which has one order of H_{pnc} and dipole each. In the above expression these are the terms linear in λ, retaining these terms give

$$E1_{PNC} = \frac{{}_P\!\left\langle \Phi_f \middle| \Omega_{es}^\dagger(f) \vec{D} \Omega_{es,pnc}(i) \middle| \Phi_i \right\rangle_P + {}_P\!\left\langle \Phi_f \middle| \Omega_{es,pnc}^\dagger(f) \vec{D} \Omega_{es}(i) \middle| \Phi_i \right\rangle_P}{\sqrt{\left\langle \tilde{\Psi}_f \middle| \tilde{\Psi}_f \right\rangle \left\langle \tilde{\Psi}_i \middle| \tilde{\Psi}_i \right\rangle}}.$$

Like in EDM the wave-operators here can be got order by order using the Bloch equation. The projection and resolvent operators can further be sub-divided into different parity

components. Considering model space for each of the states to be single reference, we can define the model space projection operators as

$$P_i = \left|\Phi_i\right\rangle_{P\,P}\left\langle\Phi_i\right| \quad \text{and} P_f = \left|\Phi_f\right\rangle_{P\,P}\left\langle\Phi_f\right|.$$

Similarly, define the corresponding complementary space projections operators as Q_i, and Q_f respectively. The complementary space can be same or different for the two wave-operators. Depending on the rank of H_{pnc}, the total angular momenta J_i of the initial and J_f of the final states respectively, the following situations can arise

1. When $J_i = J_f$, the spin-independent parity non-conserving and the residual cou-lomb interaction part being scalar operators cannot mix different angular momentum eigen-states. Hence the complementary space is the same for both the states.

2. With $J_i \neq J_f$, consider the spin-independent part in H_{pnc}, the change in the angular momentum in the transition amplitude is due to the dipole operator. Hence the two complementary spaces will be different for the two states.

3. With $J_i = J_f$, taking the spin-dependent component of H_{pnc} the complementary space will be common to both the states.

4. With $J_i \neq J_f$, taking the spin-dependent component of H_{pnc} the subspace of con-figurations with same parity as the unperturbed states will be different but for the opposite parity subspace it will be the same. This is because both the spin-dependent H_{pnc} component and dipole are rank one operators.

Once the complementary projection operators are known the corresponding resolvent oper-ators can be defined as R_i and R_f respectively. The Bloch equation for the two eigen-states can be written as

$$\left[\Omega(i), H_0\right]P_i = Q_i H' \Omega_{es}(i)P_i - \chi_{es}(i)P_i H' \Omega_{es}(i)P_i, \tag{3.24}$$

$$\left[\Omega(f), H_0\right]P_f = Q_f H' \Omega_{es}(f)P_f - \chi_{es}(f)P_f H' \Omega_{es}(f)P_f, \tag{3.25}$$

where $H' = V_{es} + H_{pnc}$, $\chi_{es}(i)$ and $\chi_{es}(f)$ are the correlation operators for the two states. Out of these the required terms are those which has V_{es} alone and those that has one order of H_{pnc}. The first order wave-operators for the two states can be written as

$$\Omega^{(1)}(\text{pnc}, i)P_i = \left(R_i H_{pnc} + R_i V_{es}\right)P_i, \text{ and } \Omega^{(1)}(\text{pnc}, f)P_f = \left(R_f H_{pnc} + R_f V_{es}\right)P_f.$$

Here the index 'pnc' has been introduced within parentheses to distinguish from the wave-operator used in the case of EDM computation. Similarly the second order wave-operator for the two states can be got using the Bloch equations:

$$\left[\Omega^{(2)}(i), H_0\right]P_i = Q_i\left(V_{es} + \lambda H_{pnc}\right)\Omega^{(1)}P_i - Q_i\Omega^{(1)}P_i\left(V_{es} + \lambda H_{pnc}\right)P_i.$$

$$\left[\Omega^{(2)}(f), H_0\right]P_f = Q_f\left(V_{es} + \lambda H_{pnc}\right)\Omega^{(1)}P_f - Q_f\Omega^{(1)}P_f\left(V_{es} + \lambda H_{pnc}\right)P_f.$$

From these equations using the resolvent operators the required second order wave-operators are:

$$\begin{aligned}
\Omega^{(2)}(\text{pnc}, i)P_i &= \left(R_i V_{es}R_i V_{es} - R_i(R_i V_{es}P_i)V_{es}\right)P_i + \lambda\left(R_i V_{es}R_i H_{pnc} + R_i H_{\text{PTV}} R_i V_{es}\right. \\
&\quad \left. - R_i(R_i H_{pnc}P_i)V_{es}\right)P_i = \left(\Omega^{(2)}_{es}(i) + \lambda\Omega^{(1)}_{pnc,es}(i)\right)P_i
\end{aligned} \tag{3.26}$$

and

$$\begin{aligned}
\Omega^{(2)}(\text{pnc}, f)P_f &= \left(R_f V_{es}R_f V_{es} - R_f(R_f V_{es}P_f)V_{es}\right)P_f + \lambda\left(R_f V_{es}R_f H_{pnc} + R_f H_{pnc}R_f V_{es}\right. \\
&\quad \left. - R_f(R_f H_{pnc}P_f)V_{es}\right)P_f = \left(\Omega^{(2)}_{es}(f) + \lambda\Omega^{(1)}_{pnc,es}(f)\right)P_f.
\end{aligned} \tag{3.27}$$

Higher order wave-operators can also be computed and sum to get the total wave-operators. This is the order by order computation of the wave-operator, the other form of computation is to compute the wave-operator in terms of iteration.

3.6   Size-Inconsistency with the Bloch Equation Based MBPT

Size-inconsistency in Bloch equation based perturbation theory is due to incomplete cancellation of unlinked terms. With Epstein-Nesbet partitioning the following are the cause of incomplete cancellation of unlinked terms

- Factorization theorem[11, 12] is not valid

- Incomplete configuration space

3.6.1 Factorization Theorem is not Valid

The energy corresponding to a CSF $\left|\Phi_i\right\rangle$ in EN-partitioning is

$$E_i = \left\langle \Phi_i \left| H_{\text{atom}} \right| \Phi_i \right\rangle.$$

Let $|\Phi_0\rangle$ be the model space configuration and ΔE denote the energy difference that contributes to the denominator, then for the doubly excited configuration $|\Phi_{ab}^{rs}\rangle$ the contribution to the energy denominator is

$$\Delta E_{ab}^{rs} = \left\langle \Phi_0 \left| H_{\text{atom}} \right| \Phi_0 \right\rangle - \left\langle \Phi_{ab}^{rs} \left| H_{\text{atom}} \right| \Phi_{ab}^{rs} \right\rangle.$$

Energy denominators satisfy the factorization theorem when they are additive. For the doubly excited configuration $|\Phi_{ab}^{rs}\rangle$ the energy denominator should satisfy

$$\Delta E_{ab}^{rs} = \Delta E_a^r + \Delta E_b^s = \Delta E_b^r + \Delta E_a^s.$$

In general let A and a_i denote sequence of core orbital identification indices and R and r_i denote the virtual orbital identification indices then the energy denominators should satisfy the relation

$$\Delta E_A^R = \sum_i \Delta E_{a_i}^{r_i}, \quad \text{where} \quad A = \prod_i a_i \text{ and } R = \prod_i r_i.$$

The above relation is satisfied by the mono-energetic Hamiltonians but energies in EN-partitioning is non mono-energetic as it include non-dynamic correlation energy and hence

$$\Delta E_A^R \neq \sum_i \Delta E_{a_i}^{r_i}.$$

As a result the factorization theorem is no longer satisfied and leads to incomplete cancellation of unlinked diagrams at each order of perturbation.

The EN partition amounts to inclusion of all hole-hole, hole-particle and particle-particle ladders in H_0 which are 'space-diagonal' in the sense that the orbital indices before and after scattering are the same.

3.6.2   Incomplete Configuration Space

The energies used in the EN-partitioning can be made to satisfy the factorization theorem by a suitable modification such that

$$\left\langle \Phi_0 \middle| \overline{H}^{EN} \middle| \Phi_0 \right\rangle - \left\langle \Phi_A^R \middle| \overline{H}^{EN} \middle| \Phi_A^R \right\rangle = \sum_i \Delta \overline{E}_{a_i}^{r_i}.$$

Where $\overline{H}^{EN}$ is the modified EN-partitioning scheme Hamiltonian. This is possible when $\overline{H}^{EN}$ is defined such that it does not include ladder diagrams connecting disconnected pieces. Consider the Bloch equation

$$\left[\Omega_{es}, \overline{H}_0 \right] P = Q \overline{H}_{es} \Omega_{es} P - \chi_{es} P \overline{H}_{es} \Omega_{es} P.$$

From the linked diagram theorem

$$\left[\Omega_{es}, \overline{H}_0 \right] P = Q \left(\overline{H}_{es} \Omega_{es} P - \chi_{es} P \overline{H}_{es} \Omega_{es} P \right)_{\text{linked}}$$

The term $Q\overline{H}_{es}\Omega_{es}P$ contains both connected and disconnected terms. Among the disconnected terms, there are some which have no disconnected closed parts. These are legitimate and should be retained and are included in $(Q\overline{H}_{es}\Omega_{es}P)_{\text{linked}}$. Terms with disconnected closed parts contribute to $(Q\overline{H}_{es}\Omega_{es}P)_{\text{unlinked}}$, these cancel the disconnected terms from $\chi_{es}P\overline{H}_{es}\Omega_{es}P$ where χ_{es} and $P\overline{H}_{es}\Omega_{es}P$ have no common label–the exclusion principal obeying(EPO) terms. The rest of $\chi_{es}P\overline{H}_{es}\Omega_{es}P$ are EPV type and remains uncancelled. That is

$$\chi_{es}\left(P\overline{H}_{es}\Omega_{es}P \right)_{\text{closed}} - \left(\chi_{es}PH_{es}\Omega_{es}P \right)^{\text{EPO}} = 0.$$

Now to have only the legitimate terms in a non-perturbative evaluation of Ω_{es} upto a given rank $n = 2$, say, we should analyze the structure of Bloch equation as follows

$$\begin{aligned}
\left[\Omega_{es}(1), H_0 \right] &= Q\overline{H}_{es}^1 P + Q\left(\overline{H}_{es}^1 \Omega_{es}(1) \right)^1 P + Q\left(\overline{H}_{es}^1 \Omega_{es}(2) \right)^1 P + Q\left(\overline{H}_{es}^2 \Omega_{es}(1) \right)^1 P \\
&\quad + Q\left(\overline{H}_{es}^2 \Omega_{es}(2) \right)^1 - \chi_{es}(1)\left(P\overline{H}_{es}^1 \Omega_{es}(1)P + P\overline{H}_{es}^2 \Omega_{es}(2) \right)^{\text{EPV}} \\
&\quad - \chi_{es}(1)\left(P\overline{H}_{es}^1 \Omega_{es}(1)P + \overline{H}_{es}^2 \Omega_{es}(2) \right)^{\text{EPO}}
\end{aligned}$$

Where $\overline{H}_{es}^1$ and $\overline{H}_{es}^2$ are the one-body and two-body terms in the residual coulomb interaction, $(AB)^n$ denote n-body terms and $\Omega_{es}(n)$ represents n-body wave-operator. The

third term in the above equation can generate a disconnected closed part. Since we don't distinguish the connected and disconnected pieces of $\Omega_{es}(2)$, we do not know which part of $\Omega_{es}(2)$ generates the disconnected closed part. However if we keep track of the EPO renormalization terms, this will be made to cancel.

To see this, note that $(\chi_{es}(n)(P\overline{H}_{es}^{i}\Omega_{es}(i))P)^{\text{EPO}}$ is an $(n+l)$-body operator and when $i=1$ it has two-body terms. If we retain this , this will cancel the disconnected closed part from the third term. The other EPO term is three-body, and should be deleted. Thus

$$\left[\Omega_{es}(1), H_0\right] = Q\left(\overline{H}_{es}\right)^1_c P + Q\left(\overline{H}_{es}^1\Omega_{es}(1)\right)^1_c P + Q\left(\overline{H}_{es}^1\Omega_{es}(2)\right)^1_c P + Q\left(\overline{H}_{es}^2\Omega_{es}(1)\right)^1_c P$$
$$+ Q\left(\overline{H}_{es}^2\Omega_{es}(2)\right)^1_c - \chi_{es}(1)\left(P\overline{H}_{es}^1\Omega_{es}(1)P + P\overline{H}_{es}^2\Omega_{es}(2)\right)^{\text{EPV}}$$
$$- \chi_{es}(1)\left(PH_{es}{}^1\Omega_{es}(1)P\right)^{\text{EPO}}.$$

By $(AB)_c$ we now mean that there are common labels between A and B hence connected.

Consider now Ω_{es}^2:

$$\left[\Omega_{es}(2), H_0\right] = Q\overline{H}_{es}^2 P + Q\left(\overline{H}_{es}^1\Omega_{es}(1)\right)^2_d P + Q\left(\overline{H}_{es}^1\Omega_{es}(2)\right)^2_c P + Q\left(\overline{H}_{es}^2\Omega_{es}(1)\right)^2_c P$$
$$+ Q\left(\overline{H}_{es}^2\Omega_{es}(2)\right)^2_c - \chi_{es}(2)\left(P\overline{H}_{es}^1\Omega_{es}(1)P + P\overline{H}_{es}^2\Omega_{es}(2)P\right)^{\text{EPV}}$$
$$- \chi_{es}(2)\left(PH_{es}{}^1\Omega_{es}(1)P + PH_{es}{}^2\Omega_{es}(2)\right)^{\text{EPO}}.$$

Now the last two terms generate three and four body terms of Ω_{es} and should be deleted. The rest are either connected or a legitimate disconnected term like the second term in the above equation. In general with a blind computation within a configuration space limited till n-tuply excited configurations the renormalization term has EPO part till $n+2$-body terms. Configurations space being limited to n-tuply excited configurations $Q\overline{H}_{es}\Omega_{es}$ does not contain terms that will cancel these terms. Though the factorization theorem is satisfied the incompleteness in the configurations space leads to incomplete cancellation of unlinked terms. The above equations for Ω_{es} with EPO terms deleted are the generalized CEPA equations. Thus the condition of configuration space being complete is more fundamental to curing the size-consistency.

3.7 Size Consistent Theory in Closed-Shell Systems

3.7.1 Size Consistency with Linked Diagram Theorem

The wave-operator can be made size-consistent if only the linked terms in the Bloch equation can be retained[3]. With this approach the unlinked terms are completely excluded and the incomplete cancellation of the unlinked terms can altogether be avoided. To maintain size consistency the Bloch equation should satisfy linked diagram theorem

$$\left[\Omega_{es}, H_0\right] P = Q\left(H_{es}\Omega_{es}P - \chi_{es}PH_{es}\Omega_{es}P\right)_{\text{linked}} = Q\left(H_{es}\Omega_{es}P - \chi_{es}W\right)_{\text{linked}}. \quad (3.28)$$

Redefine the wave-operator in terms of degrees of excitation. The wave-operator and correlation-operators for a system of N particles is

$$\Omega_{es} = I + \Omega_{es}(1) + \Omega_{es}(2) + \Omega_{es}(3) + \ldots = \sum_{m=0}^{N} \Omega_{es}(m) \text{ and } \chi_{es} = \sum_{m=1}^{N} \Omega_{es}(m).$$

Where in $\Omega_{es}(m)$ m denotes the degree of excitation. Considering only till double excitation the wave-operator and correlation operator assumes the form

$$\Omega_{es} = \sum_{m=0}^{2} \Omega_{es}(m) \text{ and } \chi_{es} = \sum_{m=1}^{2} \Omega_{es}(m)$$

Since no valence lines are involved in closed-shell systems the diagrammatic representation of the wave-operators are
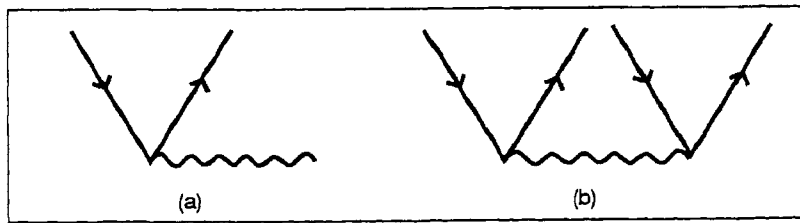
Figure 3.1: Diagrams for the wave-operators (a)$\Omega_{es}(1)$ and (b) $\Omega_{es}(2)$.

For W it is just a number and the diagrammatic representations of the residual coulomb interaction are
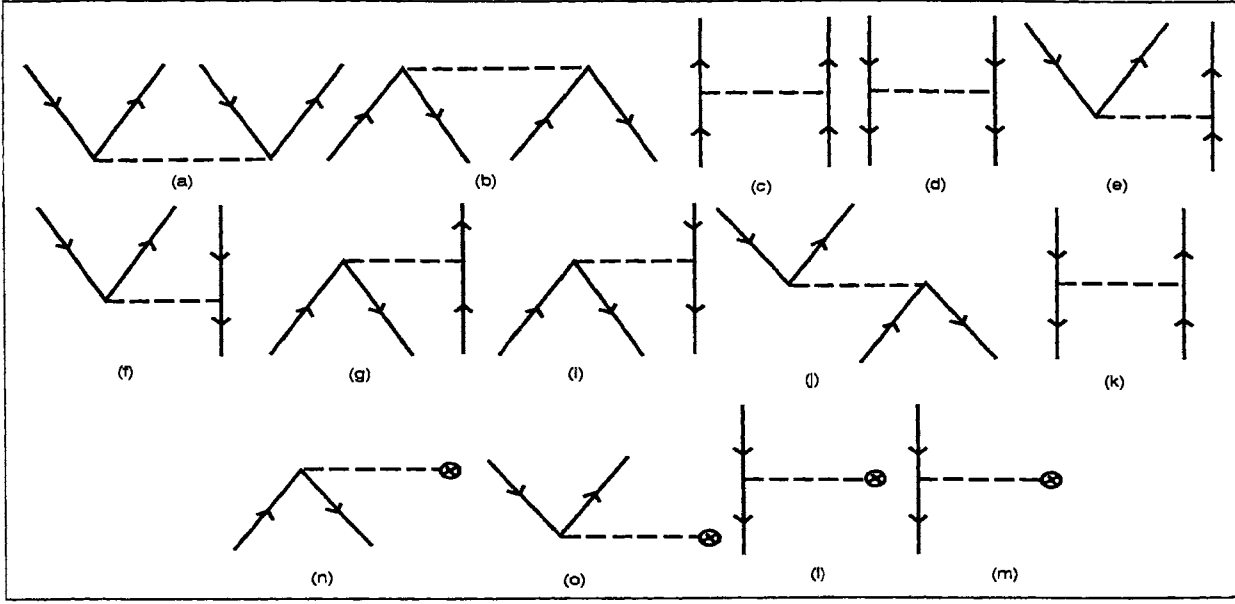
Figure 3.2: The diagrams for the residual Coulomb interaction H_{es}.

From (3.28), the equation for the singly-excited wave-operator is

$$\left[\Omega_{es}(1), H_0\right] P = Q\left(H_{es}P + H_{es}\Omega_{es}(1)P + H_{es}\Omega_{es}(2)P - \Omega_{es}(1)W\right)_{1,\text{linked}}.$$

Similarly, the equation for the doubly-excited wave-operator is

$$\left[\Omega_{es}(2), H_0\right] P = Q\left(H_{es} + H_{es}\Omega_{es}(1)P + H_{es}\Omega_{es}(2)P - \Omega_{es}(2)W\right)_{2,\text{linked}}.$$

Let $|\Phi_0\rangle$ be the reference configuration and $\{|\Phi_\alpha\rangle\}$ be the configuration space spanned by singly and doubly excited configurations. The wave-operators can then be expressed as

$$\Omega_{es}(1) = \sum_{ar} \left|\Phi_a^r\right\rangle\left\langle\Phi_0\right|x_a^r \ \text{ and } \ \Omega_{es}(2) = \sum_{abrs} \left|\Phi_{ab}^{rs}\right\rangle\left\langle\Phi_0\right|x_{ab}^{rs}.$$

Where x_a^r and x_{ab}^{rs} are the excitation amplitudes. Let $\{|\Phi_i\rangle\} = |\Phi_0\rangle + \{|\Phi_\alpha\rangle\}$, then H_{es} can also be expressed as

$$H_{es} = \sum_{i,j} \left\langle\Phi_j\left|H_{es}\right|\Phi_i\right\rangle\left|\Phi_j\right\rangle\left\langle\Phi_i\right|.$$

Using these definitions the equation for the one-body wave-operator can be written as

$$\begin{aligned}
\left[\Omega_{es}(1), H_0\right] P &= \sum_{ar} \left[\left\langle\Phi_a^r\left|H_{es}\right|\Phi_0\right\rangle + \sum_{a'r'}\left\langle\Phi_a^r\left|H_{es}\right|\Phi_{a'}^{r'}\right\rangle x_{a'}^{r'} + \sum_{a'b'r's'}\left\langle\Phi_a^r\left|H_{es}\right|\Phi_{a'b'}^{r's'}\right\rangle x_{a'b'}^{r's'}\right. \\
&\quad \left. - x_a^r W\right]\left|\Phi_a^r\right\rangle\left\langle\Phi_0\right| \tag{3.29}
\end{aligned}$$

Similarly, for the two-body wave-operator the equation is

$$\left[\Omega_{es}(2), H_0\right] P = \sum_{abrs}\left[\left\langle\Phi^{rs}_{ab}\middle|H_{es}\middle|\Phi_0\right\rangle + \sum_{a'r'}\left\langle\Phi^{rs}_{ab}\middle|H_{es}\middle|\Phi^{r'}_{a'}\right\rangle x^{r'}_{a'} + \sum_{a'b'r's'}\left\langle\Phi^{rs}_{ab}\middle|H_{es}\middle|\Phi^{r's'}_{a'b'}\right\rangle x^{r's'}_{a'b'}\right.$$
$$\left. - x^{rs}_{ab}W\right]\left|\Phi^{rs}_{ab}\right\rangle\left\langle\Phi_0\right| \tag{3.30}$$

In (3.29) all the terms except $x^r_a W$ are connected and hence linked. Similarly in (3.30) all the terms are linked except $x^{rs}_{ab}W$ and the second term

$$\left\langle\Phi^{rs}_{ab}\middle|H_{es}\middle|\Phi^{r'}_{a'}\right\rangle x^{r'}_{a'},$$

and has the following diagrammatic representations Out of these diagrams (a) is a dis-
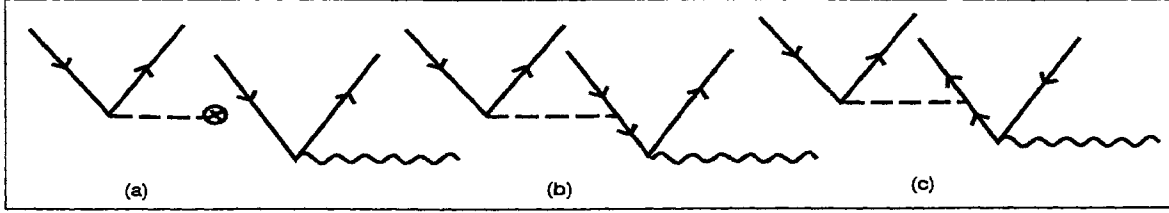
Figure 3.3: The diagrammatic representations of the term $\langle\Phi^{rs}_{ab}|H_{es}|\Phi^{r'}_{a'}\rangle x^{r'}_{a'}$

connected term but (b) and (c) are connected. The diagram (a) is still linked but if only connected terms are to be retained then it should be discarded. This can be done by retaining only those terms which does not have both a' and r' in $|\Phi^{rs}_{ab}\rangle$. With this modification all the terms in (3.30) are connected and hence linked. Thus in (3.29) the only term that has unlinked contribution is $x^r_a W$ and in (3.30) it is $x^{rs}_{ab}W$. The wave-operator is connected and size-consistent if these terms are excluded. The wave-operator equation then assumes the forms

$$\left[\Omega_{es}(1), H_0\right] P=\sum_{ar}\left[\left\langle\Phi^r_a\middle|H_{es}\middle|\Phi_0\right\rangle + \sum_{a'r'}\left\langle\Phi^r_a\middle|H_{es}\middle|\Phi^{r'}_{a'}\right\rangle x^{r'}_{a'} + \sum_{a'b'r's'}\left\langle\Phi^r_a\middle|H_{es}\middle|\Phi^{r's'}_{a'b'}\right\rangle x^{r's'}_{a'b'}\right]\left|\Phi^r_a\right\rangle\left\langle\Phi_0\right|$$
$$\tag{3.31}$$

Similarly, for the two-body wave-operator the equation is

$$\left[\Omega_{es}(2), H_0\right] P=\sum_{abrs}\left[\left\langle\Phi^{rs}_{ab}\middle|H_{es}\middle|\Phi_0\right\rangle + \sum_{a'r'}\left\langle\Phi^{rs}_{ab}\middle|H_{es}\middle|\Phi^{r'}_{a'}\right\rangle x^{r'}_{a'} + \sum_{a'b'r's'}\left\langle\Phi^{rs}_{ab}\middle|H_{es}\middle|\Phi^{r's'}_{a'b'}\right\rangle x^{r's'}_{a'b'}\right]\left|\Phi^{rs}_{ab}\right\rangle\left\langle\Phi_0\right|$$
$$\tag{3.32}$$

Applying the modifications to the second term in (3.32) all the terms are now connected and linked too. This is the form of the equations for CEPA-0. So far the perturbation Hamiltonian has been H_{es} alone. With the PT-reversal violating Hamiltonian H_{PTV} included the perturbation Hamiltonian is

$$H' = H_{es} + H_{PTV}.$$

The corresponding wave-operators are

$$\Omega(1) = \Omega_{es}(1) + \Omega_{PTV}(1) \text{ and } \Omega(2) = \Omega_{es}(2) + \Omega_{PTV}(2).$$

Wave-operators $\Omega_{es}(1)$ and $\Omega_{es}(2)$ are same as before but $\Omega_{PTV}(1)$ and $\Omega_{PTV}(2)$ are wave-operators that connect $\{|\Phi_i\rangle\}$ to $\{|\overline{\Phi}_i\rangle\}$, where $\{|\overline{\Phi}_i\rangle\}$ is the configuration space opposite in parity to $|\Phi_0\rangle$. Within the total configuration space $\Omega_{PTV}(1)$ and $\Omega_{PTV}(2)$ can be represented as

$$\Omega_{PTV}(1) = \sum_{ar} \left|\overline{\Phi}_a^r\right\rangle\left\langle\Phi_0\left|\overline{x}_a^r\right. \text{ and } \Omega_{PTV}(2) = \sum_{abrs} \left|\overline{\Phi}_{ab}^{rs}\right\rangle\left\langle\Phi_0\left|\overline{x}_{ab}^{rs}\right.\right.$$

The equations for $\Omega_{PTV}(1)$ is

$$\left[\Omega_{PTV}(1), H_0\right]P = \sum_{ar}\left[\left\langle\overline{\Phi}_a^r\left|H_{PTV}\right|\Phi_0\right\rangle + \sum_{a'r'}\left\langle\overline{\Phi}_a^r\left|H_{PTV}\right|\Phi_{a'}^{r'}\right\rangle x_{a'}^{r'} + \sum_{a'b'r's'}\left\langle\overline{\Phi}_a^r\left|H_{PTV}\right|\Phi_{a'b'}^{r's'}\right\rangle x_{a'b'}^{r's'}\right.$$
$$\left.+\sum_{ct}\left\langle\overline{\Phi}_a^r\left|H_{es}\right|\overline{\Phi}_c^t\right\rangle\overline{x}_c^t + \sum_{cdtu}\left\langle\overline{\Phi}_a^r\left|H_{es}\right|\overline{\Phi}_{cd}^{tu}\right\rangle\overline{x}_{cd}^{tu}\right]\left|\overline{\Phi}_a^r\right\rangle\left\langle\Phi_0\right| \qquad (3.33)$$

In expression (3.33) the condition that H_{PTV} should be treated to first order is taken care of by excluding terms of the form $\langle\Phi_i|H_{PTV}|\overline{\Phi}_j\rangle\overline{x}$. The equation for $\Omega_{PTV}(2)$ is

$$\left[\Omega_{PTV}(2), H_0\right]P = \sum_{abrs}\left[\sum_{a'b'r's'}\left\langle\overline{\Phi}_{ab}^{rs}\left|H_{PTV}\right|\Phi_{a'b'}^{r's'}\right\rangle x_{a'b'}^{r's'} + \sum_{ct}\left\langle\overline{\Phi}_{ab}^{rs}\left|H_{es}\right|\overline{\Phi}_c^t\right\rangle\overline{x}_c^t\right.$$
$$\left.+\sum_{cdtu}\left\langle\overline{\Phi}_{ab}^{rs}\left|H_{es}\right|\overline{\Phi}_{cd}^{tu}\right\rangle\overline{x}_{cd}^{tu}\right]\left|\overline{\Phi}_{ab}^{rs}\right\rangle\left\langle\Phi_0\right| \qquad \cdot \qquad (3.34)$$

The term $\langle\overline{\Phi}_{ab}^{rs}|H_{PTV}|\Phi_0\rangle$ does not contribute as H_{PTV} being a one-body interaction Hamiltonian it cannot produce double excitation. In addition the term $\sum_{a'r'}\langle\overline{\Phi}_{ab}^{rs}|H_{PTV}|\Phi_{a'}^{r'}\rangle x_{a'}^{r'}$ has been excluded as it is always disconnected. The second term in (3.34) can still give disconnected terms but they can be avoided by using the same remedy as applied to

$$\left\langle\Phi_{ab}^{rs}\left|H_{es}\right|\Phi_{a'}^{r'}\right\rangle x_{a'}^{r'}.$$

Hence all the terms are connected in the expression for $\Omega_{PTV}(1)$ and $\Omega_{PTV}(2)$.

3.7.2 Size Consistency with Connected Diagrams

The other way of separating the wave-operator is in terms of cluster operators. The cluster-operator T_n is defined as

$$T_n = \Big(\Omega(n)\Big)_{\text{conn}} \quad \text{and} \quad T = \sum_{n=1}^{N} T_n$$

The wave-operators are related to the cluster operators as

$$\Omega(n) = T_n + \sum_{p=1}^{p_{\max}} \sum_{i=1}^{i_{\max}} \frac{1}{i!j!} \Big\{ \Big(T_p\Big)^i \sum_{l=p+1}^{n-p} \Big(T_l\Big)^j \Big\}, \qquad (3.35)$$

where

$$i_{\max} = \text{integer}(n/p), \quad j_{\text{rem}} = \frac{(n - p \times i)}{l}, \quad p_{\max} = \begin{cases} p/2 & \text{if } p \text{ is even} \\ (p-1)/2 & \text{if } p \text{ is odd} \end{cases}$$

and

$$j = \begin{cases} j_{\text{rem}} & \text{if } j_{\text{rem}} \text{ is an integer} \\ -\infty & \text{if } j_{\text{rem}} \text{ is not an integer} \end{cases}$$

That is when j is not an integer the second term in (3.35) does not contribute to the wave-operator. The equation for the cluster-operator with the residual Coulomb interaction as the perturbation is

$$\Big[T_{\text{es}}, H_0\Big] P = \Big(Q H_{\text{es}} \Omega_{\text{es}} P - \chi_{\text{es}} W P\Big)_{\text{conn}}$$

Taking only the linear terms of single and double cluster-operators, the wave-operator is

$$\Omega_{\text{es}} = 1 + T_{\text{es}}(1) + T_{\text{es}}(2) \quad \text{and} \quad W = H_{\text{es}} T.$$

The wave-operator Ω_{es} has been approximated by the linear cluster terms for the following reasons:

- The correlation introduced by T_1^2 is very small compared to the contribution from T_2. By including the T_2 a major part of the electron-electron correlation effect is taken care of.

- Among the four-body cluster operators T_2^2 is the major contributor but in the present formalism this term can not be included as the CSF coupling is not in particle-hole form.

- Though T_1 does not contribute significantly in the electron-electron correlation it is important as H_{PTV} and the dipole operators are single-electron operators.

For closed-shell systems $\chi_{\text{es}}W$ is always unlinked and hence can be avoided from the cluster equation. The cluster-operator equation is

$$\left[T_{\text{es}}, H_0\right] P = \left(Q H_{\text{es}} \Omega_{\text{es}} P\right)_{\text{conn}}$$

This cluster equation does not include the EPV diagrams, the linked EPV diagrams are to be avoided but unlinked EPV terms are to be retained. With suitable transformations the unlinked EPV terms can be converted into connected terms[12], thus the cluster-operator equation is

$$\left[T_{\text{es}}, H_0\right] P = \left(Q H_{\text{es}} \Omega_{\text{es}} P\right)_{\text{linked}}^{\text{EPV}} + \left(Q H_{\text{es}} \Omega_{\text{es}} P\right)_{\text{conn}}^{\text{EPO}}$$

Where the first term is EPV and second term is non-EPV. By suitable rearrangement

$$\left(Q H_{\text{es}} \Omega_{\text{es}} P\right)_{\text{linked}}^{\text{EPV}} = -\left(Q \chi_{\text{es}} W P\right)^{\text{EPV}}$$

The cluster-operator equations now takes the form

$$\left[T_{\text{es}}, H_0\right] P = \left(Q H_{\text{es}} \Omega_{\text{es}} P\right)_{\text{conn}}^{\text{EPO}} - \left(Q \chi_{\text{es}} W P\right)^{\text{EPV}}$$

With these definitions the single and double cluster-operator equations with residual coulomb interaction as the perturbation are

$$\left[T_{\text{es}}(1), H_0\right] P = \sum_{ar} \left[\left\langle \Phi_a^r \middle| H_{\text{es}} \middle| \Phi_0 \right\rangle + \sum_{a'r'} \left\langle \Phi_a^r \middle| H_{\text{es}} \middle| \Phi_{a'}^{r'} \right\rangle \mathcal{T}_{a'}^{r'} + \sum_{a'b'r's'} \left\langle \Phi_a^r \middle| H_{\text{es}} \middle| \Phi_{a'b'}^{r's'} \right\rangle \mathcal{T}_{a'b'}^{r's'} \right.$$
$$\left. - \left(\mathcal{T}_a^r W\right)^{\text{EPV}} \right] \middle| \Phi_a^r \right\rangle \left\langle \Phi_0 \middle|. \tag{3.36}$$

The cluster amplitudes are denoted using $\mathcal{T}$ to distinguish from the single-particle cluster amplitudes represented by t. Here the computation is at the CSF level and $\mathcal{T}_a^r$ means the cluster amplitude of the cluster excitation operator that excites the reference CSF state $|\Phi_0\rangle$ to the CSF $|\Phi_a^r\rangle$. The same definition can be extended to the double excitation cluster amplitudes too.

$$\left[T_{\text{es}}(2), H_0\right] P = \sum_{abrs} \left[\left\langle \Phi_{ab}^{rs} \middle| H_{\text{es}} \middle| \Phi_0 \right\rangle + \sum_{a'r'} \left\langle \Phi_{ab}^{rs} \middle| H_{\text{es}} \middle| \Phi_{a'}^{r'} \right\rangle \mathcal{T}_{a'}^{r'} + \sum_{a'b'r's'} \left\langle \Phi_{ab}^{rs} \middle| H_{\text{es}} \middle| \Phi_{a'b'}^{r's'} \right\rangle \mathcal{T}_{a'b'}^{r's'} \right.$$
$$\left. - \left(\mathcal{T}_{ab}^{rs} W\right)^{\text{EPV}} \right] \middle| \Phi_{ab}^{rs} \right\rangle \left\langle \Phi_0 \middle|. \tag{3.37}$$

Similarly, the PT-violating cluster-operators T_{PTV} can also be evaluated using the equations

$$\left[T_{\mathrm{PTV}}(1), H_0\right]P = \sum_{ar}\left[\left\langle\overline{\Phi}_a^r\middle|H_{\mathrm{PTV}}\middle|\Phi_0\right\rangle + \sum_{a'r'}\left\langle\overline{\Phi}_a^r\middle|H_{\mathrm{PTV}}\middle|\Phi_{a'}^{r'}\right\rangle\mathcal{T}_{a'}^{r'} + \sum_{a'b'r's'}\left\langle\overline{\Phi}_a^r\middle|H_{\mathrm{PTV}}\middle|\Phi_{a'b'}^{r's'}\right\rangle\mathcal{T}_{a'b'}^{r's'}\right.$$
$$\left. + \sum_{ct}\left\langle\overline{\Phi}_a^r\middle|H_{\mathrm{es}}\middle|\overline{\Phi}_c^t\right\rangle\overline{\mathcal{T}}_c^t + \sum_{cdtu}\left\langle\overline{\Phi}_a^r\middle|H_{\mathrm{es}}\middle|\overline{\Phi}_{cd}^{tu}\right\rangle\overline{\mathcal{T}}_{cd}^{tu} - \left(\overline{t}_a^r W\right)^{\mathrm{EPV}}\right]\middle|\overline{\Phi}_a^r\right\rangle\left\langle\Phi_0\middle|(3.38)$$

and

$$\left[T_{\mathrm{PTV}}(2), H_0\right]P = \sum_{abrs}\left[\sum_{a'b'r's'}\left\langle\overline{\Phi}_{ab}^{rs}\middle|H_{\mathrm{PTV}}\middle|\Phi_{a'b'}^{r's'}\right\rangle\mathcal{T}_{a'b'}^{r's'} + \sum_{ct}\left\langle\overline{\Phi}_{ab}^{rs}\middle|H_{\mathrm{es}}\middle|\overline{\Phi}_c^t\right\rangle\overline{t}_c^t\right.$$
$$\left. + \sum_{cdtu}\left\langle\overline{\Phi}_{ab}^{rs}\middle|H_{\mathrm{es}}\middle|\overline{\Phi}_{cd}^{tu}\right\rangle\overline{\mathcal{T}}_{cd}^{tu} - \left(\overline{\mathcal{T}}_{ab}^{rs}W\right)^{\mathrm{EPV}}\right]\middle|\overline{\Phi}_{ab}^{rs}\right\rangle\left\langle\Phi_0\middle| \qquad (3.39)$$

Using these cluster-operators

$$\Omega_{\mathrm{es,edm}} = \Omega_{\mathrm{PTV}}(1) + \Omega_{\mathrm{PTV}}(2).$$

The required value of the atomic EDM $\vec{D}_a$ can be computed using the operators as

$$\vec{D}_a = 2\left\langle\Phi_0\middle|\Omega_{\mathrm{es}}^\dagger\vec{D}\Omega_{\mathrm{PTV}}\middle|\Phi_o\right\rangle.$$

The equations describing the cluster equations are similar to the equation CEPA-2 equations[13. 14].

References

[1] Ann-Marie Martensson-Pendrill, *Methods in computational Chemistry, Volume 5: Atomic and molecular properties*, Edited by Stephen Wilson (Plenum Press, New York,1992).

[2] Ingvar Lindgren and John Morrison, *Atomic Many-Body Theory*(Springer, New York, 1982).

[3] J. Goldstone, Proc. Roy. Soc.(London) **A239**, 267(1957).

[4] Takashi Kagawa, Yoshie Honda and Shuji Kiyokawa, Phys. Rev. A **44**, 7092(1991).

[5] Hugh P. Kelly, Phys. Rev. **131**,684(1963).

[6] Hugh P. Kelly, Phys. Rev. **132**,2091(1963), Hugh P. Kelly, Phys. Rev. **134**,A1450(1964).

[7] Hugh P. Kelly, Phys. Rev., **136**,B896(1964).

[8] C. Bloch, Nucl. Phys. **6**, 329(1958).

[9] Paul. S. Epstein, Phys. Rev. **28**, 695(1926).

[10] R. K. Nesbet, Pro. Roy. Soc. London, **A250** 312(1955).

[11] N. M. Hugenholtz, Physica **23**, 481(1957).

[12] L. M. Frantz and R. L. Mills **15**, 16(1960).

[13] W. Kutzelnigg, Methods in Electronic Structure Theory, Ed by H. F. Schaefer (Plenum, New York, 1977).

[14] R. Ahlrichs, Comp. Phys. Comm. **17**, 31(1979).

s

Chapter 4

Computation of Electric Dipole Moment with Different Many-Body Methods and Comparison

4.1 The Orbitals and the Configurations

4.1.1 Bound and Continuum Orbitals

The orbitals used in the CSF based perturbation theory can be of any form but it should satisfy the following properties:

- completeness

- orthonormality.

These conditions are satisfied by a set of orbitals generated using a single particle Hamiltonian like the Hartree-Fock potential. Similarly, a set of orbitals generated using the [1] V^{N-1} potential satisfies these conditions too. We have used V^{N-1} orbitals in our calculation. The completeness criterion of the orbital space is determined by the convergence of the property of interest and the ground state energy E_0.

For atomic Yb the occupied-orbitals are generated first with the ground state configuration $|6s^2\rangle$. The virtual orbital $|\psi_i\rangle$ is generated using the configuration $|6s\psi_i\rangle$ where the orbitals till $6s$ are frozen. The total angular momentum of the configuration is chosen as the smaller of the two got after coupling the angular momentum of $|6s\rangle$ and $|\psi_i\rangle$. The

disadvantage of using the V^{N-1} potential is that to make the orbitals complete the positive continuum spectrum must be included. Though the continuum contribution to EDM is not very significant, the quadrature of the matrix elements involving continuum orbitals always incur errors. Energies of the occupied and the bound virtuals are tabulated in Table 4.1 according to symmetry.

<div align="center">Table 4.1</div>

Orb.	Energy	Orb.	Energy	Orb.	Energy
1s	−2267.650 00	11p*	−0.0099 12	5d	−0.0788 17
2s	−388.8923 64	2p	−331.4874 09	6d	−0.0421 41
3s	−89.7094 89	3p	−73.0939 62	7d	−0.0254 43
4s	−18.6724 43	4p	−13.3735 81	8d	−0.0169 63
5s	−2.4395 07	5p	−1.1827 91	9d	−0.0121 03
6s	−0.1965 16	6p	−0.0971 30	10d	−0.0090 66
7s	−0.0781 08	7p	−0.0468 76	4f*	−0.5389 89
8s	−0.0388 68	8p	−0.0293 26	5f*	−0.0201 77
9s	−0.0236 02	9p	−0.0179 81	6f*	−0.0140 08
10s	−0.0158 87	10p	−0.0126 99	7f*	−0.0102 85
11s	−0.0114 30	11p	−0.0094 45	8f*	−0.0078 69
12s	−0.0086 19	3d*	−59.1919 29	9f*	−0.0062 14
2p*	−370.0552 26	4d*	−7.7779 63	10f*	−0.0050 30
3p*	−81.4222 13	5d*	−0.1000 42	4f	−0.4801 86
4p*	−15.2751 03	6d*	−0.0444 43	5f	−0.0200 43
5p*	−1.4191 60	7d*	−0.0262 77	6f	−0.0139 19
6p*	−0.1244 56	8d*	−0.0173 73	7f	−0.0102 25
7p*	−0.0537 68	9d*	−0.0123 38	8f	−0.0078 27
8p*	−0.0292 38	10d*	−0.0092 14	9f	−0.0061 84
9p*	−0.0188 94	3d	−57.3906 05	10f	−0.0050 08
10p*	−0.0134 43	4d	−7.4220 74		

In order to check on the completeness of the bound virtual orbitals E_0 is computed with the addition of each orbital of different symmetries. For each symmetry the orbital

Table 4.2: CI-energy for each of the symmetry with increasing CSFs

Sl. No.	CSFs	Energy	Change in Energy
1	$\lvert 6s^2\rangle + \lvert 7s^2\rangle + \lvert 6s7s\rangle$	$-14067.6717\ 58$	$-0.0002\ 80$
2	$+\lvert 8s^2\rangle + \lvert(6\text{-}7)s8s\rangle$	$-14067.6718\ 83$	$-0.0001\ 25$
3	$+\lvert 9s^2\rangle + \lvert(6\text{-}8)s9s\rangle$	$-14067.6719\ 40$	$-0.0000\ 57$
4	$+\lvert 10s^2\rangle + \lvert(6\text{-}9)s10s\rangle$	$-14067.6719\ 70$	$-0.0000\ 30$
5	$+\lvert 11s^2\rangle + \lvert(6\text{-}10)s11s\rangle$	$-14067.6719\ 88$	$-0.0000\ 18$
6	$+\lvert 12s^2\rangle + \lvert(6\text{-}11)s12s\rangle$	$-14067.6720\ 00$	$-0.0000\ 02$
7	$\lvert 6s^2\rangle + \lvert 6p*^2\rangle$	$-14067.6786\ 17$	$-0.0071\ 39$
8	$+\lvert 7p*^2\rangle + \lvert 6p*\ 7p*\rangle$	$-14067.6798\ 38$	$-0.0012\ 21$
9	$+\lvert 8p*^2\rangle + \lvert(6\text{-}7)p*\ 8p*\rangle$	$-14067.6800\ 97$	$-0.0002\ 59$
10	$+\lvert 9p*^2\rangle + \lvert(6\text{-}8)p*\ 9p*\rangle$	$-14067.6802\ 24$	$-0.0001\ 27$
11	$+\lvert 10p*^2\rangle + \lvert(6\text{-}9)p*\ 10p*\rangle$	$-14067.6803\ 23$	$-0.0000\ 99$
12	$+\lvert 11p*^2\rangle + \lvert(6\text{-}10)p*\ 11p*\rangle$	$-14067.6803\ 80$	$-0.0000\ 57$
13	$\lvert 6s^2\rangle + \lvert 6p^2\rangle$	$-14067.6774\ 75$	$-0.0059\ 97$
14	$+\lvert 7p^2\rangle + \lvert 6p7p\rangle$	$-14067.6796\ 90$	$-0.0022\ 15$
15	$+\lvert 8p^2\rangle + \lvert(6\text{-}7)p8p\rangle$	$-14067.6811\ 61$	$-0.0014\ 71$
16	$+\lvert 9p^2\rangle + \lvert(6\text{-}8)p9p\rangle$	$-14067.6814\ 10$	$-0.0002\ 49$
17	$+\lvert 10p^2\rangle + \lvert(6\text{-}9)p10p\rangle$	$-14067.6815\ 75$	$-0.0001\ 65$
18	$+\lvert 11p^2\rangle + \lvert(6\text{-}10)p11p\rangle$	$-14067.6816\ 84$	$-0.0001\ 09$
19	$\lvert 6s^2\rangle + \lvert 5d*^2\rangle$	$-14067.6740\ 44$	$-0.0025\ 66$
20	$+\lvert 6d*^2\rangle + \lvert 5d*\ 6d*\rangle$	$-14067.6742\ 00$	$-0.0001\ 56$
21	$+\lvert 7d*^2\rangle + \lvert(5\text{-}6)d*\ 7d*\rangle$	$-14067.6742\ 35$	$-0.0000\ 35$
22	$+\lvert 8d*^2\rangle + \lvert(5\text{-}7)d*\ 8d*\rangle$	$-14067.6742\ 48$	$-0.0000\ 13$
23	$+\lvert 9d*^2\rangle + \lvert(5\text{-}8)d*\ 9d*\rangle$	$-14067.6742\ 55$	$-0.0000\ 07$
24	$+\lvert 10d*^2\rangle + \lvert(5\text{-}9)d*\ 10d*\rangle$	$-14067.6742\ 58$	$-0.0000\ 03$

Sl. No.	CSFs	Energy	Change in Energy
25	$\lvert 6s^2\rangle + \lvert 5d^2\rangle$	$-14067.6744\ 68$	$-0.0029\ 90$
26	$+\lvert 6d^2\rangle + \lvert 5d6d\rangle$	$-14067.6750\ 81$	$-0.0006\ 13$
27	$+\lvert 7d^2\rangle + \lvert (5\text{-}6)d7d\rangle$	$-14067.6752\ 29$	$-0.0001\ 48$
28	$+\lvert 8d^2\rangle + \lvert (5\text{-}7)d8d\rangle$	$-14067.6752\ 86$	$-0.0000\ 57$
29	$+\lvert 9d^2\rangle + \lvert (5\text{-}8)d9d\rangle$	$-14067.6753\ 14$	$-0.0000\ 28$
30	$+\lvert 10d^2\rangle + \lvert (5\text{-}9)d10d\rangle$	$-14067.6753\ 30$	$-0.0000\ 16$

space is increased by one at time and E_0 is computed using CI. The CSF space for CI is the ground state CSF $\lvert \Phi_0\rangle$ and the set of CSFs which has same angular momentum and parity as $\lvert \Phi_0\rangle$ generated using the virtual orbitals of the symmetry. Completeness of the virtual orbital space is assumed when E_0 converges to the fourth place of decimal. Ground state energy for each of the symmetry are given in the Table 4.2. In the Table 4.2 the change in energy is the difference between E_0 of the present set of CSFs and the earlier set. For each symmetry the starting comparison is the ground state CSF energy. Table shows that the convergence pattern is different for each symmetry. Compared to $7s$ the inclusion of $6p*$ orbital introduces a larger change in E_0 and is a result of $6p*$ being closer in energy to $6s$ than $7s$. But the change in E_0 with the inclusion of $7p*$ is much smaller than with the inclusion of $7p$. Since the energy of $7p$ is higher than $7p*$ the energy separation from $6s$ cannot explain this. This is due to the configuration mixing between those other than $\lvert \Phi_0\rangle$. Energy values for the $f*$ and f are not included as they converge with a single virtual orbital. For the computation six bound virtual orbitals for each symmetry is taken, the orbital space $(1\text{-}12)s$, $(2\text{-}11)p*$, $(2\text{-}11)p$, $(3\text{-}10)d*$, $(3\text{-}10)d$, $(4\text{-}10)f*$ and $(4\text{-}10)f$.

In the continuum orbital space the number of points used in the Gauss-Laguerre quadrature decides the number of orbitals to be included [2, 3, 4]. The continuum orbitals are identified by the symmetry and the linear momentum k, where $0 \le k \le \infty$. They are assigned negative principal quantum numbers to distinguish from the bound orbitals and are generated by using the energy $\epsilon_k = k^2/2$. To include the complete continuum spectrum the contribution from the continuum orbitals has to be integrated over the whole

spectrum. Consider the lowest order contribution to the atomic EDM with the continuum orbitals as the intermediate orbital

$$(\text{EDM})_{\text{cntm}} = \int_0^\infty dk \langle \psi_{6s} | \vec{D} | \psi_{P_-}(k) \rangle \langle \psi_{P_-}(k) | H_{\text{PTV}} | \psi_{6s} \rangle \left(\Delta E(k) \right)^{-1} = \int_0^\infty dk f(k),$$

where $\Delta E(k) = (\epsilon_{6s} - \epsilon_{P_-}(k))$ and $f(k) = \langle \psi_{6s} | \vec{D} | \psi_{P_-}(k) \rangle \langle \psi_{P_-}(k) | H_{\text{PTV}} | \psi_{6s} \rangle (\Delta E(k))^{-1}$.

Quadrature within the continuum spectrum can be simplified by discretizing it using the Gauss-Laguerre quadrature. This reduces the integration over the entire continuum spectrum to a sum over the roots of the Laguerre polynomials. If n is the number of roots used in the Gauss-Laguerre quadrature and the k_i the ith Laguerre root the above integration reduces to

$$(\text{EDM})_{\text{cntm}} = \sum_{i=1}^{n} w_i e^{-k_i} f(k_i).$$

With this form of quadrature the continuum orbitals are required only for energies corresponding to the roots of the Laguerre polynomials. For convenience the roots are normalized to 20 such that the new roots are $k_i' = (20 \times k_i)/k_n$ and the corresponding energies are given by

$$\epsilon_{k_i} = \frac{1}{2} \left(\frac{20 \times k_i}{k_n} \right)^2.$$

Using the normalized roots the integration is

$$(\text{EDM})_{\text{cntm}} = \left(\frac{20}{k_n} \right) \sum_{i=1}^{n} w_i e^{k_i'} f(k_i'). \tag{4.1}$$

This is the required integration for the continuum spectrum [5]. The same expression can also be used for CSFs by reducing the matrix elements to the orbital level.

4.1.2 The Configuration Space Considered

The configuration space is spanned by the CSFs constructed from the V^{N-1} orbitals. The configurations are generated by single or double excitations from the occupied orbitals to the bound and the continuum virtual orbitals in all possible ways such that it gives the required final angular momentum. For the single reference MBPT the reference CSF of Yb is $|6s^2\rangle$ and from now on it will be referred as $|\Phi_0\rangle$. Hence the occupied orbitals are $(1-6)s,(2-5)p*, (2-5)p,(3-4)d*, (3-4)d,4f*$ and $4f$ respectively. The configuration space

generated is not a complete active space but complete for the single and double excitations from the most important outer occupied orbitals within the converged orbital orbital space. The occupied-orbital shells of the configurations that has been considered are

single excitation: $|4f*^6\,4f^86s\rangle$, $|4f*^5\,6s^2\rangle$ $|4f^76s^2\rangle$, $|5p*^1\,6s^2\rangle$ $|5p^36s^2\rangle$ and $|5s^16s^2\rangle$

double excitation: $|4f*^64f^8\rangle$, $|4f*^56s\rangle$ $|4f^76s\rangle$, $|4f*^46s^2\rangle$, $|4f^66s^2\rangle$, $|4f*^54f^76s^2\rangle$ $|5p*^16s\rangle$, $|5p^36s\rangle$, $|5p*^14f^56s^2\rangle$, $|5p^34f*^56s^2\rangle$, $|5p*^34f^56s^2\rangle$, $|5p^34f^56s^2\rangle$, $|5s^16s\rangle$, $|5s^14f*^5\,6s^2\rangle$, $|5s^14f^76s^2\rangle$, $|5s^15p*^1\,6s^2\rangle$ and $|5s^15p^36s^2\rangle$.

The remaining electrons are arranged in the virtual orbitals in all possible ways. Of all the CSFs the even parity with CSF with $J=0$ and odd parity CSFs with $J=1$ are selected. Table4.3 gives the number of even and odd parity configurations generated from these in non-relativistic notation. Though not included in the table, CSFs with excitations from $5s$ are also included in the configuration space.

Table 4.3: The number of the CSFs with different occupied configurations.

Sl.no	Occupied part	Configurations		Sl.no	Occupied part	Configurations	
		Even	Odd			Even	Odd
1	$|6s\rangle$	6	12	2	$|4f^{14}\rangle$	147	287
3	$|4f^{13}6s^2\rangle$	12	18	4	$|4f^{13}6s^1\rangle$	1224	3618
5	$|4f^{12}6s^2\rangle$	3045	7739	6	$|5p^54f^{14}6s^2\rangle$	12	30
7	$|5p^54f^{14}6s^1\rangle$	1044	1668	8	$|5p^54f^{13}6s^2\rangle$	3604	2394

The total number of odd and even parity CSFs with bound virtual orbitals are 9930 and 17087 respectively. The modulus of the EN-partitioned energies of the CSFs-the diagonal Hamiltonian matrix elements-are as shown in the histograms below The two histograms are plotted such the the lowest $|E|$ is shifted to zero and the the range between the lowest and the highest are divided into ten units. The zero on $|E|$ axis are 14064.9531 and 14065.0068 hartrees for the even and odd parity CSFs respectively. Similarly, the highest $|E|$ are 14067.6720 and 14067.5996 hartrees respectively. From the histogram the number of configurations with low and high energies are less as the number of CSFs that can be constructed with the basis set considered are less where as the number of the configurations that can give the intermediate energy are large. This has the advantage
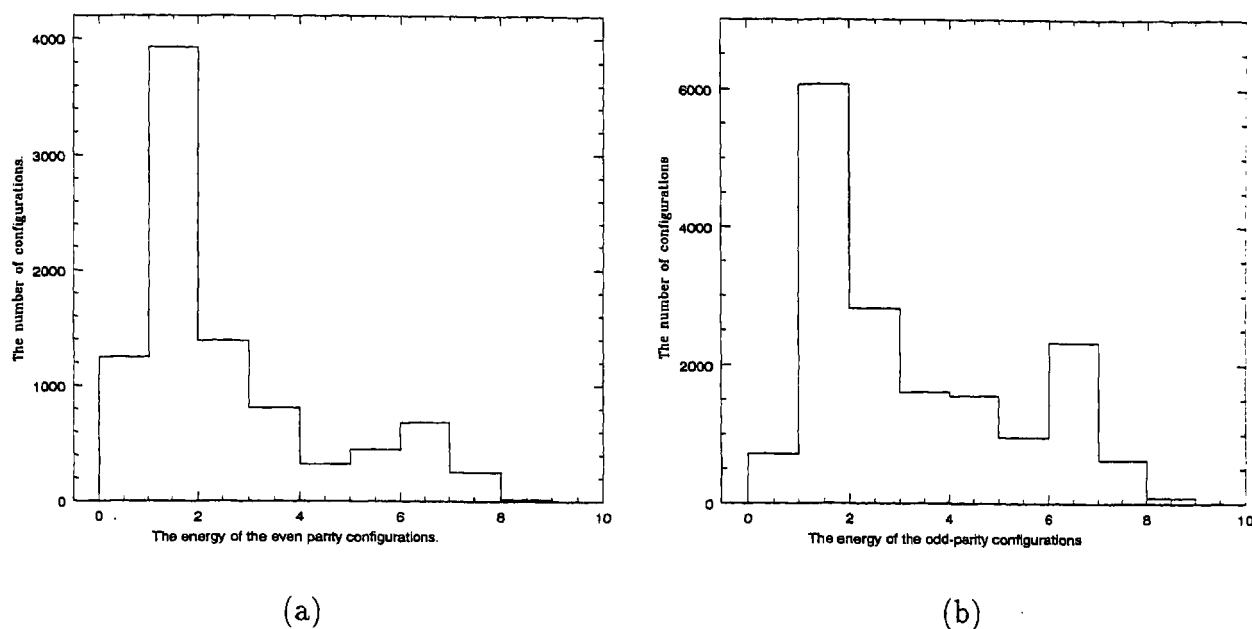
Figure 4.1: Histogram of $|E|$ for the even parity CSFs.

that the perturbation series converges fast as only a few of the configurations are quite close to $|\Phi_0\rangle$ and the energy separation with the rest of the CSFs is quite large.

Number of odd parity CSFs in the intermediate energy is more than the even parity as the odd parity configuration space can have many possible intermediate couplings to give $J = 1$, to limit the number of CSFs within the memory limitations a filtering has been done. In the filtering process double excitations beyond the converged orbitals are not included for the d and f symmetries. Another constraint on the choice of configurations is: there shouldn't be more than four open shells in the non-relativistic notation and eight in the relativistic form, choosing only singly and doubly excited configurations satisfies this condition for a closed-shell atom like Yb. This constraint is due to the angular co-efficient computation program.

Continuum orbitals when used in the framework of single particle formulations are numerically more appropriate as the error accumulation is less severe. In the CSF approach the error accumulation becomes large as the computation of CSF energies requires integrals with some of the highly contracted inner occupied orbitals. These integrals can be avoided altogether in the single particle approach. The CSF energies of the configurations with

continuum spin orbitals are given in Table4.4. In Table4.4 the continuum orbitals are

Table 4.4: Energy of the CSF $|6s\psi\rangle$ where ψ is a continuum orbital and ϵ_k is its energy.

Sl. No.	Orbital	ϵ_k	ΔE_s	CSF	CSF Energy	ΔE_c
1	$-1s$	0.0019 46	0.1984 62	$|6s-1s\rangle$	$-14067.3111\ 21$	0.3603 57
2	$-2s$	0.0543 83	0.2508 99	$|6s-2s\rangle$	$-14065.8681\ 66$	1.8033 12
3	$-3s$	0.3324 73	0.5289 89	$|6s-3s\rangle$	$-14062.9640\ 38$	4.7074 40
4	$-4s$	1.1668 80	1.3633 96	$|6s-4s\rangle$	$-14058.7320\ 33$	8.9394 45
5	$-5s$	3.0737 78	3.2702 94	$|6s-5s\rangle$	$-14053.1998\ 19$	14.4716 59
6	$-6s$	6.8075 28	7.0040 44	$|6s-6s\rangle$	$-14046.0824\ 58$	21.5890 20
7	$-7s$	13.4515 33	13.6480 49	$|6s-7s\rangle$	$-14037.3452\ 57$	30.3262 21
8	$-8s$	24.5806 82	24.7771 97	$|6s-8s\rangle$	$-14026.6947\ 39$	40.9767 39
9	$-9s$	42.5746 12	42.7711 28	$|6s-9s\rangle$	$-14013.6933\ 15$	53.9781 63
10	$-10s$	71.3005 65	71.4970 81	$|6s-10s\rangle$	$-13997.6760\ 78$	69.9954 00

distinguished from the bound by the negative principal quantum numbers. Though twelve point Gauss-Laguerre quadrature has been chosen, only the first ten configurations of the form $|6s-ns\rangle$ have been considered in the table.

The quantities ΔE_c and ΔE_s are defined as

$$\Delta E_c = \left\langle 4f^{14}6s\psi \middle| H_{\text{atom}} \middle| 4f^{14}6s\psi \right\rangle - \left\langle 4f^{14}6s^2 \middle| H_{\text{atom}} \middle| 4f^{14}6s^2 \right\rangle$$

and

$$\Delta E_s = \left\langle 4f^{14}6s\psi \middle| h_{\text{HF}} \middle| 4f^{14}6s\psi \right\rangle - \left\langle 4f^{14}6s^2 \middle| h_{\text{HF}} \middle| 4f^{14}6s^2 \right\rangle = \epsilon_\psi - \epsilon_{6s}$$

A non-single particle Hamiltonian like EN-partitioning includes a part of the static correlation and hence give configuration energy lower than the single particle Hamiltonian energy. As the static correlation is included in both configurations and is stronger in the ground state configuration, ΔE_c should be larger than the single particle value ΔE_s. Consider the configuration $|6s7s\rangle$, with EN-partitioning its energy is $-14067.5341\ 25$ and ΔE_c is 0.1373 57 hartrees respectively. The single particle energy difference between $7s$ and $6s$ orbitals is 0.1184 08 hartrees and this is the value of ΔE_s for $|6s7s\rangle$. The difference between ΔE_c and ΔE_s can be accounted to different strengths of static correlation in $|\Phi_0\rangle$

and $|6s7s\rangle$. Where as with the continuum orbitals the difference can be due to numerical error accumulation too.

Energies of Yb^+ and Yb^{2+} computed using the V^{N-1} orbitals are $-14067.4749\ 62$ and $-14067.0646\ 69$ hartrees respectively, the corresponding configurations are $|5p^64f^{14}6s\rangle$ and $|5p^64f^{14}\rangle$ respectively. Taking the difference with the energy of $|\Phi_0\rangle$ gives the first ionization potential as $0.1965\ 16$ hartrees and the double ionization potential as $0.6068\ 09$ hartrees. Consider the first two continuum orbitals, their energies are lower than double particle excitation energy of $6s$ shell. Which implies that the energy of $|6s - 1s\rangle$ and $s|6s - 2s\rangle$ should be between that of Yb^+ and Yb^{2+}, this is so for the configuration with the first but not for the second one. This could be due to decrease in the strength of the correlation with higher energies on the other hand as the energy of the continuum orbitals increase they get more contracted towards the core and enhance the error accumulation in quadratures involving the continuum orbitals.

4.2 The Matrix elements in EN-Partitioning

4.2.1 The Residual Coulomb Interaction

The energy E_i of a CSF $|\Phi_i\rangle$ in the EN-partitioning can be written in terms of orbitals as

$$E_i = \left\langle \Phi_i \middle| H_{\text{atom}} \middle| \Phi_i \right\rangle = \sum_i A(i,i)\left\langle \psi_i \middle| t \middle| \psi_i \right\rangle + \sum_{i>j} B(ij,ij)\left\langle \psi_i\psi_j \middle| \left(1 - P_{12}\right)\frac{1}{r_{12}} \middle| \psi_i\psi_j \right\rangle.$$

Where P_{12} is the exchange permutation operator, $A(i,i)$ and $B(ij,ij)$ are the angular factors required in reducing the CSF matrix elements to orbital level. The angular factor for the exchange part is $B(ij,ji)$ and $B(ij,ij) \neq B(ij,ji)$. Similarly, the Moller-Plesset partitioning with Hartree-Fock potential gives the energy of this configuration as

$$E_i^{\text{MP}} = \left\langle \Phi_i \middle| h_{\text{HF}} \middle| \Phi_i \right\rangle = \sum_{i \in |\Phi_i\rangle} q_i\epsilon_i.$$

Where q_i is the occupation number of the ith orbital and ϵ_i is the corresponding single-particle energy. The EN-energy can be expressed in terms of the Moller-Plesset energy for closed-shell CSFs as

$$E_i = E_i^{\text{MP}} - \sum_{i \in |\Phi_i\rangle}\left[\sum_{b \notin |\Phi_i\rangle}\left\langle \psi_i\psi_b \middle| \left(1 - P_{12}\right)\frac{1}{r_{12}} \middle| \psi_i\psi_b \right\rangle\right] - \frac{1}{2}\sum_{r \in |\Phi_i\rangle}\left[\sum_{b \in |\Phi_i\rangle}\left\langle \psi_r\psi_b \middle|\right.\right.$$

$$\left(1 - P_{12}\right)\frac{1}{r_{12}}\left|\psi_r\psi_b\right\rangle\right] + \frac{1}{2}\sum_{r\in|\Phi_i\rangle}\left[\sum_{s\in|\Phi_i\rangle}\left\langle\psi_r\psi_s\right|\left(1 - P_{12}\right)\frac{1}{r_{12}}\left|\psi_r\psi_s\right\rangle\right].$$

For open-shell CSFs angular factors make it difficult to arrive at a straight forward relation. If the model space is spanned by the reference CSF alone then terms other than E_i^{MP} contributes to a shift in the energy denominator and each of the matrix element combined with appropriate numerator is a sum of ladder diagrams to all orders. Ladder diagrams can be grouped into three classes: (i) particle-particle (ii) particle-hole and (iii) hole-hole. The second and third term in the above equation is particle-hole class and the last term is particle-particle class. The summation over hole-hole class of ladder diagrams is given by the reference state energy in the energy denominator. Since the diagonal elements are the energy in EN-partitioning the histograms in the earlier section gives a comparison of the diagonal terms and their range but with V^{N-1} potential as the central field potential.

The residual Coulomb interaction H_{es} in EN-partitioning is the off-diagonal matrix elements of H_{atom} within the whole of configuration space under consideration and can be represented as

$$H_{\mathrm{es}} = \sum_{i\neq j}\left\langle\Phi_i\left|H_{\mathrm{atom}}\right|\Phi_j\right\rangle\left|\Phi_i\right\rangle\left\langle\Phi_j\right| = \sum_{i\neq j}\left\langle\Phi_i\left|\sum_m\left(t + \sum_{n>m}\frac{1}{r_{mn}}\right)\right|\Phi_j\right\rangle\left|\Phi_i\right\rangle\left\langle\Phi_j\right|$$

Let the CSF $|\Phi_i\rangle$ be singly excited wrt $|\Phi_j\rangle$ and both are singly excited wrt the reference CSF $|\Phi_0\rangle$. One of the possible form of $|\Phi_i\rangle$ and $|\Phi_j\rangle$ is

$$\left|\Phi_i\right\rangle = \left|\Phi_a^r\right\rangle \text{ and } \left|\Phi_j\right\rangle = \left|\Phi_a^s\right\rangle.$$

The matrix element of the residual coulomb interaction between these two CSFs can be converted into orbital matrix elements as [6]

$$\left\langle\Phi_a^r\left|\sum_m\left(t + \sum_{n>m}\frac{1}{r_{mn}}\right)\right|\Phi_a^s\right\rangle = A(r,s)\left\langle\psi_r\left|t\right|\psi_s\right\rangle + \sum_{\alpha\neq a}B(r\alpha,s\alpha)\left\langle\psi_r\psi_\alpha\right|\left(1 - P_{12}\right)\frac{1}{r_{12}}\left|\psi_s\psi_\alpha\right\rangle.$$

$$(4.2)$$

Where $|\psi_\alpha\rangle$s are the orbitals common to both $|\Phi_a^r\rangle$ and $|\Phi_a^s\rangle$. If $\{|\psi_r\}\in|\Phi_a^r\rangle$ and $\{|\psi_s\}\in|\Phi_a^s\rangle$ then $\{|\psi_\alpha\rangle\} = \{|\psi_r\rangle\}\cap\{|\psi_s\rangle\}$. Similarly, for CSFs $|\Phi_{ab}^{rs}\rangle$ and $|\Phi_{ab}^{tu}\rangle$ which are doubly excited wrt each other and the reference state $|\Phi_0\rangle$ the matrix element that contributes to H_{es} is

$$\left\langle\Phi_{ab}^{rs}\left|\sum_m\left(t + \sum_{n>m}\frac{1}{r_{mn}}\right)\right|\Phi_{ab}^{tu}\right\rangle = B(rs,tu)\left\langle\psi_r\psi_s\right|\left(1 - P_{12}\right)\frac{1}{r_{12}}\left|\psi_t\psi_u\right\rangle. \qquad (4.3)$$

The single-electron part of the Hamiltonian does not contribute in the above expression as it cannot excite two electrons. Similarly, there are doubly excited configurations which are coupled by single excitation/de-excitation, the matrix elements of which can be evaluated in terms of orbitals. Two configurations which are connected by triple or higher excitations/de-excitations are not coupled directly—two configurations are coupled directly by an interaction Hamiltonian if its matrix elements *wrt* the configurations is non-zero—but can be coupled when H_{es} is treated to higher orders. An example of such configurations in Yb is $|4f*^6 4f^8 6p*^2\rangle$ and $|5p*^1 6s^1 6p^2\rangle$, both are doubly excited with respect to the $|\Phi_0\rangle$ but between them it is a triple excitation. This is a motivation for treating H_{es} to high orders as it includes different forms of configuration coupling. The other possible direct con-
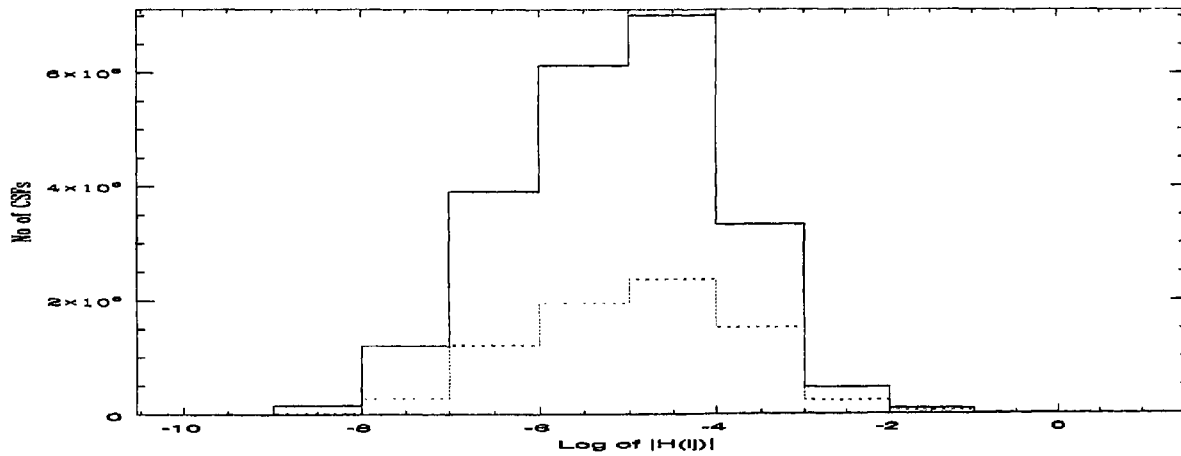
Figure 4.2: Histogram of $|H(ij)|$ for the even and odd parity CSFs.

figuration coupling is between the singly and doubly excited configurations which can be evaluated similar to the earlier cases. Expressions (4.2) and (4.3) are typical examples as only the particle to particle excitation has been considered. The other forms of excitations are hole to hole and hole-particle to hole-particle.

The histogram in the Fig:4.2 gives the number of the offdiagonal coupling terms and the log of absolute value of $H(ij)$, which represents the residual coulomb interaction coupling between the two CSFs $|\Phi_i\rangle$ and $|\Phi_j\rangle$. The solid line is for the odd parity configurations and the dashed line for the even parity configurations. It can be inferred that very few configurations are coupled very strongly, but several of CSFs couple in the range 10^{-3}—

10^{-4}, so when a sufficiently large configuration space is taken these terms will add upto to give non-trivial contributions.

4.2.2 The PT-Violating and Dipole Interaction Terms

Consider the PT-violating interaction which is dependent on the nuclear density its matrix element between two CSFs is non-zero only when they are connected by a single excitation/de-excitation from s to $p*$ symmetry orbitals or vice-versa. Within the CSF space considered, the CSFs that correspond to these effects can connect through the PT-violating interaction in the following manner (i)$|\Phi_0\rangle$ and singly excited CSFs (ii) between singly excited CSFs (iii) singly and doubly excited CSFs and (iv) between doubly excited CSFs. The matrix elements of H_{PTV} can be computed in terms of single particle orbitals like in the case of H_{es} by using appropriate radial and angular factors

$$\left\langle \Phi_i \middle| H_{\mathrm{PTV}} \middle| \Phi_j \right\rangle = T(i,j,k,l) \left\langle \psi_k \middle| H_{\mathrm{PTV}} \middle| \psi_l \right\rangle.$$

Where $T(i,j,k,l)$ is the angular factor to convert from the CSF level to the orbital level. The above expression shows that the same single-particle matrix element can contribute to many different configuration couplings via H_{PTV}. An example is: the coupling between $|6s^2\rangle$ and $|6s6p*\rangle$ is the same as between $|6s6p*\rangle$ and $|6p*^2\rangle$. In this respect a single particle approach will reduce the number of excitations considerably but it introduces complications when higher order perturbations are considered as the excited configurations are purely defined by the perturbations rather than defined apriori as in EN-partitioning. At the single particle level the strength of the coupling can be enhanced in the following cases:

- when one of the orbitals lie deep in the core, it is highly contracted towards the nuclear region and hence the H_{PTV} coupling is quite strong.

- continuum orbitals due to their high kinetic energy penetrates deeper into the nuclear region. As a result the H_{PTV} coupling gets stronger when one of the orbitals involved is a continuum.

But, in both cases the energy difference in the denominator suppresses the contribution to the final expectation value of EDM significantly. In the Table4.5 the H_{PTV} reduced matrix

element between the $7s$ and $np*$ are given. The values of the matrix elements has been

Table 4.5: Matrix element of H_{PTV} *wrt* $np*$ and $7s$ orbital

Sl. No.	n	$\langle np* \|\| H_{PTV} \|\| 7s \rangle$	Sl. No.	n	$\langle np* \|\| H_{PTV} \|\| 7s \rangle$
1	12	$-0.0298\ 19$	2	11	$0.0483\ 86$
3	10	$0.0627\ 50$	4	9	$0.0656\ 03$
5	8	$0.0879\ 94$	6	7	$-0.1724\ 47$
7	6	$-0.3191\ 55$	8	5	$-1.7866\ 83$
9	4	$-5.1915\ 37$	10	3	$-10.8463\ 18$
11	2	$-21.8273\ 41$			

parameterized in terms of $C_T \sigma_{Nz} \times 10^{-12}$, where C_T is the TPT coupling constant and σ_{Nz} is the component of nuclear-spin along the z-axis. The expression has been computed for the z-component. These matrix elements do contribute to the lowest order EDM and can contribute through one or more order of residual coulomb interaction too. The core $p*$ contributes via coupled perturbed Hartree-Fock terms, whereas virtual $p*$ orbitals contribute through correlation terms. One important trend in the matrix elements is the flip in sign and the continuous decrease in magnitude towards the outer orbitals. This can contribute to cancellations in the value of EDM if there is no corresponding sign flip in the dipole contribution.

Within the configuration space considered $|\Phi_0\rangle$ is coupled to only a few CSFs from the odd parity CSF space through the H_{PTV}, these are single excitations from $6s$ to virtual $p*$ orbitals $|6s(6\text{-}11)p*\rangle$, from $5p*$ to the virtual s orbitals $|5p*^1\ (7\text{-}12)s\rangle$ and excitations from $5s$ to $|6s(6-11)p*\rangle$. Only these CSFs from the odd parity get connected to $|\Phi_0\rangle$ with H_{PTV} alone as perturbation and hence contribute to $\Omega_{es,edm}^{(0)}$. If one considers one order of H_{es} as a perturbation, then $|\Phi_0\rangle$ gets connected to all the CSFs in the even parity space as all of them are generated by excitation(s) from $|\Phi_0\rangle$. If H_{PTV} is applied as the next perturbation, the number of odd parity CSFs that gets coupled to the even parity space is 6447. This is because the whole of the even parity space is coupled directly to only 6447 CSFs in the odd parity space through H_{PTV}. This is a part of $\Omega_{es,edm}^{(1)}$ but not the whole as there is another contribution from applying H_{es} to $\Omega_{es,edm}^{(0)}$. The difference

between the two is: in the first component H_{es} is applied in the even parity space whereas in the second case it is applied in the odd parity space. The non-zero coupling from the later component are those CSFs that contribute to $\Omega^{(0)}_{es,edm}$. Starting from $\Omega^{(2)}_{es,edm}$ all the configurations in the odd parity space have non-zero contribution, this is due to the configuration coupling due to the residual coulomb interaction. In short the contribution to EDM from odd parity configurations other than those contributing to $\Omega^{(0)}_{es,edm}$ is due to the residual coulomb interaction.

The Dipole interaction term unlike H_{PTV} depends linearly on r and has the selection rules $\Delta J = 0, \pm 1$ and $\Delta M = 0$ for the transverse mode. So $|\Phi_0\rangle$ is connected to more configurations through the dipole term in odd parity space than in the case of H_{PTV}. In the present computation the dipole term is not treated as a perturbation. As described in earlier sections, the dipole operator is used to compute the expectation value and is the required value of the EDM in the ground state of atomic Yb. But the value of EDM remains the same when the dipole is treated as the perturbation and the expectation value of H_{PTV} is computed. This is more of a theoretical consistency check as in real physical systems the dipole term is the measure of the EDM as a linear response to an external field.

4.3 The Lowest Order EDM

The expression for the lowest order contribution to EDM from the virtual orbital $np*$ is

$$\left(\vec{D}_a\right)_{np*} = \frac{\langle 6s|\vec{D}|np*\rangle\langle np* |H_{PTV}|6s\rangle}{\epsilon_{6s} - \epsilon_{np*}}.$$

where ϵ_{6s} and ϵ_{np*} are the single particle energies of $6s$ and $np*$ orbitals respectively. Combining both H_{PTV} and dipole terms the lowest order contributions to EDM from the first few virtual $p*$ orbitals are tabulated in Table4.6. The values in the table above have been parameterized in terms of $C_T \sigma_{Nz} \times 10^{-12} ea_0$. This is at the level of single particle. A similar computation can be done at the level of configurations using CSFs instead of single particle orbitals. The expression for the EDM in terms of the CSFs is

$$\left(\vec{D}_a\right)_{np*} = \frac{\left\langle 6s^2(J{=}0)\left|\vec{D}\right|6snp*\,(J{=}1)\right\rangle\left\langle 6snp*\,(J{=}1)\left|H_{PTV}\right|6s^2(J{=}0)\right\rangle}{E_0 - E_{np*}}.$$

Table 4.6: Lowest order contribution to EDM at the single particle level.

n	$\langle 6s||\vec{D}||np*\rangle$	$\langle np*||H_{\text{PTV}}||6s\rangle$	$\epsilon_{6s} - \epsilon_{np*}$	$(\vec{D}_a)_{np*}$	Cumulated $(\vec{D}_a)_{np*}$
6	3.6696 93	−9.4176 66	−0.0720 60	4.8133 79	4.8133 79
7	0.2132 37	−5.0885 95	−0.1427 47	0.0762 89	4.8896 68
8	−0.0659 96	2.5965 51	−0.1672 78	0.0102 66	4.8999 34
9	−0.0374 63	1.9358 25	−0.1776 22	0.0049 77	4.9049 11
10	−0.0271 61	1.8516 32	−0.1830 73	0.0027 57	4.9076 68
11	−0.0188 43	1.4277 90	−0.1866 04	0.0014 47	4.9091 15
12	0.0125 74	−0.8798 99	−0.1889 95	0.0006 13	4.9097 28

Where E_{np*} is the energy of the CSF $|6snp*\ (J=1)\rangle$. The values got using the single particle approach and the CSFs should be the same except for the effect of the static correlation, which will change the value of the energy denominator from the single particle energy denominator.

From Table4.6 it is clear that at the single particle level the lowest order contribution is dominated by $6p*$ and the contribution from the other virtual $p*$ orbitals is marginal. Like in $7s$ there is a flip in the sign of H_{PTV} matrix element for the intermediate energy virtual $p*$ orbitals but a corresponding sign flip in the dipole matrix element maintains the sign of EDM. If not for the accompanying sign flip it can lead to cancellations. The fall in the contribution from the virtual $p*$ starting from $n=7$ is due to a decrease in the H_{PTV} coupling and the widening energy gap between $np*$ and $6s$. Compared to $6p*$ the $\vec{D}$ coupling with $7p*$ is more than one order of magnitude down and the energy gap is almost twice. In addition H_{PTV} coupling also decreases but at a slower pace compared to $\vec{D}$ coupling. Over all there is a rapid fall in the $\vec{D}$ coupling till $9p*$ after which it continues to fall but at a slower pace. The magnitude of the energy difference falls very fast for the first two bound virtual $p*$ but is relatively stable after as the energy separation become smaller for the high lying orbitals.

The contribution from the continuum orbitals to the lowest order can also be computed in the same way. To include the whole of continuum $p*$ orbitals space first we have to compute the required matrix elements and apply the Gauss-Laguerre quadrature. The

(a)   (b)
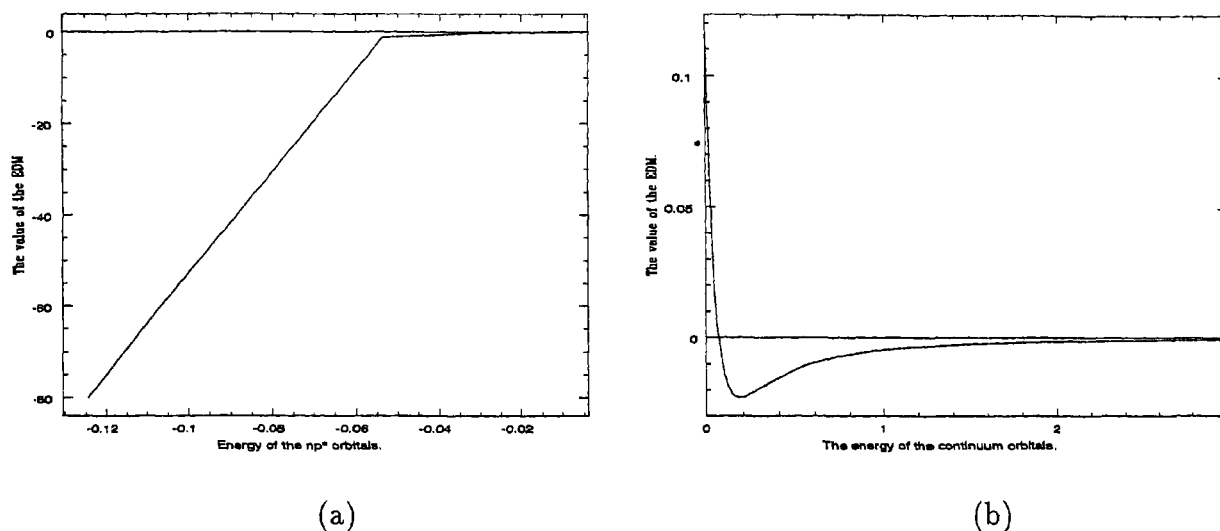
Figure 4.3: The contribution from the continuum orbitals.

individual contributions from the continuum $p*$ orbitals are as in Table4.7. The last column in the table gives the total value of EDM till that continuum orbital. Though the 12 point Gauss-Laguerre quadrature has been used only the first 9 points have been given as the contribution from the rest is very small. The quadrature can be done using the expression (4.1). The Fig:4.3 shows the EDM contributions from the bound and continuum contributions plotted against the orbital energies. For the continuum orbitals the plot is generated with more data points than required for the Gauss-Laguerre quadrature. Trends in the contribution from the bound and continuum orbitals are very different and this is clearly brought out in the plots. The column for $\vec{D}_a$ in Table4.7 is the individual contribution from the continuum orbitals weighted by the corresponding Laguerre weight factors. The last column is the cumulated value of $\langle \vec{D} \rangle$ and the final value is the total contribution from the continuum orbitals.

The individual contribution from $-1p*$ is larger than the contribution from $7p*$ but its contribution to the overall quadrature gets suppressed as the weight factor is less than unity. The dipole matrix element flips in sign with increase in energy but magnitude of the energy denominator and the H_{PTV} matrix element increase monotonically. This also flips the sign of the contribution to EDM. Since the energy has been scaled to 20 the contribution from the whole of the continuum $p*$ spectrum is the final value multiplied

by $(20/k_{12})$, which gives the contribution from $p*$ continuum orbitals to the lowest order EDM as $0.0145\ 856 C_T \sigma_{Nz} \times 10^{-12} e a_0$. Adding up with the contribution from the bound $np*$ virtuals the value of EDM is $4.9243\ 136 C_T \sigma_{Nz} \times 10^{-12} e a_0$.

Table 4.7: Lowest order contribution to EDM from continuum orbitals.

n	$\langle 6s||\vec{D}||np*\rangle$	$\langle np*||H_{\mathrm{PTV}}||6s\rangle$	$\epsilon_{6s} - \epsilon_{np*}$	$\vec{D}_a$	Cumulated $\vec{D}_a$
-1	$0.0898\ 41$	$-24.5982\ 44$	$-0.1984\ 62$	$0.0328\ 211$	$0.0328\ 211$
-2	$0.0109\ 44$	$-24.8677\ 07$	$-0.2508\ 99$	$0.0056\ 102$	$0.0384\ 313$
-3	$-0.0344\ 06$	$-25.9005\ 69$	$-0.5289\ 89$	$-0.0097\ 214$	$0.0287\ 099$
-4	$-0.0169\ 05$	$-27.2879\ 55$	$-1.3633\ 96$	$-0.0014\ 750$	$0.0272\ 349$
-5	$-0.0074\ 59$	$-28.2745\ 33$	$-3.2702\ 94$	$-0.0001\ 618$	$0.0270\ 731$
-6	$-0.0033\ 11$	$-28.8716\ 73$	$-6.6110\ 12$	$-0.0000\ 161$	$0.0270\ 569$
-7	$-0.0014\ 56$	$-29.2848\ 00$	$-13.6480\ 49$	$-0.0000\ 012$	$0.0270\ 557$
-8	$-0.0006\ 47$	$-29.6175\ 00$	$-24.7771\ 29$	$-0.0000\ 001$	$0.0270\ 556$
-9	$-0.0002\ 87$	$-29.9291\ 47$	$-42.7711\ 29$	$-0.0000\ 000$	$0.0270\ 556$

An important feature of the continuum is that the contribution from $-1p*$ is quite large compared to the contribution from the whole of the continuum spectrum. This implies that the important contribution from the continuum is from a small region in the k-space near the origin. This is evident from the individual values in Table 4.7. For completeness of the computation the continuum orbitals is important as the contribution from the continuum is larger than that of $8p*$. At the single particle level $6p*$ is the most important virtual orbital, it accounts for 97.747% of the lowest order EDM. The remaining $p*$ orbitals including the continuum accounts for only 2.225% and the continuum alone contributes only 0.296% to the total value.

4.4 The CI and Bloch Equation Based Formulations

4.4.1 Comparison of the Different Methods

As described in the previous chapter, atomic EDM can be computed by diagonalizing within the whole configuration space. It involves two diagonalization, one within each of

the even and the odd-parity sub-spaces. Since atomic EDM is the expectation value of the dipole operator *wrt* the ground state , for atomic Yb only the lowest energy ASF in the even parity sub-space is required. Within the odd-parity sub-space all the ASFs are required as they are the intermediate states. Though the $5d$ orbital does not contribute to the atomic EDM directly, it is very important for the correlation effects as there are CSFs containing $5d$ which mix strongly with $|\Phi_0\rangle$. Other configurations that mix strongly with $|\Phi_0\rangle$ are the double excitations from $6s^2$ to the lower s and p orbitals. Among the odd-parity ASFs the most important CSF is $|6s6p*\rangle$ and similar to the even-parity sub-space configurations with excitations to $5d$ are important. For comparison the value of EDM computed with CI, the perturbed CI(PCI) and the Bloch equation based formulation are as tabulated in Table4.8. The unit for EDM used in Table4.8 is the same as in earlier tables.

Table 4.8: Comparison of results from different methods.

Sl. No	No of CSFs		CI	PCI		MBPT	
	Odd	Even		H_{PTV}	$\vec{D}_a$	$[-4]$	$[-8]$
1	100	100	6.4263 76	6.4263 76	6.4263 76	6.4264 27	6.4263 76
2	100	300	6.4263 71	6.4263 71	6.4263 71	6.4264 22	6.4263 71
3	100	500	6.4294 36	6.4294 36	6.4294 36	6.4294 95	6.4294 36
4	100	1000	6.4295 56	6.4295 56	6.4295 56	6.4296 12	6.4295 56
5	500	1000	6.0965 02	6.0965 02	6.0965 02	6.0964 68	6.0965 02
6	500	1500	6.0964 05	6.0964 05	6.0964 05	6.0963 72	6.0964 06

The CSFs considered are single excitations from $6s, 4f*$ and $4f$ and double excitations with the occupied-orbital configuration $|4f^{13}6s^1\rangle$. The sequence of the CSFs is arranged in increasing principal quantum numbers and corresponds roughly to increasing energy. The results using PCI have been given for both the interactions treated as perturbations separately. Results under the heading H_{PTV} are computed treating H_{PTV} as the perturbation in the PCI formulation and similarly for $\vec{D}$.

CI and PCI are diagonalization based methods and include the residual coulomb interaction within the configuration space to all order, whereas in the Bloch equation based MBPT approach, the order of residual coulomb interaction is decided by the convergence

(a)   (b)
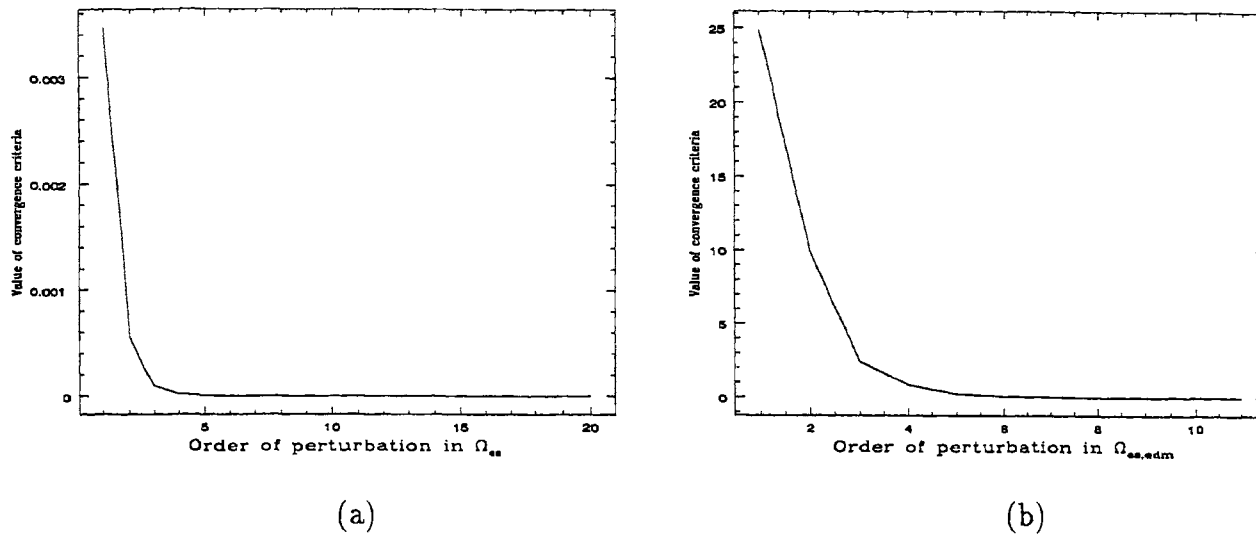
Figure 4.4: The convergence of the wave-operators

criterion. For the results tabulated the wave-operator is computed till the order which contributes more than 10^{-10} to the CSF coefficients with the residual coulomb interaction. With the H_{PTV} included as perturbation two sets of computation are done; one with the convergence criteria set to 10^{-4} and another to 10^{-8}. These are tabulated in the columns labelled as $[-4]$ and $[-8]$ respectively. Higher convergence criteria with H_{PTV} has been chosen as it has a scaling factor of G_F. Results in the table emphasizes the following points

- The results from CI and PCI are in perfect agreement thereby suggesting that the physical effects incorporated in the two approaches are the same even though the formulations are different. The value of EDM computed with PCI is the same whether H_{PTV} or $\vec{D}$ is treated as the perturbation.

- The result does not change significantly with the inclusion of CSFs which has excitations to high lying orbitals. This is another test for the convergence of the orbital basis set in terms of all the interactions involved in the computation where as the test for convergence in the single–particle picture was without the residual coloumb interaction.

Though the details of the formalisms are different, the physical effects included in all the

procedures are the same, so the results from MBPT should be identical with the CI and PCI results. Consider the first column in the MBPT results where the convergence criteria is set to 10^{-4}, this result differs from those of CI and PCI by an order of 10^{-4}. This can be accounted as due to different physical effects included. Higher value of the convergence criteria mean lower order of residual coloumb interaction in the odd-parity configuration sub-space. As shown in the table when the convergence criteria is decreased to 10^{-8}, there is almost perfect agreement between the results from various methods. When the convergence criteria is set to 10^{-4} the order at which the wave-operator converges is 22 for Ω_{es} in the even-parity CSF space and 12 for $\Omega_{es,edm}$ in the odd-parity space, which means 22 and 12 orders of residual coulomb interaction is included in the even-parity and odd-parity configuration spaces respectively. This establishes the one to one correspondence of the physical effects included in each of the methods.

The MBPT based approach has the best efficiency among the various approaches in terms of the memory usage and run time. Consider the last case with 500 even parity CSFs and 1500 odd-parity CSFs, the time taken with CI, PCI and MBPT approaches are 5:58:23,00:15:39 and 00:7:07 hrs respectively. Ratio of the time taken with runtime of CI normalized to 100 is 100:4.366:1.986, this clearly shows the advantage of the MBPT based formalism in terms of run time. For the MBPT approach, the time taken is with the convergence criteria set to 10^{-8}. Part of the CI and PCI approaches which takes most time is the matrix diagonalization and the enhanced run time efficiency of MBPT is the absence of diagonalization. As shown in the Fig:4.4, the convergence of Ω_{es} is much faster than that of $\Omega_{es,edm}$. This is due to the strong coupling with H_{PTV}. However one point to be noted is that H_{PTV} is parameterized in terms of G_F, which will be included later while computing $\vec{D}_a$.

The computation has been done with excitations from $6s,4f*$ and $4f$ alone. This checks the importance of the high-lying bound virtuals. It is also necessary to check the importance of excitations from the occupied orbitals, for which only the lowest virtuals in each symmetry are selected and the configurations with excitations from deeper cores are included gradually. The result for such a sequence of runs is tabulated in Table 4.8. The sequence of runs show that the excitations from the $4f$ orbitals contribute significantly

to the value of EDM but the excitations from the $5p$ and $5s$ are not so important. This justifies the choice of excitations till the $5s$ occupied orbital. Configurations with excitation from

Table 4.9: Contributions from the occupied orbitals.

Sl. no	CSFs(non-rel)		Value of $\vec{D}_a$
	Even CSFs	Odd CSFs	
1	$\lvert 6s^2\rangle + \lvert 7s^2\rangle + \lvert 6p^2\rangle + \lvert 5d^2\rangle$ $+\lvert 5f^2\rangle + \lvert 6s7s\rangle + \lvert 6p5f\rangle$	$\lvert 6s6p\rangle + \lvert 7s6p\rangle + \lvert 6p5d\rangle$ $+\lvert 5d5f\rangle$	4.8402 78
2	$+\lvert 4f^{13}(6p+5f)\rangle$ $+\lvert 4f^{13}6s(7s6p+7s5f$ $+6p5d+5d5f)\rangle + \lvert 4f^{12}(7s^2$ $+6p^2+5d^2+5f^2+7s5d$ $+6p5f)\rangle$	$+\lvert 4f^{13}(7s+5d)\rangle$ $+\lvert 4f^{13}6s(7s^2+5d^2+7s5d$ $+6p5f)\rangle + \lvert 4f^{12}(7s6p$ $+7s5f+6p5d+5d5f)\rangle$	4.7842 17
3	$+\lvert 5p^56p\rangle + \lvert 5p^56s(7s6p$ $+7s5f+6p5d+5d5f)\rangle$ $+\lvert 5p^54f^{13}(7s^2+6p^2+5d^2$ $+5f^2+7s5d+6p5f)\rangle$ $+\lvert 5p^4(7s^2+6p^2+5d^2+5f^2$ $+7s5d+6p5f)\rangle$	$+\lvert 5p^5(7s+5d)\rangle + \lvert 5p^56s(7s^2$ $+5d^2+7s5d+6p5f)\rangle$ $+\lvert 5p^54f^{13}(7s6p+7s5f+6p5d$ $+5d5f)\rangle + \lvert 5p^4(7s6p+7s5f$ $+6p5d+5d5f)\rangle$	4.7486 74
4	$+\lvert 5s7s\rangle + \lvert 5s6s(7s^2+5f^2$ $+5d^2+5f^2+7s5d+6p5f)\rangle$ $+\lvert 5s4f^{13}(7s6p+7s5f+6p5d+$ $+5d5f)\rangle + \lvert 5s5p^5(7s6p$ $+7s5f+6p5d++5d5f)\rangle$	$+\lvert 5s6p\rangle + \lvert 5s6s(7s6p+7s5d$ $+6p5d+5d5f)\rangle + \lvert 5s4f^{13}(7s^2$ $+6p^2+5d^2+5f^2+7s5d$ $+6p5f)\rangle + \lvert 5s5p^5(7s^2++6p^2$ $+5d^2+5f^2+7s5d+6p5f)\rangle$	4.7450 89

the $4f$ occupied orbital adds to the contribution from the configurations with excitations from $6s$ but there is a cancellation with the contributions from the $5p$ and $5s$ excited configurations.

4.4.2 Bloch Equation Based MBPT

4.4.2.1 Computation of Ω_{es} and E_0

In the previous section we have compared the results from different methods. In this section we shall elaborate to a deeper extent on the results from the Bloch-equation based MBPT formalism. As mentioned in earlier sections the matrix approach to the Bloch-equation does not distinguish between different effects and the topology of the diagrams involved. As a result there are contributions from the size-inconsistent terms both in the energy expression as well as the properties computed. The fact that CI is a size-inconsistent theory and the result obtained using MBPT is the same as those from CI and PCI also establishes the size inconsistency of the matrix based MBPT method. The first part of the computation is the computation of the wave-operator Ω_{es}, using which the energy of the ground state ASF E_0 can be computed. The wave-operator Ω_{es} can be computed in an order by order sequence using the Bloch equation given in the previous chapter

$$\left[\Omega_{es}, H_0\right] P_+ = Q V_{es} \Omega_{es} P_+ - \chi_{es} P_+ V_{es} \Omega_{es} P_+,$$

where the definitions of the quantities remain the same. From the wave-operator Ω_{es} the ground state wave-function $|\Psi_0\rangle$ and energy E_0 are got as

$$\left|\Psi_0\right\rangle = \frac{\Omega_{es}\left|\Phi_0\right\rangle}{\left\langle\Phi_0\middle|\Omega_{es}^\dagger\Omega_{es}\middle|\Phi_0\right\rangle} \quad \text{and} \quad E_0 = \left\langle\Phi_0\middle|H_{es}\Omega_{es}\middle|\Phi_0\right\rangle.$$

Since the computation is done within the framework of EN-partitioning of the Hamiltonian, the first order energy correction of the ground state is zero. This is because in EN-partitioning the diagonal elements of the Hamiltonian matrix are taken as the energy of the configuration and offdiagonal elements as the perturbation.

The whole of the even parity configuration space is spanned by 9930 CSFs of which 1-4435 has its occupied as $|4f^{14}6s\rangle$, $|4f^{14}\rangle$, $|4f^{13}6s^2\rangle|4f^{13}6s\rangle$ and $|4f^{12}6s^2\rangle$, 4436-9094 corresponds to occupied of the form $|5p^54f^{14}6s^2\rangle$, $|5p^54f^{14}6s\rangle$ and $|5p^54f^{13}\rangle$ and the remaining CSFs has the occupied configurations $|5s5p^64f^{14}6s^2\rangle$, $|5s5p^64f^{14}6s\rangle$, $|5s5p^64f^{13}\rangle$, and $|5s5p^64f^{14}6p^5\rangle$. Using this set of configuration the ground state wave-function is

$$\left|\Psi_0\right\rangle = 0.9251\,23\left|6s^2\right\rangle + 0.1172\,17\left|6p*^2\right\rangle + 0.1169\,21\left|6s7s\right\rangle + 0.0996\,76\left|6p^2\right\rangle$$

$$-0.0600\ 60\big|5d^2\big\rangle + 0.0568\ 61\big|6p7p\big\rangle - 0.0497\ 43\big|5d*^2\big\rangle + 0.0480\ 54\big|6p*\ 7p*\big\rangle$$

$$+0.0443\ 18\big|6p8p\big\rangle - 0.0442\ 15\big|6s8s\big\rangle - 0.0320\ 73\big|5d6d\big\rangle + \ldots.$$

Where the wave-function has been renormalized, the normalization constant is 1.0809 37. In the above expression only first ten important CSFs have been selected. As expected most of the important CSFs in $|\Psi_0\rangle$ are doubly excited except for $|6s7s\rangle$, this being a single excitation does not interact very strongly with the ground state CSF $|6s^2\rangle$ but contributes significantly through other configurations when the residual interaction is taken to very high orders. Values of E_0 with increasing size of the even configuration space is as given in Table4.10.

Table 4.10: The energy of the ground state ASF with increasing CSF-space size.

Sl. no	No of CSF	Energy	Sl. no	No of CSF	Energy
1	100	−14067.6714 79	2	500	−14067.6755 69
3	1000	−14067.6756 60	3	2000	−14067.6942 64
5	3000	−14067.6942 68	6	4000	−14067.6949 91
7	4435	−14067.6949 91	8	5435	−14067.6974 13
9	6435	−14067.6974 21	10	7435	−14067.7019 28
11	8435	−14067.7040 97	12	9094	−14067.7040 97
13	9594	−14067.7042 26	14	9930	−14067.7042 26

Configurations are added to the configuration space in sequence of excitations from the occupied orbitals. The sequence of excitations is similar to that of Table 4.2 except that the virtual orbital space is much larger and hence the size of the configuration space is also large. As the size of the configuration space is increased more many-body effects are included in the computation. A direct measure of the importance of the even parity configurations added is the energy of the ground state ASF, the size of the change induced is a direct indication of the importance of the CSFs added.

An important quantity that can be derived from the values given in the table is the change in E_0. Define ΔE_0 as the energy difference between the CSF energy of $|6s^2\rangle$ and the energy computed using the configurations in the even-parity CSF space–correlation energy.

From the plot of ΔE_0 it is evident that the change in the ground state ASF energy is not uniform but in steps interrupted by regions of very minimal changes. Most significant changes in ΔE_0 occur while going from 100 to 500, from 1000 to 2000 and from 6435 to 7435 CSFs respectively. These changes are not the combined effect of all the CSFs added but due to a few important ones. The largest change in ΔE_0 is in going from 1000 to 2000 CSFs this corresponds to contribution from the occupied configuration $|4f^{14}\rangle$, that is double excitation from the $6s$ orbital shell. Of the remaining two, the first one is due to CSFs with occupied configuration $|4f^{13}6s\rangle$ and the other jump is due to the CSFs with occupied configuration $|5p^56s\rangle$. Each individually contributes $-0.0041\ 82$, $-0.0179\ 26$ and $-0.0045\ 07$ hartrees respectively, the combined effect amounts to 81.20% of the total change in the ground state energy due to correlation effects. The total change in E_0 due to correlation effects is $-0.0304\ 50$ hartrees. From these it can be concluded that, the most important CSFs that contribute to the correlation energy are those with the occupied configurations $|4f^{13}6s\rangle$, $|4f^{14}\rangle$ and $|5p^56s\rangle$ respectively. As to be expected the doubly excited CSFs are most important for capturing the correlation effects and among them it is the low lying double excitations from $6s$ orbital shell that gives the most significant contribution to correlation energy, it contributes 54.74% of the correlation energy.

The plot (b) in Fig:4.5 shows the need to include H_{es} to high orders to capture the correlation effects accurately. As shown in the graph the correlation effect due to one order of H_{es} is $-0.0436\ 033$ hartrees and decreases in magnitude monotonically till third order to $-0.0306\ 67$hartrees but increases in the fourth order to $-0.0343\ 38$hartrees. This trend of oscillation about the final value of ΔE_0 $-0.0327\ 48$ hartrees continues till it converges. The cycle of the oscillation has a period of four orders, that is in four orders it goes to the same side of the final value of ΔE_0 and the amplitude of the oscillation decreases with each cycle. Over all the value of ΔE_0 behaves like a damped oscillator with a cycle of four orders. If E_0 is computed by truncating the perturbation to the first few orders where the amplitude of oscillation is quite significant the value of ΔE_0 can be erroneous.

The Fig:4.6 shows the trend of wave-operator convergence. The first graph is a plot of the value of the convergence criteria against the order of perturbation and second graph is plot of $\log_{10}$ of the convergence criteria against the order of perturbation. From the
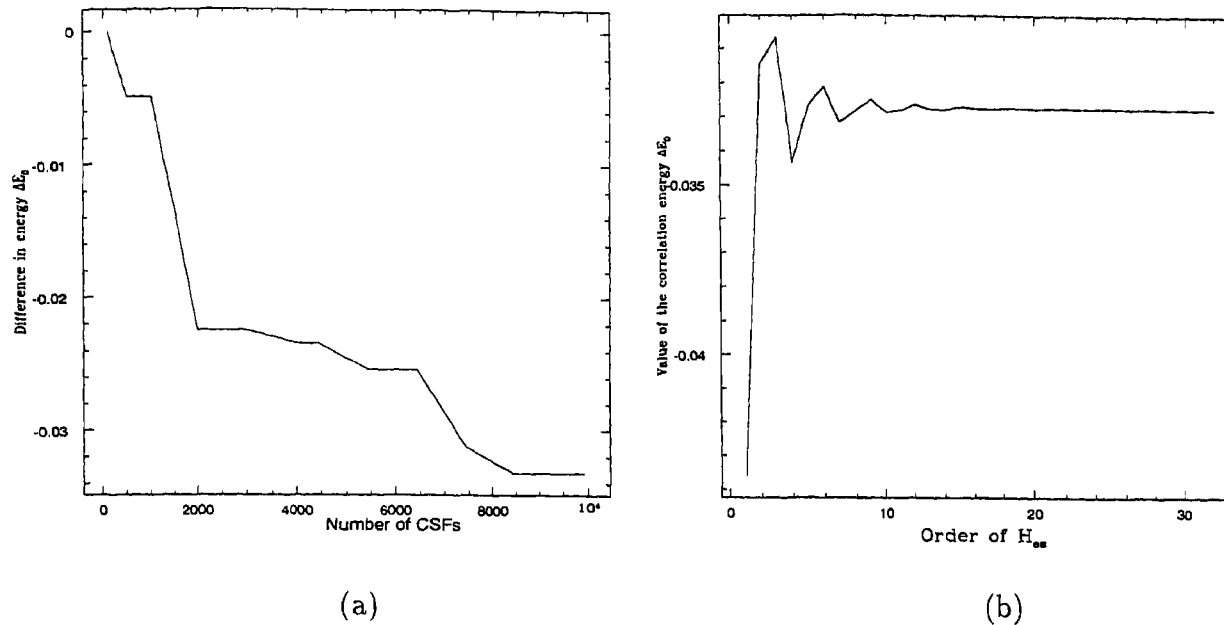
Figure 4.5: The change in energy due to many-body effects introduced by the configurations.

first graph it is evident that the convergence criteria starts off with a small value but as shown in the second graph in terms of order of magnitude, the convergence is not so fast. Still the convergence is monotonic with very regular fluctuations. As described in the last chapter, the first step for computation of the wave-operator $\Omega_{es,edm}$ is the computation of Ω_{es}, then using it various orders of $\Omega_{es,edm}$ can be computed.

4.4.2.2 Computation of $\Omega_{es,edm}$ and $\vec{D}_a$

The next step towards EDM computation is the inclusion of odd-parity CSFs within the configuration space used so far, which has been solely spanned by even-parity CSFs. Once H_{PTV} is applied to the wave-operator Ω_{es}, it maps onto the odd-parity component of the configuration space and can never be mapped back to the even-parity component as H_{PTV} is treated to first order only. This is followed by a sequence of residual coulomb interaction H_{es}, which accounts for the correlation effects in the odd-parity sub-space. In essence what is achieved is a sequence of perturbations applied to the ground state CSF $|6s^2\rangle$, where H_{PTV} is sandwiched between all possible arrangements of H_{es}. After the computation of the wave-operator Ω_{es}, it is stored in an order by order sequence. These are accessed as

(a)   (b)
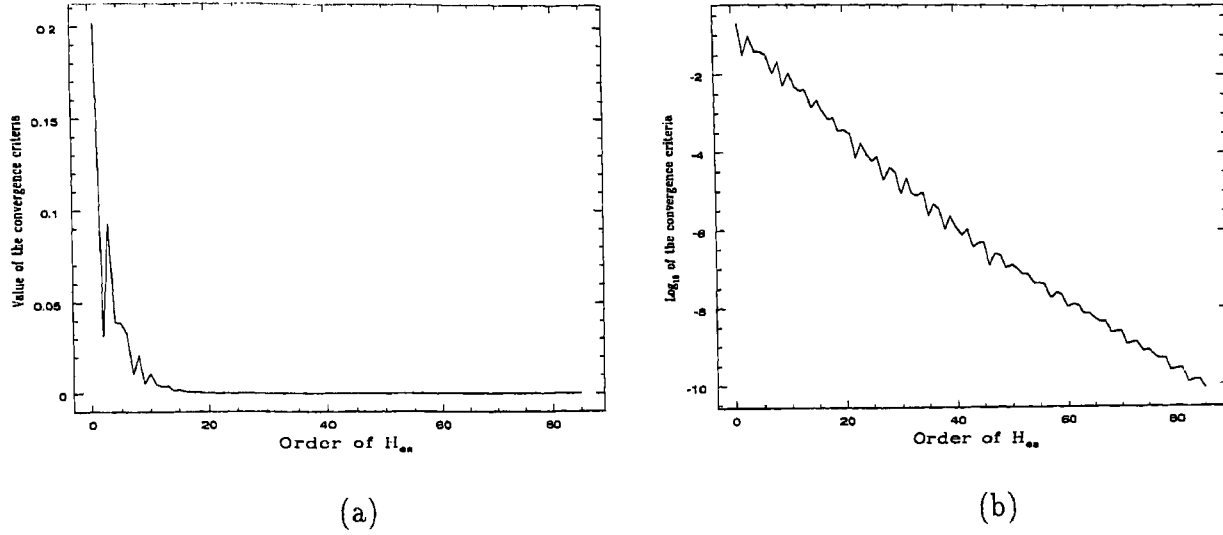
Figure 4.6: The convergence of the wave-operators

and when required during the computation of $\Omega_{es,edm}$, this is an advantage as $\Omega_{es,edm}$ is computed order by order. The wave-operator $\Omega_{es,edm}$ can be computed in an order by order sequence using the Bloch equation defined in the earlier chapter

$$\left[\Omega^{(n)}_{es,edm}, H_0\right]P_+ = \left(Q_-H_{PTV}\Omega^{(n)}_{es} + Q_-V_{es}\Omega^{(n-1)}_{es,edm} - \sum_{m=0}^{n-1}\Omega^{(m)}_{es,edm}P_+V_{es}\Omega^{(n-m-1)}_{es}\right)P_+.$$

Where the definition of all the quantities remain the same as defined in the earlier chapter. Once the wave-operator $\Omega_{es.edm}$ is computed, the mixed parity ground state wave-function $|\tilde{\Psi}_0\rangle$ can be written in terms of the wave-operators Ω_{es} and $\Omega_{es,edm}$ as

$$\left|\tilde{\Psi}_0\right\rangle = \left|\Psi_0\right\rangle + \left|\Psi^0_{corr}\right\rangle = \left(\Omega_{es} + \Omega_{es,edm}\right)\left|\Phi_0\right\rangle$$

From this expression the value of $\vec{D}_a$ can be calculated using the expression

$$\vec{D}_a = \left\langle\tilde{\Psi}_0\left|\vec{D}\right|\tilde{\Psi}_0\right\rangle = 2\left\langle\Phi_0\left|\Omega^\dagger_{es}\vec{D}\Omega_{es,edm}\right|\Phi_0\right\rangle$$

While choosing the odd-parity configurations the same criteria as in even-parity space is applied. This is because the criteria used in the even-parity space are valid for odd-parity also as these were arrived at by considering $\vec{D}_a$ which is a property that involves both the even and odd parity configurations. The whole of the odd parity configuration sub-space is spanned by 17087 CSFs, where the CSFs 1-11676 have occupied configurations

$|4f^{14}6s\rangle$, $|4f^{14}\rangle$, $|4f^{13}6s^2\rangle$ and $|4f^{13}6s\rangle$, 11677-15768 CSFs are spanned by occupied configurations $|5p^54f^{14}6s^2\rangle$, $|5p^54f^{14}6s\rangle$ and $|5p^54f^{13}\rangle$ and 15769-17087 is spanned by CSFs with occupied configurations $|5s6s^2\rangle$, $|5s6s\rangle$, $|5s4f^{13}\rangle$ and $|5s5p\rangle$. The majority of the configurations are with the excitations from $4f$ orbital, because f has the highest total angular momentum among all the orbitals considered and the total angular momentum of the CSF $J=1$ can be got in many intermediate coupling sequences.

With this choice of configuration space, many forms of correlation effects will be picked up. The correction to the ground state $|\Psi_0\rangle$ from the opposite parity sub-space due to H_{PTV} with all the configurations considered is

$$|\Psi^0_{corr}\rangle = \mathcal{A}\Big(-55.1403\ 73\big|6s6p*\big\rangle - 17.3681\ 84\big|6s7p*\big\rangle + 10.8231\ 86\big|6s6p\big\rangle$$
$$-9.5064\ 23\big|5p*7s\big\rangle - 9.2841\ 00\big|5s6p*\big\rangle + 7.8322\ 72\big|6s8p*\big\rangle + 7.1950\ 56\big|6p*5d*\big\rangle$$
$$+5.5464\ 22\big|6s9p*\big\rangle + 5.5189\ 58\big|6p5d*\big\rangle + 5.1246\ 77\big|5p*8s\big\rangle + \ldots \Big).$$

Where $\mathcal{A} = \sqrt{2}C_T\sigma_N G_F$. In the expression for $|\Psi^0_{corr}\rangle$ only the first ten important configurations has been listed. Though the coefficients are much larger than unity when scaled by the parameter $\sqrt{2}G_F$, it becomes very small. The product of the coupling constant C_T and nuclear spin σ_N is retained throughout as a parameter and C_T can be estimated by combining with the experimental results. The above expression for $|\Psi^0_{corr}\rangle$ shows that:

- As in the lowest order single-particle case, the coefficients of the CSFs $|6snp*\rangle$ flip sign for $n \geq 8$. In the lowest order computation a complementary sign flip of the dipole matrix element will not change the sign of $\vec{D}_a$. Here there can be configurations where this does not happen.

- Most of the important CSFs are singly excited with respect to the ground state CSF $|6s^2\rangle$, where as in $|\Psi_0\rangle$ doubly excited CSFs were more important. This is because the ground state ASF $|\Psi_0\rangle$ is strongly dominated by $|6s^2\rangle$ and H_{PTV} is a single particle operator. So the singly excited odd parity CSFs that connects to $|6s^2\rangle$ through H_{PTV} contributes very strongly.

- Singly excited configurations like $|6s6p\rangle$ can contribute through three possible many-body routes. First H_{PTV} takes $|6s^2\rangle$ to $|6snp*\rangle$ then a sequence of H_{es} connects it to

$|6s6p\rangle$, second a sequence of H_{es} connects $|6s^2\rangle$ to $|6p*6p\rangle$ and H_{PTV} takes it to $|6s6p\rangle$ and third a sequence of H_{es} takes $|6s^2\rangle$ to a CSF $|\Phi_i\rangle$ which connects to $|\Phi_j\rangle$ via H_{PTV} and from there another sequence of H_{es} takes it to $|6s6p\rangle$. The importance of many-body effects is demonstrated by the presence of $|6s6p\rangle$ as the third important CSF that contributes to $|\Psi^0_{corr}\rangle$.

- The two most important doubly excited odd-parity CSFs for the evaluation of EDM are $|6p* 5d\rangle$ and $|6p5d*\rangle$. More interesting is the second as both the virtual orbitals involved cannot contribute to the H_{PTV} matrix elements. Among the possible many-body routes which can contribute to the co-efficient of $|6p5d*\rangle$ one possibility is through the deeper occupied orbitals $5p*$ and $5s$, this would contribute to core polarization effects.

The value of $\vec{D}_a$ as computed using the set of configurations with increasing number of configurations is tabulated Table 4.11. In this sequence of runs both even and odd CSFs are increased alternately or at the same time. This gives the importance of particular occupied orbitals with respect to both the even and odd parity CSF space.

Another possible sequence of run is to keep the number of either the even or odd CSFs fixed to the maximum allowed and then compute the EDM by increasing the number of CSFs in the opposite parity CSF space. The results of such a sequence of runs is given in the Table 4.12. If the earlier sequence of runs shows the importance of occupied orbitals in the whole configuration space, these two runs show the importance of the occupied orbitals in CSF sub-space of each parity.

Like in correlation energy ΔE_0 there is a significant change in the value of EDM when CSFs with double excitations from $6s$ are included. To see the change more clearly the values of $\vec{D}_a$ in the two sequence of the runs are plotted in Fig:4.7. Consider the sequence of runs with the number of even-parity CSFs fixed, the value of $\vec{D}_a$ increase as the number of the odd-parity CSFs is increased. Which means that there are no appreciable cancellations due to addition of CSFs in the odd-parity sub-space. On the other hand in the second sequence of runs where the number of odd-parity CSFs is fixed, the value of $\vec{D}_a$ decreases as the number of even-parity CSFs is increased. This trend is opposite as compared to

Table 4.11: Values of $\vec{D}_a$ for different number of even and odd parity configurations.

Sl. no	No of CSFs		$\vec{D}_a$	Sl. no	No of CSFs		$\vec{D}_a$
	Even	Odd			Even	Odd	
1	100	100	6.4264 27	17	4435	10500	4.1722 47
2	100	300	6.4264 22	18	4435	11500	4.1722 47
3	100	500	6.4294 90	19	4435	12500	4.1741 36
4	100	1000	6.4296 12	20	4435	13500	4.1740 74
5	500	1000	6.0964 68	21	4435	14500	4.2069 56
6	500	1500	6.0963 72	22	4435	15768	4.2198 86
7	500	2500	6.1282 87	23	5435	15768	4.5344 87
8	1000	2500	6.1280 27	24	6435	15768	4.5334 98
9	1000	3500	6.1242 55	25	7435	15768	4.5000 68
10	3000	4500	4.1982 77	26	8435	15768	4.4295 81
11	4000	4500	4.1721 78	27	9094	15768	4.4295 81
12	4000	5500	4.1721 75	28	9594	15768	4.4424 63
13	4000	6500	4.1722 55	29	9930	15768	4.4424 63
14	4000	7500	4.1722 61	30	9930	16768	4.4436 23
15	4000	8500	4.1722 44	31	9930	17087	4.4438 58
16	4435	9500	4.1722 46				

the earlier sequence. In both sequence of runs there is a significant change in the value of $\vec{D}_a$ when CSFs with double excitation from $6s$ orbital are added. But, the signs of the change are different, in the even CSF space the inclusion of CSFs with double excitation from $6s$ increases the value of $\vec{D}_a$ where as in the odd-parity CSFs the trend is opposite.

Consider the expression for EDM it can be expanded as

$$\vec{D}_a = 2\left(\left\langle\Phi_0\middle|\vec{D}\Omega_{\text{es,edm}}\middle|\Phi_0\right\rangle + \sum_n \left\langle\Phi_0\middle|\Omega_{\text{es}}^{\dagger(n)}\vec{D}\Omega_{\text{es,edm}}\middle|\Phi_0\right\rangle\right).$$

Which can be rewritten in terms of configuration coefficients as

$$\vec{D}_a = 2\left[\left\langle\Phi_0\middle| + \sum_i \left\langle\Phi_i\middle|\mathcal{C}_i^{(\text{es})}\right]\vec{D}\Omega_{\text{es,edm}}\middle|\Phi_0\right\rangle = 2\sum_j \left[\left\langle\Phi_0\middle| + \sum_{i\neq 0}\left\langle\Phi_i\middle|\mathcal{C}_i^{(\text{es})}\right]\vec{D}\mathcal{C}_j^{(\text{es,edm})}\middle|\overline{\Phi}_j\right\rangle.$$

$$(4.4)$$

Table 4.12: Values of $\vec{D}_a$ for different number of even and odd parity configurations.

No of CSFs		$\vec{D}_a$	Sl. no	No of CSFs		$\vec{D}_a$
Even CSFs	Odd CSFs			Even CSFs	Odd CSFs	
9930	12	3.3654 83	10	7	17087	8.2430 89
9930	30	3.3605 54	11	19	17087	8.2430 89
9930	3648	3.4095 46	12	1243	17087	7.6831 05
9930	3846	4.3895 21	13	1390	17087	4.2645 44
9930	11676	4.3895 43	14	4435	17087	4.2118 95
9930	14070	4.3916 11	15	4448	17087	4.1837 51
9930	14100	4.3760 30	16	6713	17087	4.5282 75
9930	15768	4.4424 65	17	9094	17087	4.4333 81
9930	17087	4.4438 58	18			

Where the definitions of all quantities are the same as defined in previous chapter. Within the whole configuration space, the contribution from the first term is 5.4394 39 and the contribution from the second term is -0.6417 31, which is just 11.80% of the first term. Five most important configurations in the second term from the even-parity sub-space are $|6p*^2\rangle$, $|6p^2\rangle$, $|6p*\ 7p*\rangle$, $|5d*^2\rangle$ and $|6p7p\rangle$ and their contributions are -0.8119 50, 0.2065 15, -0.1001 58, 0.0738 55 and 0.0599 84 respectively, the values of EDM are in units of $C_T\sigma_N \times 10^{-12}ea_0$. All these are doubly excited configurations and mixes with the ground state CSF significantly but the singly excited CSF $|6s7s\rangle$ which is the third important CSF in $|\Psi_0\rangle$ does not contribute strongly. In addition there is shift in the sequence of the important CSFs compared to the sequence in terms of contribution to $|\Psi_0\rangle$, this is due to difference in dipole and H_{PTV} coupling strengths between different CSFs.

Within the whole CSF space considered the value of $\vec{D}_a$ is 4.4438 58. In absolute terms this is down by 0.4804 56 compared to the lowest order result of 4.9243 136 computed in an earlier section. A major contribution to this difference is the many-body effects, this is because the direct contributions from the CSFs added to the configuration space is small. Which implies that the contribution from the many-body effects is just 10.81%

(a)   (b)
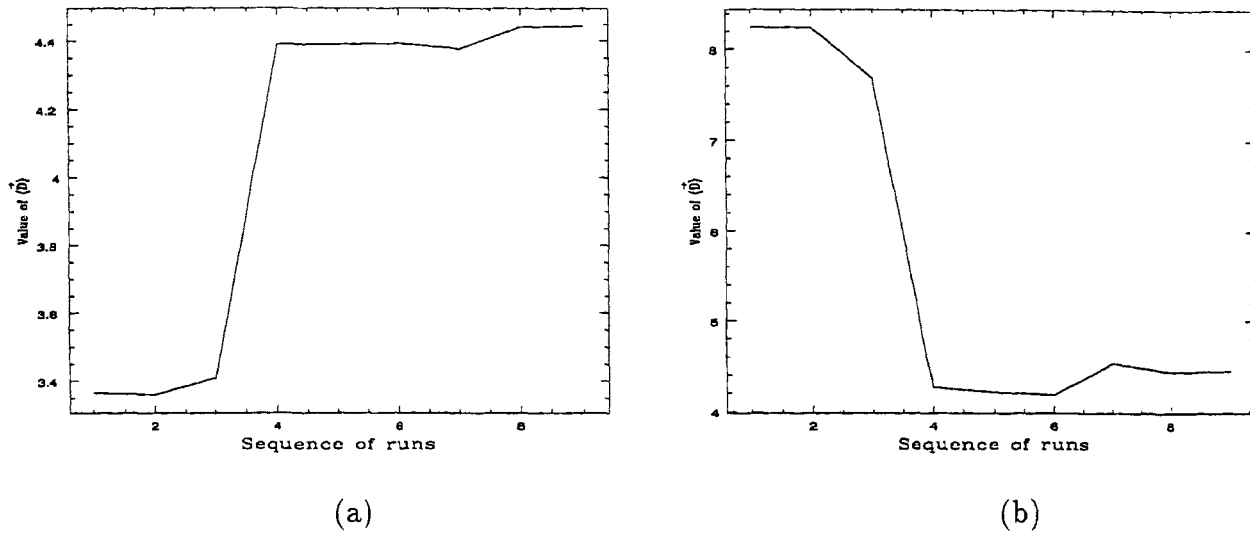
Figure 4.7: The value of $\vec{D}_a$

of the total value and the change is opposite in sign. An added advantage of the order by order approach is that the contribution to EDM can be computed in terms of the order of residual coulomb interaction. Earlier while computing the ground state ASF energy it was shown how a truncation in the order of H_{es} perturbation can give an inaccurate value of E_0.

4.5   The Size-Consistent Formulations

4.5.1   Size Consistency with the Linked Diagram Theorem

The simplest remedy to avoid the size inconsistent terms in the matrix based Bloch-equation formulation is to select only the linked terms in the computation. A very simple method is the CEPA-0 formalism. The wave-operators in this approach are computed iteratively and the renormalization terms are excluded from the Bloch equation. The wave-operators are then defined in terms of the excitation amplitudes. From the description in the previous chapter, the wave-operator with H_{es} as the perturbation in the even-parity CSF space in terms of excitation amplitudes are:

$$\Omega_{es}(1) = \sum_{ar} \left|\Phi_a^r\right\rangle\left\langle\Phi_0\right|x_a^r \text{ and } \Omega_{es}(2) = \sum_{abrs} \left|\Phi_{ab}^{rs}\right\rangle\left\langle\Phi_0\right|x_{ab}^{rs}.$$

Similarly, the wave-operators with the perturbation H_{PTV} included are

$$\Omega_{\mathrm{PTV}}(1) = \sum_{ar} \left|\overline{\Phi}_a^r\right\rangle\left\langle\Phi_0\right|\overline{x}_a^r \text{ and } \Omega_{\mathrm{PTV}}(2) = \sum_{ar} \left|\overline{\Phi}_{ab}^{rs}\right\rangle\left\langle\Phi_0\right|\overline{x}_{ab}^{rs}$$

The equation for the wave-operators $\Omega_{\mathrm{es}}(1)$ and $\Omega_{\mathrm{es}}(2)$ are

$$\left[\Omega_{\mathrm{es}}(1), H_0\right]P = \sum_{ar} \left[\left\langle\Phi_a^r\left|H_{\mathrm{es}}\right|\Phi_0\right\rangle + \sum_{a'r'}\left\langle\Phi_a^r\left|H_{\mathrm{es}}\right|\Phi_{a'}^{r'}\right\rangle x_{a'}^{r'} + \sum_{a'b'r's'}\left\langle\Phi_a^r\left|H_{\mathrm{es}}\right|\Phi_{a'b'}^{r's'}\right\rangle x_{a'b'}^{r's'}\right]$$
$$\left|\Phi_a^r\right\rangle\left\langle\Phi_0\right|$$

$$\left[\Omega_{\mathrm{es}}(2), H_0\right]P = \sum_{abrs} \left[\left\langle\Phi_{ab}^{rs}\left|H_{\mathrm{es}}\right|\Phi_0\right\rangle + \sum_{a'r'}\left\langle\Phi_{ab}^{rs}\left|H_{\mathrm{es}}\right|\Phi_{a'}^{r'}\right\rangle x_{a'}^{r'} + \sum_{a'b'r's'}\left\langle\Phi_{ab}^{rs}\left|H_{\mathrm{es}}\right|\Phi_{a'b'}^{r's'}\right\rangle x_{a'b'}^{r's'}\right]$$
$$\left|\Phi_{ab}^{rs}\right\rangle\left\langle\Phi_0\right|.$$

and the equations for the wave-operators $\Omega_{\mathrm{PTV}}(1)$ and $\Omega_{\mathrm{PTV}}(2)$ are

$$\left[\Omega_{\mathrm{PTV}}(1), H_0\right]P = \sum_{ar}\left[\left\langle\overline{\Phi}_a^r\left|H_{\mathrm{PTV}}\right|\Phi_0\right\rangle + \sum_{a'r'}\left\langle\overline{\Phi}_a^r\left|H_{\mathrm{PTV}}\right|\Phi_{a'}^{r'}\right\rangle x_{a'}^{r'} + \sum_{a'b'r's'}\left\langle\overline{\Phi}_a^r\left|H_{\mathrm{PTV}}\right|\Phi_{a'b'}^{r's'}\right\rangle x_{a'b'}^{r's'}\right.$$
$$\left. + \sum_{ct}\left\langle\overline{\Phi}_a^r\left|H_{\mathrm{es}}\right|\overline{\Phi}_c^t\right\rangle\overline{x}_c^t + \sum_{cdtu}\left\langle\overline{\Phi}_a^r\left|H_{\mathrm{es}}\right|\overline{\Phi}_{cd}^{tu}\right\rangle\overline{x}_{cd}^{tu}\right]\left|\overline{\Phi}_a^r\right\rangle\left\langle\Phi_0\right| \qquad (4.5)$$

$$\left[\Omega_{\mathrm{PTV}}(2), H_0\right]P = \sum_{abrs}\left[\sum_{a'b'r's'}\left\langle\overline{\Phi}_{ab}^{rs}\left|H_{\mathrm{PTV}}\right|\Phi_{a'b'}^{r's'}\right\rangle x_{a'b'}^{r's'}\right.$$
$$\left. + \sum_{ct}\left\langle\overline{\Phi}_{ab}^{rs}\left|H_{\mathrm{es}}\right|\overline{\Phi}_c^t\right\rangle\overline{x}_c^t + \sum_{cdtu}\left\langle\overline{\Phi}_{ab}^{rs}\left|H_{\mathrm{es}}\right|\overline{\Phi}_{cd}^{tu}\right\rangle\overline{x}_{cd}^{tu}\right]\left|\overline{\Phi}_{ab}^{rs}\right\rangle\left\langle\Phi_0\right| \qquad (4.6)$$

As discussed in the previous chapter, only the connected components are picked up from the term $\left\langle\Phi_{ab}^{rs}|H_{\mathrm{es}}|\Phi_{a'}^{r'}\right\rangle x_{a'}^{r'}$ in the equation for $\Omega_{\mathrm{es}}(2)$. The discussion on the implementation of the component selection scheme is given in a later section in this chapter. The results–the value of $\vec{D}_a$ and energies–obtained when compared with the results from cluster approach give a measure of the contribution from the renormalization terms in the Bloch-equation. The values of $\vec{D}_a$ computed using the sequence followed in the matrix based Bloch-equation are tabulated in Table 4.13. In this formalism, the renormalization terms and the many-body effects they give rise to are excluded. The value of $\vec{D}_a$ computed within the whole CSF space in this formalism is 5.9421 36 and exceeds the result from the matrix based method by 1.4982 78. Compared to the lowest order result it is higher by 1.0178 22. That is, the many-body effects arising from the size-consistent normal terms in the Bloch-equation increases the value of $\vec{D}_a$ whereas the effect of the renormalization

Table 4.13: Value of $\vec{D}_a$ computed using the CEPA-0 formalism.

Sl. no	No of CSFs		$\vec{D}_a$	Sl. no	No of CSFs		$\vec{D}_a$
	Even	Odd			Even	Odd	
1	9930	12	3.8250 23	10	7	17087	8.4499 64
2	9930	30	3.8426 96	11	19	17087	8.4499 64
3	9930	3648	3.9252 41	12	1243	17087	8.3408 14
4	9930	3846	5.7783 09	13	1390	17087	5.5126 26
5	9930	11676	5.7783 88	14	4435	17087	5.5091 16
6	9930	14070	5.7820 42	15	4448	17087	5.3769 11
7	9930	14100	5.8370 85	16	6713	17087	5.6132 71
8	9930	15768	5.9437 56	17	9094	17087	5.9275 26
9	9930	17087	5.9421 36				

terms tend to lower the value of $\vec{D}_a$. But, the many-body effects from the renormalization terms alone cannot be isolated as any change in the renormalization terms effects the other terms in the next order.

4.5.2 Cluster Based Formulation

The cluster based formalism is not an order by order formalism but an iterative scheme in which the Bloch equation is cast in terms of the order of excitation rather than the order of perturbation. Except for the cases where there is a change in the order of excitation the matrix elements of H_{es} used in order by order approach can still be used. Where there is a change in the order of excitation modifications are required in the matrix element generation so that it picks up only the connected components and leave out the unconnected contributions. Compared to size of the configuration space these are few and with little modifications this can be done.

4.5.2.1 The Singly Excited Amplitude Cluster Equation

Consider the cluster amplitude with only the residual coulomb interaction as the perturbation. The modified Bloch equation for the singly excited cluster amplitudes as given in Chapter3 is

$$\left[T_{es}(1), H_0\right] P = \sum_{ar} \left[\left\langle \Phi_a^r \middle| H_{es} \middle| \Phi_0 \right\rangle + \sum_{a'r'} \left\langle \Phi_a^r \middle| H_{es} \middle| \Phi_{a'}^{r'} \right\rangle \mathcal{T}_{a'}^{r'} + \sum_{a'b'r's'} \left\langle \Phi_a^r \middle| H_{es} \middle| \Phi_{a'b'}^{r's'} \right\rangle \mathcal{T}_{a'b'}^{r's'} - \left(\mathcal{T}_a^r W\right)^{EPV}\right] \middle| \Phi_a^r \right\rangle \left\langle \Phi_0 \middle|. \tag{4.7}$$

The diagrammatic representation of the first three terms in the single-excitation cluster operator equation are given in Fig4.8. The different terms in the cluster equation that
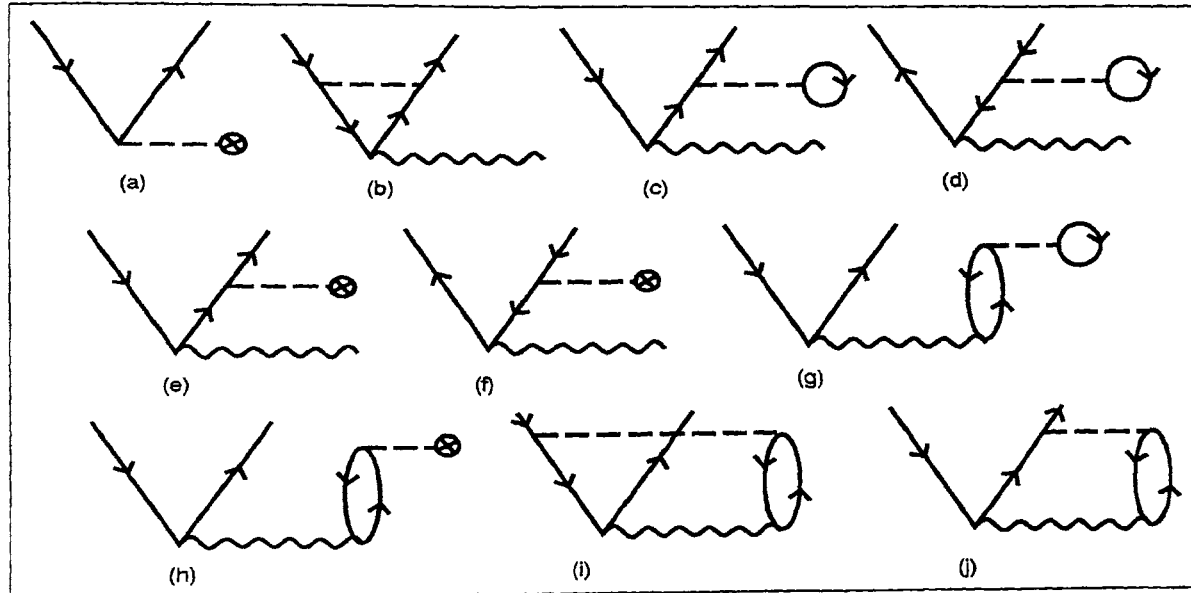
Figure 4.8: Diagrams that contributes to the single-excitation cluster amplitude.

correspond to each of the diagrams are as described:

- Diagram (a) contributes to the first term $\left\langle \Phi_a^r \middle| H_{es} \middle| \Phi_0 \right\rangle$ in the cluster equation. This term is independent of any cluster amplitudes and is an important term as the iteration will proceed from this term. Since it does not involve any of the cluster amplitudes at any stage of the iteration the contribution from this term is the same, that is what ever be the order of iteration the contribution from this term is always first order in H_{es}.

- The diagrams (b),(c),(d),(e) and (f) contributes to the second term $\langle\Phi_a^r|H_{es}|\Phi_{a'}^{r'}\rangle\mathcal{T}_{a'}^{r'}$. Here the H_{es} matrix element is coupled with the single excitation cluster amplitude. It starts contributing from the second iteration, where the cluster amplitude $\mathcal{T}_{a'}^{r'}$ is just the matrix element $\langle\Phi_{a'}^{r'}|H_{es}|\Phi_0\rangle$ in the first iteration.

- Diagrams (g),(h),(i) and (j) contributes to the third term $\langle\Phi_a^r|H_{es}|\Phi_{a'b'}^{r's'}\rangle\mathcal{T}_{a'b'}^{r's'}$ and couple the double excitation cluster amplitude with the H_{es} matrix element. This adds one more order of H_{es} to the all the terms that contribute to $\mathcal{T}_{a'b'}^{r's'}$, which implies that the lowest order in terms of H_{es} that contribute to this term is two. The same is true of the second term too. The first order contribution as stressed earlier is always picked up from the first term.

Consider diagrams (c) and (e), though they resemble the Hartree-Fock potential scattering diagram these are quite different. Take the the bubble part in diagram (c), it is summed over the occupied orbitals common to both the initial and the final CSFs in the matrix element of H_{es}. An example is if the initial and final CSFs are $|\Phi_{a'b'}^{r's'}\rangle = |7s^2\rangle$ and $|\Phi_{ab}^{rs}\rangle = |7s8s\rangle$ respectively, the bubble part in (c) has all the occupied orbitals except the $6s$ orbital. This is because both the CSF does not have $6s$, where as in the Hartree-Fock scattering diagram the bubble should have contribution from all the occupied orbitals. A similar description is true of diagrams (d) and (f) too.

The first three terms does not introduce any unlinked diagrams as the wave-operator is linear in cluster operator $\Omega_{es} = 1 + T_{es}(1) + T_{es}(2)$. Non-linear terms like $T_{es}(1)^2$ can produce unlinked diagrams that contribute to single excitation cluster amplitude equation. The linear approximation is justified as the configurations space is confined only upto double excitation and the contribution from the non-linear term $T_{es}(1)^2$ to the double excitation wave operator is small.

The renormalization term $\mathcal{T}_a^r W$ has both EPV and EPO terms, out of which only the EPV terms are included in the equation. The EPO part is discarded as these are unlinked terms. With suitable rearrangements it can be shown that $(\mathcal{T}_a^r W)^{EPV}$ is same as the linked EPV contribution from terms non-linear in cluster amplitude in the equation but with a negative sign, which is taken care of by the negative sign of the renormalization term.

With these terms in the equation, terms non-linear in cluster amplitude are included in the expression for the wave-operator. The non-linear terms included through $(\mathcal{T}_a^r W)^{\mathrm{EPV}}$ are $T_{es}(1)^2$ and $T_{es}(1)T_{es}(2)$, that is second order terms involving $T_{es}(1)$ amplitude will be included in the single excitation amplitude equation. This implies that the wave-operator assumes the form

$$\Omega_{es} = 1 + T_{es}(1) + T_{es}(2) + \Big[T_{es}(1)T_{es}(1) + T_{es}(1)T_{es}(2) + T_{es}(2)T_{es}(2) \Big]^{\mathrm{EPV}} \qquad (4.8)$$

Terms that are not included in the single excitation cluster amplitude equation are

$$\Big[T_{es}(1)T_{es}(1) + T_{es}(1)T_{es}(2) + T_{es}(2)T_{es}(2) \Big]^{\mathrm{EPO}}.$$

In a later section will discuss how to choose the EPV terms that originate from the renormalization term.

4.5.2.2   The Doubly Excited Cluster Amplitude Equation

The modified Bloch equation for the doubly excited cluster amplitudes as given in Chapter:3 is

$$\begin{aligned}
\Big[T_{es}(2), H_0 \Big] P &= \sum_{abrs} \Bigg[\Big\langle \Phi_{ab}^{rs} \Big| H_{es} \Big| \Phi_0 \Big\rangle + \sum_{a'r'} \Big\langle \Phi_{ab}^{rs} \Big| H_{es} \Big| \Phi_{a'}^{r'} \Big\rangle \mathcal{T}_{a'}^{r'} + \sum_{a'b'r's'} \Big\langle \Phi_{ab}^{rs} \Big| H_{es} \Big| \Phi_{a'b'}^{r's'} \Big\rangle \mathcal{T}_{a'b'}^{r's'} - \\
&\quad \Big(\mathcal{T}_{ab}^{rs} W \Big)^{\mathrm{EPV}} \Bigg] \Big| \Phi_{ab}^{rs} \Big\rangle \Big\langle \Phi_0 \Big|.
\end{aligned} \qquad (4.9)$$

The diagrammatic representation of the first three terms in the above equation are given in Fig4.9. The terms in the double-excitation cluster-operator equation can be simplified further. The first term is quite trivial and is the double excitation counter part of the first term in the single excitation cluster amplitude equation. The second term can be expanded to individual terms as

$$\begin{aligned}
\sum_{a'r'} \Big\langle \Phi_{ab}^{rs} \Big| H_{es} \Big| \Phi_{a'}^{r'} \Big\rangle \mathcal{T}_{a'}^{r'} &= \Big\langle \Phi_{ab}^{rs} \Big| H_{es} \Big| \Phi_a^r \Big\rangle \mathcal{T}_a^r + \sum_{a' \neq a,b} \Big\langle \Phi_{ab}^{rs} \Big| H_{es} \Big| \Phi_{a'}^r \Big\rangle \mathcal{T}_{a'}^r + \sum_{r' \neq r,s} \Big\langle \Phi_{ab}^{rs} \Big| H_{es} \Big| \Phi_a^{r'} \Big\rangle \mathcal{T}_a^{r'} \\
&\quad + \sum_{a' \neq a,b} \Big\langle \Phi_{ab}^{rs} \Big| H_{es} \Big| \Phi_{a'}^s \Big\rangle \mathcal{T}_{a'}^s + \sum_{r' \neq r,s} \Big\langle \Phi_{ab}^{rs} \Big| H_{es} \Big| \Phi_b^{r'} \Big\rangle \mathcal{T}_b^{r'}
\end{aligned}$$

The first term on the right has both connected and disconnected terms, for cluster equations only the connected term should be retained. The remaining terms are connected and
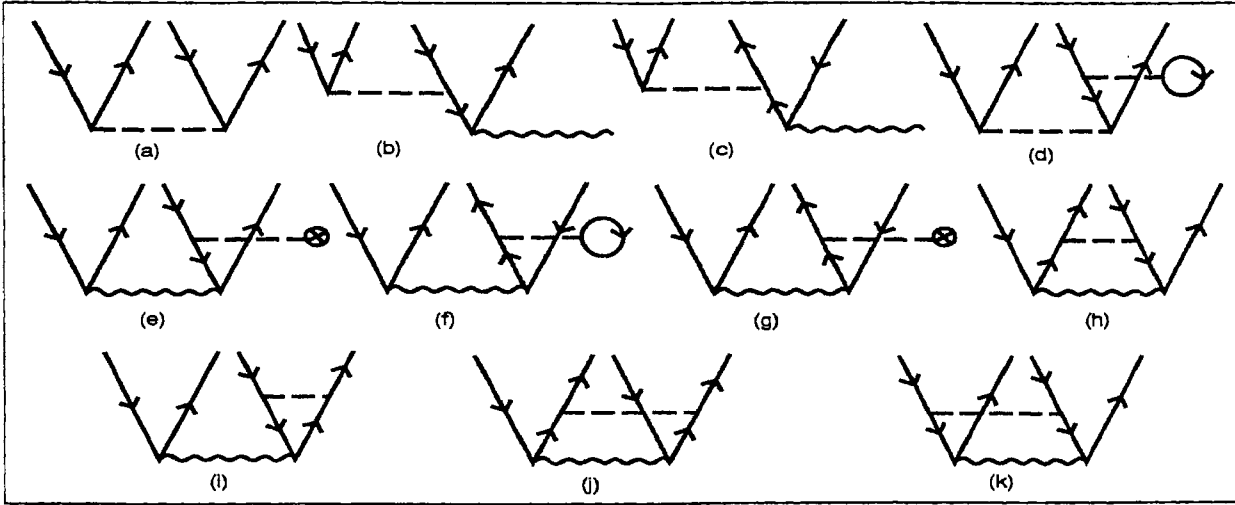
Figure 4.9: The diagrams for the terms in doubly-excited cluster operator equation.

hence linked too. Terms with $a' \neq a, b; r' \neq r, s$ does not contribute as these are triple excitations. The above equation can then be written as

$$\sum_{a'r'} \langle \Phi_{ab}^{rs} | H_{es} | \Phi_{a'}^{r'} \rangle \mathcal{T}_{a'}^{r'} = \left[\langle \Phi_{ab}^{rs} | H_{es} | \Phi_{a}^{r} \rangle \mathcal{T}_{a}^{r} \right]_{conn} + \sum_{r' \neq r, s} \left(\delta_{a'a} + \delta_{a'b} \right) \langle \Phi_{ab}^{rs} | H_{es} | \Phi_{a'}^{r'} \rangle \mathcal{T}_{a'}^{r'}$$

$$+ \sum_{a' \neq a, b} \left(\delta_{r'r} + \delta_{r's} \right) \langle \Phi_{ab}^{rs} | H_{es} | \Phi_{a'}^{r'} \rangle \mathcal{T}_{a'}^{r'}$$

Similarly, the third term can be expanded to

$$\sum_{a'b'r's'} \langle \Phi_{ab}^{rs} | H_{es} | \Phi_{a'b'}^{r's'} \rangle \mathcal{T}_{a'b'}^{r's'} = \sum_{b' \neq a, b' \neq r, s} \sum \langle \Phi_{ab}^{rs} | H_{es} | \Phi_{ab'}^{rs'} \rangle \mathcal{T}_{ab'}^{rs'} + \sum_{r' \neq r, s} \left[\langle \Phi_{ab}^{rs} | H_{es} | \Phi_{ab}^{r's} \rangle \mathcal{T}_{ab}^{r's} \right.$$

$$+ \sum_{s' \neq r, s} \langle \Phi_{ab}^{rs} | H_{es} | \Phi_{ab}^{r's'} \rangle \mathcal{T}_{ab}^{r's'} \right] + \sum_{a' \neq a, b} \left[\langle \Phi_{ab}^{rs} | H_{es} | \Phi_{a'b}^{rs} \rangle \mathcal{T}_{a'b}^{rs} \right.$$

$$+ \sum_{b' \neq a, b} \langle \Phi_{ab}^{rs} | H_{es} | \Phi_{a'b'}^{rs} \rangle \mathcal{T}_{a'b'}^{rs} \right].$$

Here all the terms are connected and terms that are triply and quadruply excited have been excluded. Each of the diagrams will have an exchange diagram too. Terms that correspond to each of the diagrams are:

- Diagram (a) correspond to the first term in the cluster equation and has no dependence any of the cluster amplitude.

- $\langle \Phi_{ab}^{rs} | H_{es} | \Phi_{a}^{r} \rangle \mathcal{T}_{a}^{r}$ contribute to diagrams (b) and (c). The final CSF in this term has a pair of hole-particle pair in common with the cluster amplitude, which means when

the connected diagrams from this term are considered one hole/particle state does not change after the H_{es} interaction. This type of diagram belong to the first type of EPV term as classified by Kelly. The diagram (b) correspond to the hole line EPV diagram and diagram (c) to particle line EPV diagram.

- $(\delta_{a'a} + \delta_{a'b})\langle\Phi_{ab}^{rs}|H_{es}|\Phi_{a'}^{r'}\rangle\mathcal{T}_{a'}^{r'}$ contribute to diagram (c). Though the topology of the diagram is same as that of $\langle\Phi_{ab}^{rs}|H_{es}|\Phi_a^r\rangle\mathcal{T}_a^r$, it is an EPO diagram. Here the H_{es} interaction changes the state of the particle and picks up the effect of core-virtual correlation, which can be classified as core-polarization effect.

- $(\delta_{r'r} + \delta_{r's})\langle\Phi_{ab}^{rs}|H_{es}|\Phi_{a'}^{r'}\rangle\mathcal{T}_{a'}^{r'}$ contribute to diagram (b). This also has similar topology with $\langle\Phi_{ab}^{rs}|H_{es}|\Phi_a^r\rangle\mathcal{T}_a^r$ but is again an EPO diagram. In this term the hole state get changed and correspond to core-core correlation effect, where one of the core gets excited to virtual state and the hole state in the cluster amplitude just change its state.

- $\langle\Phi_{ab}^{rs}|H_{es}|\Phi_{ab'}^{rs'}\rangle\mathcal{T}_{ab'}^{rs'}$ contribute to diagram (h) and (i). These are EPO diagrams where a hole-particle change to another hole-particle pair. These are the terms which include the core-virtual correlation effects.

- The term $\langle\Phi_{ab}^{rs}|H_{es}|\Phi_{ab}^{r's}\rangle\mathcal{T}_{ab}^{r's}$ contribute to diagrams (f) and (g). These are EPO diagrams where one of the particle states in $\mathcal{T}_{ab}^{r's}$ has been excited to another particle state. This term can also contribute to EPV diagrams of the first kind, if it is a hole-line EPV diagram then it will correspond to (h) and (i) and if it is particle line EPV then diagram (j).

- $\langle\Phi_{ab}^{rs}|H_{es}|\Phi_{ab}^{r's'}\rangle\mathcal{T}_{ab}^{r's'}$ contribute to diagram (j). This is a double excitation where the particle states from the cluster amplitude $\mathcal{T}_{ab}^{r's'}$ are excited different particle states but the hole states in the remain the same. These terms can capture the correlation effects due to the virtual-virtual orbitals.

- $\langle\Phi_{ab}^{rs}|H_{es}|\Phi_{a'b}^{rs}\rangle\mathcal{T}_{a'b}^{rs}$ contribute to diagram (d) and (e). This term correspond to change of the hole and captures the single-body hole-hole interaction component. These are

both EPO diagrams with the effective single-body interaction. It can contribute to the EPV diagrams, the hole line EPV diagram arising from this term is (k) and the particle line EPV diagrams are (h) and (i).

- $\langle \Phi_{ab}^{rs} | H_{es} | \Phi_{a'b'}^{rs} \rangle \mathcal{T}_{a'b'}^{rs}$ contribute to (j) and is the hole-hole correlation term.

Thus terms in the cluster equation contributes to different physical effects. So far only the first three terms in the cluster equation have been considered. The last term in the doubly excited cluster amplitude $(\mathcal{T}_{ab}^{rs} W)^{\mathrm{EPV}}$ is a renormalization term. It picks up a set of terms non-linear in cluster amplitude and these are:

$$T_{\mathrm{es}}(1)T_{\mathrm{es}}(2) + T_{\mathrm{es}}(2)T_{\mathrm{es}}(2).$$

That is, this term picks up a selected class of EPV terms having the cluster amplitude $T_{\mathrm{es}}(2)$ and non-linear in cluster amplitude. Consider the expression for W

$$W = PH_{\mathrm{es}}\Big(T_{\mathrm{es}}(1) + T_{\mathrm{es}}(2)\Big)P.$$

The non-linear cluster amplitude term $T_{\mathrm{es}}(1)T_{\mathrm{es}}(2)$ is picked up through the term $PH_{\mathrm{es}}T_{\mathrm{es}}(1)P$ in W. This implies that the term $(\mathcal{T}_{ab}^{rs} P H_{\mathrm{es}} T_{\mathrm{es}}(1))^{\mathrm{EPV}}$ can have one hole/particle EPV line or a pair of hole-particle EPV lines. Where as in the single excitation cluster amplitude equation, contribution from $T_{\mathrm{es}}(1)T_{\mathrm{es}}(2)$ is captured through the term $(\mathcal{T}_a^r P H_{\mathrm{es}} T_{\mathrm{es}}(2))^{\mathrm{EPV}}$ in $(\mathcal{T}_a^r W)^{\mathrm{EPV}}$. The number of EPV hole-lines or EPV particle-lines in this term is the same as in $PH_{\mathrm{es}}T_{\mathrm{es}}(1)P$. In general the number of EPV hole-lines and particle-lines in $(T_{\mathrm{es}}(n)PH_{\mathrm{es}}T_{\mathrm{es}}(m)P)^{\mathrm{EPV}}$ is limited by by H_{es} if $m,n > 2$ and by cluster amplitudes if $m < 2$ or $n < 2$. Though the term $T_{\mathrm{es}}(1)T_{\mathrm{es}}(2)$ is included in both the single as well as the double excitation cluster amplitude the topology of their diagrammatic representations are different. Diagrams from $(\mathcal{T}_a^r W)^{\mathrm{EPV}}$ has only a pair of hole-particle lines where as $(\mathcal{T}_{ab}^{rs} W)^{\mathrm{EPV}}$ has two pairs of hole-particle lines.

4.5.2.3 Selection of EPV Terms and Connected Terms

As the formulation is based on CSF matrix elements, terms linear in the cluster amplitude does not introduce EPV diagrams. Because, terms linear in cluster amplitude can be

EPV only when there are CSFs which violate exclusion principle, which is not possible. The EPV diagrams arises from renormalization terms which are non-linear in cluster amplitude . The diagrams representing the renormalization terms are just the cluster diagrams multiplied by energy diagrams and hence unlinked but these can suitably be rearranged to give connected diagrams.

As a step in selecting the EPV terms all the orbitals–the occupied as well as the virtual– are given integer labels. These labels are chosen to be prime numbers. Since each CSF can be identified by the hole and particle states in it, each CSF can be identified by the product of the prime number labels of these holes and particles. For the ith CSF let this number be N_i. Along with this, the labels of the holes and particles are also retained and for the ith CSF let these be k_i, l_i, m_i and n_i. These five numbers–the hole/particle labels and their product–are sufficient to identify a CSF as the configuration space has CSFs till double excitation only. If the CSF is singly excited, then only three numbers are required to identify it–the label for the hole and particle and their product. To maintain consistency the remaining two indices are filled with another prime number not used in labeling the occupied/virtual orbitals. Let this prime number be N_p. According to this scheme, the ground/reference state is identified by $(N_p)^4, N_p, N_p, N_p$ and N_p. Similarly, labels are also given to the cluster amplitudes.

Once the CSFs and cluster amplitudes are labelled the required terms $(\mathcal{T}_a^r W)^{EPV}$ are those where the number N identifying the CSF in W can be divided by one or more of the numbers in $klmn$ identifying the cluster amplitude $\mathcal{T}_a^r$. The number of possible division is the number of common hole/particle lines between $\mathcal{T}_a^r$ and W. During the selection process division by N_p should be discarded as this does not represent any hole of particle states.

The term $\langle \Phi_{ab}^{rs} | H_{es} | \Phi_{a'}^{r'} \rangle \mathcal{T}_{a'}^{r'}$ in the doubly excited cluster amplitude equation has disconnected components if both the hole and particle states in the initial CSF are present in the final CSF. These should be discarded and only the connected components should be chosen. This is implemented while computing the matrix elements of H_{es}. During the matrix element computation using the initial and final CSF labels the total number of hole states are computed. If this is equal to three then these are the terms that will contribute

to $\langle\Phi_{ab}^{rs}|H_{\text{es}}|\Phi_{a'}^{r'}\rangle\mathcal{T}_{a'}^{r'}$. In the next step the connected component is chosen by selecting the H_{es} matrix element which has r'. With this the doubly excited cluster amplitude equation has only connected components. Though disconnected the discarded components are still linked.

4.5.2.4   The computation of the cluster amplitudes $T_{\text{PTV}}(1)$ and $T_{\text{PTV}}(2)$

After computing the cluster amplitudes $T_{\text{es}}(1)$ and $T_{\text{es}}(2)$, to compute the expectation value $\vec{D}_a$ the next step is the computation of cluster amplitudes $T_{\text{PTV}}(1)$ and $T_{\text{PTV}}(2)$. The equation for the cluster amplitude $T_{\text{PTV}}(1)$ from Chapter3 is

$$\left[T_{\text{PTV}}(1), H_0\right]P = \sum_{ar}\left[\langle\overline{\Phi}_a^r|H_{\text{PTV}}|\Phi_0\rangle + \sum_{a'r'}\langle\overline{\Phi}_a^r|H_{\text{PTV}}|\Phi_{a'}^{r'}\rangle\mathcal{T}_{a'}^{r'} + \sum_{a'b'r's'}\langle\overline{\Phi}_a^r|H_{\text{PTV}}|\Phi_{a'b'}^{r's'}\rangle\mathcal{T}_{a'b'}^{r's'}\right.$$
$$+ \sum_{ct}\langle\overline{\Phi}_a^r|H_{\text{es}}|\overline{\Phi}_c^t\rangle\overline{\mathcal{T}}_c^t + \sum_{cdtu}\langle\overline{\Phi}_a^r|H_{\text{es}}|\overline{\Phi}_{cd}^{tu}\rangle\overline{\mathcal{T}}_{cd}^{tu}$$
$$\left.- \left(\overline{\mathcal{T}}_a^r W\right)^{\text{EPV}}\right]|\overline{\Phi}_a^r\rangle\langle\Phi_0| \tag{4.10}$$

and the equation for the cluster amplitude $T_{\text{PTV}}(2)$ is:

$$\left[T_{\text{PTV}}(2), H_0\right]P = \sum_{abrs}\left[\sum_{a'b'r's'}\langle\overline{\Phi}_{ab}^{rs}|H_{\text{PTV}}|\Phi_{a'b'}^{r's'}\rangle\mathcal{T}_{a'b'}^{r's'} + \sum_{ct}\langle\overline{\Phi}_{ab}^{rs}|H_{\text{es}}|\overline{\Phi}_c^t\rangle\overline{\mathcal{T}}_c^t + \right.$$
$$\left.\sum_{cdtu}\langle\overline{\Phi}_{ab}^{rs}|H_{\text{es}}|\overline{\Phi}_{cd}^{tu}\rangle\overline{\mathcal{T}}_{cd}^{tu} - \left(\overline{\mathcal{T}}_{ab}^{rs} W\right)^{\text{EPV}}\right]|\overline{\Phi}_{ab}^{rs}\rangle\langle\Phi_0|. \tag{4.11}$$

In the above equations $\mathcal{T}_a^r$ and $\mathcal{T}_{ab}^{rs}$ are the cluster amplitudes computed with H_{es} as perturbation. As it is a single-reference computation W has no contribution from the odd-parity CSF space. It is the same as in the computation of $T_{\text{es}}(1)$ and $T_{\text{es}}(2)$. The same procedure in computing $T_{\text{es}}(1)$ and $T_{\text{es}}(2)$ are used to select the connected terms from the cluster amplitude equation of $T_{\text{PTV}}(1)$ and $T_{\text{PTV}}(2)$. To understand the effect of size inconsistent terms, three sequences of computations are done. First T_{es} is computed with EPV renormalization terms but $T_{\text{PTV}}(1)$ and $T_{\text{PTV}}(1)$ are computed without the renormalization terms, second T_{es} are computed with the EPV renormalization terms and $T_{\text{PTV}}(1)$ and $T_{\text{PTV}}(1)$ are computed with the full renormalization term and finally all the cluster amplitudes are computed by selecting only the EPV terms in the cluster equations. The results of these computations are the contents of the next section.

Once all the required cluster amplitudes are computed the wave-operators are defined as

$$\Omega_{\mathrm{es}} = T_{\mathrm{es}}(1) + T_{\mathrm{es}}(2) \quad \text{and} \quad \Omega_{es,edm} = T_{\mathrm{PTV}}(1) + T_{\mathrm{PTV}}(2).$$

Using these cluster amplitudes the expectation value $\vec{D}_a$ can be computed using the expression

$$\vec{D}_a = 2\Big\langle \Phi_0 \Big| \Omega_{\mathrm{es}}^\dagger \vec{D} \Omega_{es,edm} \Big| \Phi_o \Big\rangle.$$

In terms of computation the selection procedure of the EPV terms make it slower compared to the ordinary matrix based Bloch-equation implementation. This is due to the conditional statements required during the EPV renormalization term selection procedure, due to which this method compromises the gain in using Bloch-equation based formulations over the matrix diagonalization schemes. But this method has the advantage of a stronger foundation on many-body physics as it is a size-consistent method. As pointed out earlier it does leave out certain size-consistent terms which are non-linear in the cluster amplitude and EPO but it is a very good approximation as the contribution from these terms is expected to be very small.

4.5.2.5   Results

The computation of $\vec{D}_a$ requires the wave-operators Ω_{es} and $\Omega_{es,edm}$. As described in the earlier section an important part of the non-linear cluster amplitudes can be included in the cluster amplitude equation by choosing appropriate terms. Consider the cluster amplitudes T_{es} computed with the equations (4.10) and (4.11) but cluster amplitudes $T_{es,edm}$ are computed using the equations

$$\Big[T_{\mathrm{PTV}}(1), H_0 \Big] P = \sum_{ar} \Bigg[\Big\langle \overline{\Phi}_a^r \Big| H_{\mathrm{PTV}} \Big| \Phi_0 \Big\rangle + \sum_{a'r'} \Big\langle \overline{\Phi}_a^r \Big| H_{\mathrm{PTV}} \Big| \Phi_{a'}^{r'} \Big\rangle \mathcal{T}_{a'}^{r'} + \sum_{a'b'r's'} \Big\langle \overline{\Phi}_a^r \Big| H_{\mathrm{PTV}} \Big| \Phi_{a'b'}^{r's'} \Big\rangle \mathcal{T}_{a'b'}^{r's'}$$
$$+ \sum_{ct} \Big\langle \overline{\Phi}_a^r \Big| H_{\mathrm{es}} \Big| \overline{\Phi}_c^t \Big\rangle \overline{\mathcal{T}}_c^t + \sum_{cdtu} \Big\langle \overline{\Phi}_a^r \Big| H_{\mathrm{es}} \Big| \overline{\Phi}_{cd}^{tu} \Big\rangle \overline{\mathcal{T}}_{cd}^{tu} - \mathcal{T}_a^r W \Bigg] \Big| \overline{\Phi}_a^r \Big\rangle \Big\langle \Phi_0 \Big| \quad (4.12)$$

and

$$\Big[T_{\mathrm{PTV}}(2), H_0 \Big] P = \sum_{abrs} \Bigg[\sum_{a'b'r's'} \Big\langle \overline{\Phi}_{ab}^{rs} \Big| H_{\mathrm{PTV}} \Big| \Phi_{a'b'}^{r's'} \Big\rangle \mathcal{T}_{a'b'}^{r's'} + \sum_{ct} \Big\langle \overline{\Phi}_{ab}^{rs} \Big| H_{\mathrm{es}} \Big| \overline{\Phi}_c^t \Big\rangle \overline{\mathcal{T}}_c^t$$
$$+ \sum_{cdtu} \Big\langle \overline{\Phi}_{ab}^{rs} \Big| H_{\mathrm{es}} \Big| \overline{\Phi}_{cd}^{tu} \Big\rangle \overline{\mathcal{T}}_{cd}^{tu} - \mathcal{T}_{ab}^{rs} W \Bigg] \Big| \overline{\Phi}_{ab}^{rs} \Big\rangle \Big\langle \Phi_0 \Big|. \quad (4.13)$$

That is the cluster amplitudes $\overline{T}_a^r$ and $\overline{T}_{ab}^{rs}$ are computed along with the EPO-renormalization terms $(\overline{T}_a^r W)^{\mathrm{EPO}}$ and $(\overline{T}_{ab}^{rs} W)^{\mathrm{EPO}}$, which are size-inconsistent terms as they are unlinked. From these cluster amplitudes the wave-operators Ω_{es} and $\Omega_{es,edm}$ can be computed. The wave-operator Ω_{es} is size-consistent and $\Omega_{es,edm}$ is different from the matrix based Bloch equation implementation in the following ways

- The terms other than the renormalization in equations (4.12) and (4.13) doesn't introduce disconnected terms. But in the matrix based Bloch equation the non-renormalization terms include disconnected terms and leads to inclusion of size-inconsistent terms.

- Ω_{es} is connected and enters into the cluster amplitudes $\overline{T}_a^r$ and $\overline{T}_{ab}^{rs}$ through $\mathcal{T}_a^r$ and $\mathcal{T}_{ab}^{rs}$ in eq(4.5) and (4.6).

The results for a sequence of runs are tabulated in Table4.14. As in the Bloch-equation case the computation has two sequences, first the number of even-parity CSF is kept fixed and the number of odd-parity CSF is increased and in the second this is reversed. Comparing the value of $\vec{D}_a$ calculated using cluster amplitudes $\mathcal{T}_a^r, \mathcal{T}_{ab}^{rs}$, $\overline{T}_a^r$ and $\overline{T}_{ab}^{rs}$ and matrix Bloch-equation gives a measure of the following contributions:

- Terms other than the connected-EPV terms in $\Omega_{es,edm}$, that is the contribution from $(T_{es}W)^{\mathrm{EPO}}$.

- The disconnected components in the non-renormalization terms. This is because computation in matrix Bloch-equation does not distinguish between different terms, where as in cluster approach only the connected terms from the non-renormalization terms are selected.

With the condition that the contribution from the EPO connected terms is less important compared to the EPV terms, the difference between this result and matrix based Bloch-equation result gives an estimate of the contribution from the size inconsistent terms. For ·the first sequence, where the number of even-parity CSF is fixed and odd-parity CSF is slowly increased, the maximum difference here is compared with the Bloch-equation.

Table 4.14: Values of $\vec{D}_a$ computed with the EPO components included in the cluster amplitudes $\mathcal{T}$.

Sl. no	No of CSFs		$\vec{D}_a$	Sl. no	No of CSFs		$\vec{D}_a$
	Even	Odd			Even	Odd	
1	9930	12	3.1704 91	10	7	17087	8.4499 64
2	9930	30	3.1682 67	11	19	17087	8.4499 64
3	9930	3648	3.2196 53	12	1243	17087	7.8521 84
4	9930	3846	4.2130 96	13	1390	17087	4.3783 45
5	9930	11676	4.2130 54	14	4435	17087	4.3042 71
6	9930	14070	4.2147 05	15	4448	17087	4.2332 39
7	9930	14100	4.2039 41	16	6713	17087	4.2802 30
8	9930	15768	4.2539 59	17	9094	17087	4.2375 23
9	9930	17087	4.2446 91	18			

In the plot given in Figure:4.10 $\Delta\vec{D}_a$ denotes the difference in the value of $\vec{D}_a$ computed with the matrix Bloch-equation formalism and the wave-operator $\Omega_{es,edm}$ which has the EPO component in the renormalization term. The maximum difference occurs for the run with 6713 even-parity CSFs and 17087 odd-parity CSFs, here the value of $\Delta\vec{D}_a$ is 0.2950 36 and is 6.53% of the total value. That is, computing the wave-operator Ω_{es} in a size consistent form with only the EPV renormalization terms included in the cluster equation suppresses $\vec{D}_a$ by 6.52%. As to be expected, the change in the slope of the plots shows that the effect of the term $(\mathcal{T}W)^{EPO}$ depends on the form of the CSFs included.

Another property that can be compared to gain an insight on the contribution of the size-inconsistent term is the energy of the ground state E_0. The value of E_0 computed using the wave-operator Ω_{es} derived here has no contribution from the size inconsistent terms but it excludes some of the less important size-consistent terms. The difference in the value E_0 computed using the Bloch-equation and Ω_{es} derived from the cluster equation gives the contribution from the size inconsistent terms. Like in $\vec{D}_a$ the approximation is that the contribution form the EPO size consistent terms non-linear in cluster amplitudes is very small. then the difference in the result can in principle be accounted to the size inconsistent terms.

(a)   (b)
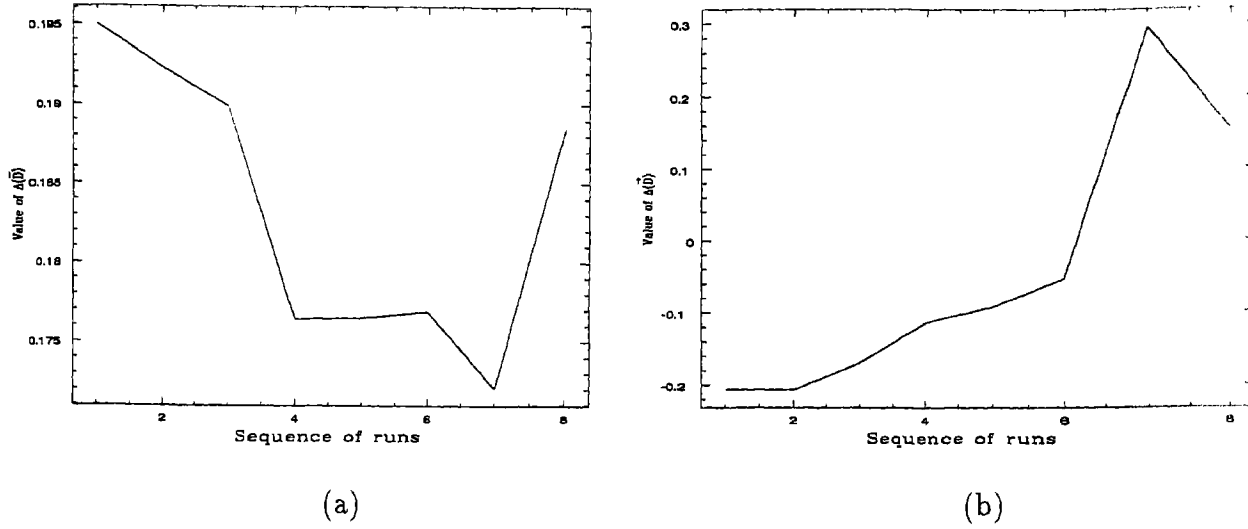
Figure 4.10: The difference in the value of $\vec{D}_a$ computed with the Bloch-equation method and the one computed with the EPO terms included in $\Omega_{es,edm}$

Table 4.15: Values of $\vec{D}_a$ computed with $\mathcal{T}$ and $\overline{\mathcal{T}}$ without the renormalization terms

Sl. no	No of CSFs		$\vec{D}_a$	Sl. no	No of CSFs		$\vec{D}_a$
	Even	Odd			Even	Odd	
1	9930	12	4.0881 90	10	7	17087	8.4499 64
2	9930	30	4.1068 68	11	19	17087	8.4499 64
3	9930	3648	4.1930 93	12	1243	17087	8.3422 09
4	9930	3846	6.0871 38	13	1390	17087	5.8034 52
5	9930	11676	6.0872 28	14	4435	17087	5.7982 02
6	9930	14070	6.0911 65	15	4448	17087	5.6605 25
7	9930	14100	6.1507 87	16	6713	17087	5.9071 87
8	9930	15768	6.2649 69	17	9094	17087	6.2474 91
9	9930	17087	6.2635 39				

One way to check the contribution from a particular term is to do the computation with and without it, then compare the results. The earlier sequence of runs have established the magnitude of the contribution from the EPO terms. The over all contribution of the renormalization term in the cluster amplitudes $\overline{\mathcal{T}}$ can be estimated by computing the cluster amplitudes $\overline{\mathcal{T}}_a^r$ and $\overline{\mathcal{T}}_{ab}^{rs}$ without the renormalization terms, then compare the

results with the values computed with the renormalization terms included. These cluster amplitudes can be computed using the cluster equations (4.5) and (4.6), except that the

Table 4.16: Values of $\vec{D}_a$ computed with CEPA-2.

Sl. no	No of CSFs		$\vec{D}_a$	Sl. no	No of CSFs		$\vec{D}_a$
	Even	Odd			Even	Odd	
1	9930	12	3.3130 75	10	7	17087	8.4499 64
2	9930	30	3.3133 86	11	19	17087	8.4499 64
3	9930	3648	3.3684 39	12	1243	17087	7.8528 23
4	9930	3846	4.4589 69	13	1390	17087	4.3791 81
5	9930	11676	4.4589 33	14	4435	17087	4.3758 71
6	9930	14070	4.4608 15	15	4448	17087	4.3558 36
7	9930	14100	4.4581 78	16	6713	17087	4.4547 38
8	9930	15768	4.5149 07	17	9094	17087	4.4981 25
9	9930	17087	4.5065 25				

excitation amplitudes in these equations should be replaced with the cluster amplitudes. The cluster amplitudes $\mathcal{T}_a^r$ and $\mathcal{T}_{ab}^{rs}$ which includes the effect of renormalization terms are computed using the equations (4.7) and (4.9).The value of $\vec{D}_a$ calculated using the wave-operator got from the cluster amplitudes computed using the above cluster equations are as given in Table 4.15. The form of the wave-operators Ω_{es} and $\Omega_{es,edm}$ in the earlier computations do not include the EPV-renormalization terms at the same time. All the cluster amplitudes can be made size consistent using the cluster amplitude equations with only the EPV-renormalization terms. The Values of $\vec{D}_a$ computed using the sequence of runs followed so far are tabulated in Table 4.16.

4.6 Schiff Moment in Atomic Yb

Unlike the atomic EDM due to TPT-electron-nucleus interaction, only the first order computation of Schiff moment induced atomic EDM is presented. This is more of an exploratory computation. Computation of Schiff moment require $\mathcal{B}$ given in eq(2.7). To get $\mathcal{B}$, $(P_{n'1}(r)P_{n-1}(r) + Q_{n'1}(r)Q_{n-1}(r))$ is evaluated at the first ten grid points and a

power series is fitted using general least square fit as in eq(2.8). The power series is then divided by r^3. Which gives

$$\left\langle n'p* \left| H_S \right| ns \right\rangle = \frac{S}{I(I+1)} I_z \mathcal{B}$$

For the $6p*$ orbital using a power series with $N = 5$ gives the value of $a_3 = -4605.3404\,79$. To get the Schiff moment induced atomic EDM this is to be multiplied by appropriate factors arising from the nuclear sector. A similar evaluation can be done by changing the number of grid points considered in the product of the orbitals and terms in the power series expansion. An important result got from the fit is that the coefficients a_1 and a_2 are very small and can be neglected, if it were not value of $\mathcal{B}$ would have diverge.

The next step in the computation of the atomic EDM due to the Schiff moment is to compute the expectation value of the dipole operator. That is, the expression for the atomic EDM arising from the Schiff moment involving only the most important orbitals is

$$\vec{D}_a = \frac{2\left\langle 6s_{1/2} \left| \vec{D} \right| 6p_{1/2} \right\rangle \left\langle 6p_{1/2} \left| H_s \right| 6s_{1/2} \right\rangle}{\epsilon_{6s_{1/2}} - \epsilon_{6p_{1/2}}}.$$

Where $\epsilon_{6s_{1/2}}$ and $\epsilon_{6p_{1/2}}$ are the single particle energies of the spin orbitals $6s_{1/2}$ and $6p_{1/2}$ respectively. For the orbitals considered the values of the single particle energies are $\epsilon_{6s_{1/2}} = -0.1965\,16$ hartrees and $\epsilon_{6p_{1/2}} = -0.1244\,56$ respectively. Substituting the earlier results and considering the stretched nuclear spin-state $I_z = \frac{1}{2}$ this can be written as

$$\vec{D}_a = \left(8.5213\,08 \times 10^4\right) \times \left\langle 6s_{1/2} \left| \vec{D} \right| 6p_{1/2} \right\rangle S$$

At this stage there is an order of magnitude enhancement as the energy difference $\epsilon_{6s_{1/2}} - \epsilon_{6p_{1/2}} = -0.0720\,06$ is very small. It also introduces a sign flip. The value of the required dipole matrix element is $1.4981\,46$, using this in the above expression gives the value of $\vec{D}_a = 12.7661\,63 \times 10^4 S e a_0$. Where e is the charge of electron and a_0 is the Bohr radius. The value of the atomic EDM is parameterized in terms of the Schiff moment S, one can make an estimate using nuclear structure computations. Such calculations have been done for ^{131}Xe, ^{199,201}Hg and ^{203,205}Tl [7]. Here computation is done in the electronic space and the nuclear contribution S has been retained as a parameter. The computation can be extended to other $p*$ symmetry orbitals. Since the nuclear excitation energies are large as

Table 4.17: Single particle lowest order Schiff moment induced atomic EDM.

n	$\langle 6s\|\|\vec{D}\|\|np* \rangle$	$\mathcal{B}_{np*}$	$\epsilon_{6s} - \epsilon_{np*}$	$\vec{D}_a$	Cumulated $\vec{D}_a$
6	3.6696 93	−4605.3404 79	−0.0720 60	−12.7661 63	−12.7661 63
7	0.2132 37	−2061.2401 86	−0.1427 47	−0.1676 05	−12.9337 68
8	−0.0659 96	1399.0146 59	−0.1672 78	0.0300 44	−12.9037 24
9	−0.0374 63	1009.3739 29	−0.1776 22	0.0115 88	−12.8921 36
10	−0.0271 61	728.9374 67	−0.1830 73	0.0058 87	−12.8862 49
11	−0.0188 43	−581.4480 19	−0.1866 04	−0.0031 96	−12.8894 45
12	0.0125 74	−496.0062 43	−0.1889 95	−0.0017 96	−12.8912 41

compared to the atomic excitation energies, the nuclear part can be taken the same. The values of $\mathcal{B}$, dipole matrix elements and the value of $\vec{D}_a$ along with the cumulated values are given in Table 4.17. The total lowest contribution to Schiff moment from the virtual $p*$ symmetry is $-12.8912\ 41 \times 10^4 Sea_0$. Like in the TPT electron-nucleus atomic EDM, here too the major contribution is from the $6p*$. But unlike in the TPT case, the change in the sign of $\mathcal{B}$ is not compensated by a sign change in the dipole matrix element. As a result there is a small cancellation in the contribution from the high the intermediate $p*$ symmetry bound virtual orbitals.

References

[1] Hugh P. Kelly Phys. Rev. **131**, 684(1963).

[2] W. F. Perger and Vasan Karighattam, Comp. Phys. Comm. **66**, 192(1991).

[3] W. F. Perger, Z. Halabuka and D. Trautmann, Comp. Phys. Comm. **76**, 250(1993).

[4] *Handbook of Mathematical Functions*, Edited by M. Abromowitz and A. Stegun(Dover Publications, 1972).

[5] W. F. Perger, Ph.D. Thesis submitted to Colorado State Univ.(1987).

[6] I. P. Grant, Adv. Phys. **19**, 747(1970).

[7] V. V. Flambaum, I. B. Khriplovich and O. P. Sushkov, Nuclear Physics. **A 449**. 750-760(1986).

Chapter 5

Parity-Nonconservation in Atomic Yb

5.1 Introduction

One of the possible odd parity electromagnetic moments of a nucleus is the anapole moment. This is purely magnetic in character and arises due to a toroidal current distribution in the nucleus. The electromagnetic interaction between the nuclear anapole moment and the atomic electrons gives rise to a nuclear spin-dependent(NSD) parity non-conserving interaction which leads to a mixing of opposite parity atomic states. This results in a finite $E1$ amplitude between two atomic states of the same parity. Being a magnetic dipole moment of the nucleus, it is dependent on the nuclear spin. In addition to the interaction arising from the anapole moment of the nucleus there is another nuclear spin-dependent PNC interaction which is due to the neutral weak current. So the nuclear spin-dependent PNC $E1$ amplitude is in general a combination of these two contributions. The total interaction Hamiltonian that is odd under parity in an atom is therefore

$$H_{\text{PNC}} = \frac{G_F}{2\sqrt{2}} \sum_i \left(Q_W \gamma_{5i} + \frac{\mu_{W'}}{I} \vec{I} \cdot \vec{\alpha}_i \right) \rho_N(r_i), \qquad (5.1)$$

where G_F is the Fermi coupling constant, Q_W is the weak charge of the nucleus, I is the nuclear spin, γ_{5i} and $\vec{\alpha}_i$ are the Dirac matrices for the electrons, $\rho_N(r_i)$ is the nuclear density and $\mu_{W'}$ can be considered as a weak nuclear moment arising from both types of NSD–PNC interaction.. In (5.1) the first term is the nuclear-spin independent neutral weak current interaction and the second term which is dependent on the nuclear spin is the combined contribution from the nuclear anapole moment and the neutral weak current. In

our calculations we do not distinguish between the two nuclear spin-dependent components but major part of the contribution is from the nuclear anapole moment[1].

With the recent discovery of the nuclear anapole moment in atomic caesium[2] the first step in the long quest for this peculiar moment has been taken. It will be of great significance if it can be measured in other atomic systems too. In this paper we show that atomic Yb maybe a promising candidate for nuclear anapole experiments. The advantage of using atomic Yb lies in the presence of very closely spaced states $6s6p(^1P_1)$ and $6s5d(^3D_1)$ [3], this leads to a large $E1$ amplitude for the NSD–PNC interaction between the ground state $6s^2(^1S_0)$ and the excited state $6s5d(^3D_1)$. Using $6s5d(^3D_1)$ as the final state mixes the contribution from both spin-independent and NSD–PNC effects. The added advantage in selecting atomic Yb is the presence of $6s5d(^3D_2)$ [4] whose energy level is just below and closer to $6s6p(^1P_1)$ as compared with the $6s5d(^3D_1)$ energy level. When this is used as the final state only the spin-dependent PNC interaction contributes to the $E1$ amplitude and unlike the case of $6s5d(^3D_1)$ there will be no contribution from the spin-independent component of the PNC interaction.

5.2 Effective Hamiltonian for the Atomic Parity-Nonconservation

5.2.1 Nuclear Spin-Dependent Effective Hamiltonian

Let $|\Psi_i\rangle$ and $|\Psi_f\rangle$ be the initial and final hyperfine atomic states between which the $E1$ transition amplitude is to be computed. These states are of same parity. Here hyperfine states states are considered as the PNC interaction has a nuclear spin-dependent component. Due to the presence of PNC interaction these atomic states mix with atomic states of opposite parity and assume the form $|\tilde{\Psi}_i\rangle$ and $|\tilde{\Psi}_f\rangle$ respectively. These are given by

$$\left|\tilde{\Psi}_i\right\rangle = \left|\Psi_i\right\rangle + \sum_{I\neq i} \frac{1}{E_i - H_0}\left|\Psi_I\right\rangle\left\langle\Psi_I\left|H_{\text{PNC}}^{\text{NSD}}\right|\Psi_i\right\rangle$$

and

$$\left|\tilde{\Psi}_f\right\rangle = \left|\Psi_f\right\rangle + \sum_{I\neq f} \frac{1}{E_f - H_0}\left|\Psi_I\right\rangle\left\langle\Psi_I\left|H_{\text{PNC}}^{\text{NSD}}\right|\Psi_f\right\rangle$$

where $|\Psi_I\rangle$ is of opposite parity to $|\Psi_i\rangle$ and $|\Psi_f\rangle$ and H_0 represents the atomic Hamiltonian. Let $\vec{D}$ be the electric dipole operator, the $E1$ transition amplitude between these mixed parity states is

$$\mathbf{D}_{fi} = \left\langle \tilde{\Psi}_f \middle| \vec{D} \middle| \tilde{\Psi}_i \right\rangle = \sum_{I \neq i} \frac{\left\langle \Psi_f \middle| \vec{D} \middle| \Psi_I \right\rangle \left\langle \Psi_I \middle| H_{\mathrm{PNC}}^{\mathrm{NSD}} \middle| \Psi_i \right\rangle}{E_i - E_I} + \sum_{I \neq f} \frac{\left\langle \Psi_f \middle| H_{\mathrm{PNC}}^{\mathrm{NSD}} \middle| \Psi_I \right\rangle \left\langle \Psi_I \middle| \vec{D} \middle| \Psi_i \right\rangle}{E_f - E_I} \quad (5.2)$$

With appropriate rearrangement of the above terms the nuclear spin part can be separated out and derive an effective Hamiltonian in the electronic space alone[5]. This can be done by rewriting expression (5.2) as:

$$\sum_{I \neq i} \left\langle \Psi_f \middle| \vec{D} \frac{1}{E_i - H_0} \middle| \Psi_I \right\rangle \left\langle \Psi_I \middle| H_{\mathrm{PNC}}^{\mathrm{NSD}} \middle| \Psi_i \right\rangle + \sum_{I \neq f} \left\langle \Psi_f \middle| H_{\mathrm{PNC}}^{\mathrm{NSD}} \middle| \Psi_I \right\rangle \left\langle \Psi_I \middle| \frac{1}{E_f - H_0} \vec{D} \middle| \Psi_i \right\rangle, \quad (5.3)$$

since the intermediate states are of opposite parity to the initial and the final states, the inequality condition in the summation can be dropped. Then using the completeness condition of the intermediate states we can avoid the summation over the intermediate states in the first term by using the identity

$$\sum_I \left| \Psi_I \right\rangle \left\langle \Psi_I \middle| \frac{1}{E_f - H_0} = \frac{1}{E_f - H_0}.$$

Similarly, the second term can also be modified, then expression (5.3) assumes the form

$$\left\langle \Psi_f \middle| \left(\vec{D} \frac{1}{E_i - H_0} H_{\mathrm{PNC}}^{\mathrm{NSD}} + H_{\mathrm{PNC}}^{\mathrm{NSD}} \frac{1}{E_f - H_0} \vec{D} \right) \middle| \Psi_i \right\rangle.$$

Define

$$D_{\mathrm{eff}}^{\mathrm{NSD}} = \vec{D} \frac{1}{E_i - H_0} H_{\mathrm{PNC}}^{\mathrm{NSD}} + H_{\mathrm{PNC}}^{\mathrm{NSD}} \frac{1}{E_f - H_0} \vec{D},$$

then the nuclear spin-dependent $E1$ transition amplitude reduced matrix element $E1_{\mathrm{PNC}}^{\mathrm{NSD}}$ is

$$E1_{\mathrm{PNC}}^{\mathrm{NSD}} = \left\langle \Psi_f \middle\| D_{\mathrm{eff}}^{\mathrm{NSD}} \middle\| \Psi_i \right\rangle.$$

Redefine the nuclear spin-dependent PNC part as

$$H_{\mathrm{PNC}}^{\mathrm{NSD}} = \frac{G_f \mu_{W'}}{2\sqrt{2}I} \vec{I} \cdot \vec{A},$$

where $\vec{A} = \sum_i \vec{\alpha}_i \rho_N(r_i)$. Then using the relation for coupling of two tensor operators the expression for the effective dipole operator can be written as

$$D_{\mathrm{eff}}^{\mathrm{NSD}} = \frac{G_F \mu_{W'}}{2\sqrt{2}I} \sum_k (-1) \frac{[k]^{1/2}}{\sqrt{3}} \left\{ \vec{I}^1 \left[\left(\vec{D} \frac{1}{E_i - H_0} \vec{A} \right)^k + (-1)^k \left(\vec{A} \frac{1}{E_f - H_0} \vec{D} \right)^k \right] \right\}^1.$$

At this stage the separation of the nuclear spin and the electron part is at the operator level. By decoupling the hyperfine states we can completely separate out the nuclear spin part and the integration over the electron coordinates. The reduced matrix element $T1^{\text{NSD}}$ in $E1$ transition amplitude that depends on the electron coordinate alone is:

$$\left\langle \Psi(\Gamma_f J_f) \middle\| \left\{ \left[\vec{D} \frac{1}{E_i - H_0} \vec{A} \right]^k + (-1)^k \left[\vec{A} \frac{1}{E_f - H_0} \vec{D} \right]^k \right\} \middle\| \Psi(\Gamma_i J_i) \right\rangle. \tag{5.4}$$

Where Γ_f is the additional quantum numbers required to define the atomic state uniquely and $k = 0, 1, 2$. The complete expression for the matrix element is as given in the Appendix:A. Define $\Delta J = J_f - J_i$, then for each value of k the allowed values of ΔJ are: $k = 0$, $\Delta J = 0$; $k = 1$, $\Delta J = 0, \pm 1$ and $k = 2$, $\Delta J = 0, \pm 1, \pm 2$ respectively. Suppose if a similar effective Hamiltonian were to be derived for the spin-independent component of the PNC then instead of $\vec{A}$ there will be a scalar. Then possible value of k is 1 and the corresponding selection rule is $\Delta J = 0, \pm 1$, this implies that only the spin-dependent component can have $\Delta J = \pm 2$. This could be of immense importance to conduct experiments for the detection of anapole moments.

The electron part is computed first and then it is multiplied by the required factors for the nuclear spin-dependent part to get the full expression.

5.2.2 Nuclear Spin-Independent Effective Hamiltonian

Consider the first part in the interaction Hamiltonian (5.1), the nuclear spin-independent part of the atomic parity-nonconservation. Define $H_{\text{PNC}}^{\text{NSI}}$ as the NSI-PNC Hamiltonian, then

$$H_{\text{PNC}}^{\text{NSI}} = \frac{G_F Q_W}{2\sqrt{2}} \sum_i \gamma_5^i \rho_N(r_i) = \frac{G_F Q_W}{2\sqrt{2}} B.$$

Where $B = \sum_i \gamma_5^i \rho_N(r_i)$. Similar to the $H_{\text{PNC}}^{\text{NSD}}$, an effective dipole operator for $H_{\text{PNC}}^{\text{NSI}}$ can also be derived. Let $D_{\text{eff}}^{\text{NSI}}$ be the effective PNC-NSI dipole transition operator, then using the earlier definitions

$$D_{\text{eff}}^{\text{NSI}} = \vec{D} \frac{1}{E_i - H_0} H_{\text{PNC}}^{\text{NSI}} + H_{\text{PNC}}^{\text{NSI}} \frac{1}{E_f - H_0} \vec{D}.$$

The full expression of $D_{\text{eff}}^{\text{NSI}}$ is

$$D_{\text{eff}}^{\text{NSI}} = \frac{G_F \mu w'}{2\sqrt{2}} \left\{ \vec{D} \frac{1}{E_i - H_0} B + B \frac{1}{E_f - H_0} \vec{D} \right\}^1 .$$

Using which the PNC-NSI dipole transition amplitude $\text{E1}_{\text{PNC}}^{\text{NSI}}$ can be computed as

$$E1_{\text{PNC}}^{\text{NSI}} = \left\langle \Psi_f \left\| D_{\text{eff}}^{\text{NSI}} \right\| \Psi_i \right\rangle.$$

The expression for $D_{\text{eff}}^{\text{NSI}}$ is independent of the nuclear-spin I but as the initial and final atomic states are hyperfine states the angular factor depend on the nuclear spin. In the expression for $E1_{\text{PNC}}^{\text{NSI}}$, the contribution from the electron part $T1^{\text{NSI}}$ is:

$$\left\langle \Psi(\Gamma_f J_f) \left\| \left\{ \vec{D} \frac{1}{E_i - H_0} B + B \frac{1}{E_f - H_0} \vec{D} \right\} \right\| \Psi(\Gamma_i J_i) \right\rangle. \tag{5.5}$$

The full expression for $E1_{\text{PNC}}^{\text{NSI}}$ is given in Appendix:B. As mentioned in the earlier section on PNC-NSD, the selection rule for the initial and final states is $\Delta J = 0, \pm 1$, where $\Delta J = J_f - J_i$.

The PNC-NSI dipole transition amplitude $E1_{\text{PNC}}^{\text{NSI}}$ are computed with the ground state $|6s^2 \ (^1S_0)\rangle$ as the initial state and $|6s5d(^3D_1)\rangle$ as the final state. But NSD computation is analyzed in greater detail as the PNC-NSI computation is an extension to the earlier work of Bhanu Das[6], which include an indepth analysis.

The next sections discusses the method of computation and analyze the shielded two-electron potential. All these are done with respect to the NSD-PNC Hamiltonian but are applicable to the NSI-PNC case too. This can be done just by replacing the $\vec{A}$ in NSD-PNC with B and by modifying the angular factors appropriately.

5.3 Method of Computation

For our computation we use an orbital basis set generated using the V^{N-1} potential. First a Dirac-Fock run is done with the ground state configuration $|6s^2 \ (^1S_0)\rangle$, then the virtual orbital ψ_i is got by doing a computation using the configuration $|6s\psi_i(J)\rangle$. While generating the virtual orbitals, the core orbitals till $6s$ are frozen and J is taken to be the lowest value obtained by coupling the angular momentum of $6s$ and ψ_i. Using the set of

orbitals so obtained a set of configuration state functions(CSF) is constructed. From these configurations using the method of configuration-Interaction(CI), we get a set of atomic state functions(ASFs). An ASF can be written as

$$\left|\Psi(\Gamma JM)\right\rangle = \sum_i C(\gamma_i JM)\left|\Phi(\gamma_i JM)\right\rangle,$$

where γ_i represents additional quantum numbers required to describe each of the CSFs uniquely. That is, an ASF is a linear combination of a set of CSFs with the same angular momentum quantum numbers. This is in the electron space alone. To get the hyperfine states the nuclear-spin need to be coupled with the net angular momentum from the electrons. After doing the CI computation we will get the required $|\Psi_i\rangle$, $|\Psi_I\rangle$ and $|\Psi_f\rangle$, which can be use for computing the contribution from the electron part of the $E1$ transition amplitude. Consider the expression (5.4), introducing a set of intermediate states, the contribution from the electronic part of the wave-function can be written as

$$\sum_{\Gamma''J''}\left[\frac{\left\langle\Psi(\Gamma_f J_f)\left\|\vec{D}\right\|\Psi(\Gamma''J'')\right\rangle\left\langle\Psi(\Gamma''J'')\left\|\vec{A}\right\|\Psi(\Gamma_i J_i)\right\rangle}{E_i - E_I}\right.$$
$$\left. + (-1)^k\frac{\left\langle\Psi(\Gamma_f J_f)\left\|\vec{A}\right\|\Psi(\Gamma''J'')\right\rangle\left\langle\Psi(\Gamma''J'')\left\|\vec{D}\right\|\Psi(\Gamma_i J_i)\right\rangle}{E_f - E_I}\right]. \qquad (5.6)$$

After computing this the value of the $E1$ transition element can be got in terms of hyperfine states using the multiplying factors as given in the appendix. Consider the first term in expression (5.6), in terms of CSFs this can written as:

$$\sum_{\gamma''J''}\left[\left(\sum_{k,l}C(\gamma_k J_f M_f)C(\gamma_l''J''M'')\left\langle\Phi(\gamma_k J_f)\left\|\vec{D}\right\|\Phi(\gamma_l''J'')\right\rangle\right) \times \right.$$
$$\left.\left(\sum_{m,n}C(\gamma_m''J''M'')C(\gamma_n J_i M_i)\frac{\left\langle\Phi(\gamma_m''J'')\left\|\vec{A}\right\|\Phi(\gamma_n J_i)\right\rangle}{E_i - E_I}\right)\right]$$

For each intermediate state the expression within the parentheses is computed separately and final result is the sum of the product of the two.

Yb being an atom with two-electrons in the valence shell, the valence-valence correlation is very important. Though the valence shell is similar to the alkaline earth elements the additional complication in Yb is the presence of filled $4f$ shell and unfilled $5d$ shell. Both are energetically located close to the ground state valence shell $6s$, hence the contribution from the core-valence correlation is quite significant. To include these correlation

effects a large orbital basis set is required with the usual CI approach but with suitable modification[6] of the atomic Hamiltonian very useful results can be got from a limited basis set. In our computation we have used an orbital basis of limited size and included shielding parameters in the atomic Hamiltonian. The orbital basis has the most important virtual orbitals namely $5d*$, $5d,6p*$ and $6p$. Using these a set of configurations is constructed.

With the configurations obtained from the orbital basis under consideration, the values of the energies are not very good compared to the experimental values. To get energies comparable to the experimental values we use shielding parameters in the two-electron term of the atomic Hamiltonian [7]. The essence of which is as described below. Consider the two-electron term in the atomic Hamiltonian at the CSF level, it's matrix element between two CSFs $|\Phi(\gamma'J'M')\rangle$ and $|\Phi(\gamma''J''M'')\rangle$ is given by:

$$\left\langle \Phi(\gamma'J'M') \Big| \frac{1}{r_{12}} \Big| \Phi(\gamma''J''M'') \right\rangle = \sum_{k,q} \left\langle \Phi(\gamma'J'M') \Big| \left(C_q^K(1) \cdot C_q^K(2)\right) \frac{r_<^K}{r_>^{(K+1)}} \Big| \Phi(\gamma''J''M'') \right\rangle.$$

With the introduction of shielding parameters the two-electron part get modified to the following form

$$\sum_{K,q} \alpha_K \left\langle \Phi(\gamma'J'M') \Big| \left(C_q^K(1) \cdot C_q^K(2)\right) \frac{r_<^K}{r_>^{(K+1)}} \Big| \Phi(\gamma''J''M'') \right\rangle,$$

where α_ks are the shielding parameters. The values of shielding parameters lies within the range 0–1 and are adjusted such that the energy levels got after doing CI matches well with the experimental values. To maintain consistency the orbital basis set is also generated using the shielding parameters. Inconsistency results if shielding parameters are used at the CI stage alone as orbitals does not feel the effect of shielding parameter. In which case the matrix elements computed for the $E1$ transition amplitude has energy denominator computed with the shielding parameters and numerators completely devoid of the effects of shielding parameters. While fine-tuning the values of the shielding parameters importance is given to the difference in the energy level than their absolute values. This is because in the expression for the $E1$ transition amplitude the difference in the energy contributes directly to the denominator. As the size of the configuration space is increased more correlation effect will be taken care of by the configuration mixing and the values

of α_K will tend toward unity. When the configuration space is complete the values of the shielding parameters should all be unity. All computations were done by suitably modifying the GRASP code [8].

5.4   The Shielded Two-Electron Potential

To understand the effect of shielding parameters let us consider the simple case of a closed-shell configuration $|\Phi_0\rangle$ and let $\{|\psi_i\rangle\}$ be a complete set of electron orbitals. The matrix element of the two-electron part of the Hamiltonian is:

$$\left\langle \Phi_0 \Big| \frac{1}{2} \sum_{i,j}^{N,N} \frac{1}{r_{ij}} \Big| \Phi_0 \right\rangle = \frac{1}{2} \sum_{i,j}^{N,N} \left\langle \psi_i \psi_j \Big| \frac{1}{r_{12}}(1 - P_{12}) \Big| \psi_i \psi_j \right\rangle,$$

where N is the total number of electron in the configuration. Selecting out the ith orbital the interaction with the rest of electrons in the configuration is given by:

$$\sum_j^N \left\langle \psi_i \psi_j \Big| \frac{1}{r_{12}}(1 - P_{12}) \Big| \psi_i \psi_j \right\rangle = \sum_j^N \left\langle \psi_i \psi_j \Big| \sum_K \frac{r_<^K}{r_>^{(K+1)}} C^K(1) \cdot C^K(2)(1 - P_{12}) \Big| \psi_i \psi_j \right\rangle.$$

When j is summed over electrons in a closed shell by selection rule only $K = 0$ contributes in the direct term. When shielding parameters are introduced the contribution from the direct part depend on the shielding parameter α_0 alone. Thus in a closed shell CSF α_0 controls the contribution from the direct part of the two-electron term. On the other hand exchange part can have contribution from other higher multipoles too. So, for a closed shell CSF α_is with $i > 0$ modify the contribution from the exchange part alone. Here we have considered the expectation value of the atomic Hamiltonian w.r.t. a closed shell CSF and without configuration mixing.

Consider the CSFs $|\Phi_0\rangle$ and $|\Phi_I\rangle$, where the CSF $|\Phi_I\rangle$ is got by exciting two electrons a and l in $|\Phi_0\rangle$ to virtual orbitals r and s respectively. Then using Slater-Condon rules the matrix element of the two-electron part between these two CSFs is:

$$\left\langle \Phi_0 \Big| \sum_{i,j} \frac{1}{r_{ij}} \Big| \Phi_I \right\rangle = C(0, I) \left(\left\langle \psi_a \psi_l \Big| \frac{1}{r_{12}}(1 - P_{12}) \Big| \psi_r \psi_s \right\rangle \right), \qquad (5.7)$$

where $C(0, I)$ is an angular factor. This will contribute to the configuration mixing. Here both the direct and the exchange terms can have contribution from $K > 0$. Since the virtual

orbitals are very small in the small r region and due to $r_>^{-(K+1)}$ dependence of the Kth multipole component the contribution from $K > 1$ are negligibly small. Use time-independent perturbation theory with Epstein-Nesbet partitioning of the atomic Hamiltonian. Including the first order contribution from $|\Phi_I\rangle$, the CSF $|\Phi_0\rangle$ assumes the form:

$$|\overline{\Phi}_0\rangle = |\Phi_0\rangle + |\Phi_0^1\rangle = |\Phi_0\rangle + \frac{|\Phi_I\rangle\langle\Phi_I|}{E_0 - E_I}H|\Phi_0\rangle,$$

where H is the atomic Hamiltonian, $E_0 = \langle\Phi_0|H|\Phi_0\rangle$ and $E_I = \langle\Phi_I|H|\Phi_I\rangle$. The corresponding energy using intermediate normalization is:

$$\overline{E}_0 = \langle\Phi_0|H|\overline{\Phi}_0\rangle = \langle\Phi_0|H|\Phi_0\rangle + \langle\Phi_0|H\frac{|\Phi_I\rangle\langle\Phi_I|}{E_0 - E_I}H|\Phi_0\rangle. \tag{5.8}$$

Since $|\Phi_I\rangle$ is doubly excited with respect to $|\Phi_0\rangle$, only the two-electron part of the Hamiltonian will contribute in the second term. Then expression (5.8) assumes the form:

$$\overline{E}_0 = \langle\Phi_0|\left(H + \frac{1}{4}\sum_{i,j}^{N,N}\frac{1}{r_{ij}}\frac{|\Phi_I\rangle\langle\Phi_I|}{E_0 - E_I}\sum_{i',j'}^{N,N}\frac{1}{r_{i'j'}}\right)|\Phi_0\rangle. \tag{5.9}$$

Using the form of the matrix element defined in expression (5.7),

$$\overline{E}_0 = \langle\Phi_0|H|\Phi_0\rangle + C(0,I)^2\langle\psi_a\psi_l|\left(\frac{1}{r_{12}}\frac{|\psi_r\psi_s\rangle\langle\psi_r\psi_s|}{E_0 - E_I}\frac{1}{r_{12}}\right)|\psi_a\psi_l\rangle. \tag{5.10}$$

This is like introducing an extra term in the atomic Hamiltonian which effects only the electron orbitals a and l in the CSF $|\Phi_0\rangle$. Consider only the dipole component of the two-electron interaction in the second term, introducing shielding parameter α_1 it can be written as:

$$(C(0,I)\alpha_1)^2\langle\psi_a\psi_l|\left(\frac{r_<}{r_>^2}C^1(1)\cdot C^1(2)\frac{|\psi_r\psi_s\rangle\langle\psi_r\psi_s|}{E_0 - E_I}\frac{r_<}{r_>^2}C^1(1)\cdot C^1(2)\right)|\psi_a\psi_l\rangle.$$

Including all the other multipole moments and denoting the energy with the shielded two-electron potential by $\overline{E'}_0$ gives

$$\overline{E'}_0 = E'_0 + C(0,I)^2\sum_{K,K'}\left[(\alpha_K\alpha_{K'} - 1)\times\langle\psi_a\psi_l|\left(\frac{r_<^K}{r_>^{K+1}}C^K(1)\cdot C^K(2)\frac{|\psi_r\psi_s\rangle\langle\psi_r\psi_s|}{E_0' - E_I'}\frac{r_<^{K'}}{r_>^{K'+1}}\times\right.\right.$$
$$\left.C^{K'}(1)\cdot C^{K'}(2)\right)|\psi_a\psi_l\rangle + \langle\psi_a\psi_l|\left(\frac{r_<^K}{r_>^{K+1}}C^K(1)\cdot C^K(2)\frac{|\psi_r\psi_s\rangle\langle\psi_r\psi_s|}{E_0' - E_I'}\frac{r_<^{K'}}{r_>^{K'+1}}\times\right.$$
$$\left.\left.C^{K'}(1)\cdot C^{K'}(2)\right)|\psi_a\psi_l\rangle\right] \tag{5.11}$$

Where E_0' is the expectation value of the atomic Hamiltonian with respect to the CSF $|\Phi_0\rangle$ with the shielding parameters included. Since $0 \leq \alpha_K \leq 1$, $(\alpha_K \alpha_{K'} - 1) < 0$. Define $\beta_{KK'} = |\alpha_K \alpha_{K'} - 1|$, the above expression can be rewritten in the form

$$
\overline{E_0'} = E_0' + C(0, I)^2 \left(\frac{E_0 - E_I}{E_0' - E_I'} \right) \sum_{K,K'} \left[\langle \psi_a \psi_l | \left(\frac{r_<^K}{r_>^{K+1}} C^K(1) \cdot C^K(2) \frac{|\psi_r \psi_s\rangle\langle\psi_r \psi_s|}{E_0 - E_I} \frac{r_<^{K'}}{r_>^{K'+1}} \times \right. \right.
$$
$$
C^{K'}(1) \cdot C^{K'}(2) \Big) |\psi_a \psi_l\rangle - \beta_{KK'} \langle \psi_a \psi_l | \left(\frac{r_<^K}{r_>^{K+1}} C^K(1) \cdot C^K(2) \frac{|\psi_r \psi_s\rangle\langle\psi_r \psi_s|}{E_0 - E_I} \frac{r_<^{K'}}{r_>^{K'+1}} \times \right.
$$
$$
C^{K'}(1) \cdot C^{K'}(2) \Big) |\psi_a \psi_l\rangle \right]. \tag{5.12}
$$

Compare the second order term in the above expression with the one without shielding parameters (5.10), the shielding parameters introduces two forms of correction: first a decrease characterize by $\beta_{KK'}$ and second the scaling of the whole expression by a factor $A(0, I) = (E_0 - E_I)/(E_0' - E_I')$. Thus the change in energy due to shielding parameters in the second order depends on $\beta_{KK'}$ and $A(0, I)$. Depending on these parameters the change in the energy $\Delta E_0 = E_0' - E_0$ can be positive or negative. This can be extended to other higher orders in perturbation.

5.5 Results

5.5.1 The NSD-Parity-Nonconservation

Using CSFs constructed from the orbital basis set we have computed the $E1$ transition amplitude between the ground state $|6s^2(^1S_0)\rangle$ and $|6s5d(^3D_1)\rangle$ as the final state for both the spin-independent and the spin-dependent case. In both cases the intermediate states can be either with total angular momentum $J = 1$ or $J = 0$. As both the spin-independent and spin-dependent component contributes, the two cannot be separated in the final result. Using the orbital basis under consideration set of even parity CSFs got by including single excitations from $4f$ and $5p$ orbitals in non-relativistic notation with $J = 1$ are:

$\quad |6s^2)\rangle$, $|6p^2\rangle$, $|6p^2\rangle$, $|5d^2\rangle$, $|5p^5 6s^2 6p\rangle$, $|5p^5 5d^2 6p\rangle$, $|5p^5 6s5d6p\rangle$, $|4f^{13} 6s^2 6p\rangle$, $|4f^{13} 5d^2 6p\rangle$,

$\quad |4f^{13} 6s5d6p\rangle$,

and those with $J = 1$ are:

$|5d^2\rangle$, $|6s5d\rangle$, $|5p^56s^26p\rangle$, $|5p^55d^26p\rangle$, $|5p^56s5d6p\rangle$, $|4f^{13}6s^26p\rangle$, $|4f^{13}5d^26p\rangle$,
$|4f^{13}6s5d6p\rangle$.

Similarly, the odd parity CSFs that can be constructed with $J = 0$ are:

$|6s6p\rangle$, $|5d6p\rangle$, $|5p^56s^25d\rangle$, $|5p^56s6p^2\rangle$, $|5p^55d6p^2\rangle$, $|4f^{13}6s^25d\rangle$, $|5p^56s5d^2\rangle$, $|4f^{13}6s5d^2\rangle$,
$|4f^{13}6s6p^2\rangle$, $|4f^{13}5d6p^2\rangle$,

and odd parity CSFs with $J = 1$ are:

$|6s6p\rangle$, $|5d6p\rangle$, $|5p^56s^25d\rangle$, $|5p^56s5d^2\rangle$, $|5p^56s6p^2\rangle$, $|5p^55d6p^2\rangle$, $|4f^{13}6s^25d\rangle$, $|4f^{13}6s5d^2\rangle$,
$|4f^{13}5d6p^2\rangle$.

With this set of configurations the values of the energy level computed using CI without the use of shielding parameters are as given in the Table below, for comparison the experimental values are also given:

Table 5.1: Values of the energy levels without shielding parameters. The energies are given in units of cm^{-1}.

sl. no.	Configuration	Term	Energy(expt)	Energy(CI)
1.	$6s6p$	$^3P_1$	17992.007	14551.7791
2.	$6s6p$	$^1P_1$	25068.222	24145.7777
3.	$6s5d$	$^3D_1$	24489.102	24561.3827
4.	$6s5d$	$^3D_2$	24751.948	24797.6955

One thing to be noted in the above table is that the sequence of the energy level from the CI computation is not in correct order as compared to the the experimental results. Here the difficulty is two-fold as not only the sequence of the energy levels but the energy difference also need to be matched. The difficulty lies in the closeness of the $|6s6p(^1P_1)\rangle$ and the $|6s5d(^3D_1)\rangle$ levels but this is also the advantage in choosing the Yb as the possible candidate for PNC experiments. After choosing the shielding parameters $\alpha_0 = 0.997$, $\alpha_1 = 0.667$, $\alpha_2 = 0.980$ and rest equal to unity the values of the energy levels obtained are as given in the Table below

Here the values of the shielding parameters have been adjusted such that the individual energy level are off by the same order. Where special attention has been given to the energy levels of $|6s5d(^3D_1)\rangle$ and $|6s6p(^1P_1)\rangle$ as they are the energy levels of interest.

Table 5.2: Values of the energy levels with shielding parameters. The energies are given in units of cm^{-1}.

sl. no.	Configuration	Term	Energy(expt)	Energy(CI)
1.	$6s6p$	$^3P_1$	17992.007	17675.6423
2.	$6s5d$	$^3D_1$	24489.102	24429.4055
3.	$6s5d$	$^3D_2$	24751.948	24707.3242
4.	$6s6p$	$^1P_1$	25068.222	25004.6888

With this set of configurations using $|6s^2(^1S_0)\rangle$ and $|5d6s(^3D_1)\rangle$ as initial and final states respectively, the value of the spin-dependent $E1$ transition amplitude reduced matrix element with hyperfine states is $0.865 \times 10^{-11}\mu_{W'}ea_0$, the contribution from the electronic part without the nuclear-spin part is $1.059 \times 10^{-11}\mu_{W'}ea_0$. These calculations are done for the isotope $^{171}Yb_{70}$ which has a nuclear spin $1/2$, the initial and final states has total angular momentum $F_i = 1/2$ and $F_f = 3/2$. The major contribution come from the term

$$\frac{\left\langle 6s5d(^3D_1)\left\|\vec{A}\right\|6s6p(^1P_1)\right\rangle\left\langle 6s6p(^1P_1)\left\|\vec{D}\right\|6s^2(^1S_0)\right\rangle}{E(6s5d~^2D_1) - E(6s6p~^1P_1)}.$$

This term alone gives $0.731 \times 10^{-11}\mu_{W'}ea_0$ which amounts to 84.41% of the total contribution and the contribution in the electron part alone is $0.894 \times 10^{-11}\mu_{W'}ea_0$. This is because of two reasons: first the close spacing between $|6s6p(^1P_1)\rangle$ and $|6s5d(^3D_1)\rangle$ as compared to the spacing between $|6s^2(^1S_0)\rangle$ and $|6s6p(^1P_1)\rangle$ and second, mixing between configurations $|6s6p(J = 1)\rangle$ and $|6p5d(J = 1)\rangle$.

Now consider the $|5d6p(^1D_2)\rangle$ state, it is located very close to the intermediate state $|6s6p(^1P_1)\rangle$ as compared to the separation of $579.113~cm^{-1}$ between the states $|6s5d(^3D_1)\rangle$ and $|6s6p(^1P_1)\rangle$, the separation between $|6s5d(^3D_2)\rangle$ and $|6s6p(^1P_1)\rangle$ is $316.274cm^{-1}$ only. When $|6s5d(^3D_2)\rangle$ state is used as the final state, by selection rule only the spin-dependent component of the PNC contribute to the $E1$ transition amplitude. The only worry is whether there will be large cancellations as it is an intercombination state. Our computation shows there are no major cancellations. This is because the value of $E1$ transition amplitude is not governed by the configurations that goes into the final states alone but also depends on the configurations that goes into the intermediate states too. The value

of the $E1$ transition amplitude reduced matrix element with the nuclear-spin included is $-4.657 \times 10^{-11} \mu_{W'} ea_0$ and in the electron space alone it is $3.293 \times 10^{-11} \mu_{W'} ea_0$. In this case the major intermediate contribution is from the state $|6s6p(^1p_1)\rangle$. To understand why there are no major cancellation consider the ASFs $|6s6p(^1P_1)\rangle$ and $|6s5d(^3D_2)\rangle$, below are given the contribution from the five most important CSFs in each case:

$$|6s6p(^1P_1)\rangle = 0.8466|6s6p\rangle + 0.4220|6s6p*\rangle - 0.2235|5d6p\rangle - 0.2206|5d*6p*\rangle$$
$$+0.0760|5d*6p\rangle + \dots \tag{5.13}$$

$$|5d6s(^3D_2)\rangle = 0.7994|6s5d*\rangle - 0.5981|6s5d\rangle - 0.0137|4f^76s5d6p*\rangle$$
$$-0.0121|4f^75d5d*6p*\rangle - 0.0111|4f^76s5d5d*6p\rangle + \dots \tag{5.14}$$

In the above expression for the ASFs the angular momentum for each of the orbital shells are coupled in a sequence but the intermediate values are not given. That is, there will be many CSFs with the same orbitals and same final angular momentum but with different intermediate angular momenta. Here the intermediate angular momenta has been avoided as no CSF from the same orbitals doesn't contribute to the first five most important CSFs for each of the ASFs.

Consider the expression for the most important intermediate state $|6s6p(^1P_1)\rangle$, there is a significant contribution from the CSF $|5d*6p*\,(J=1)\rangle$. This in combination with the CSFs $|6s5d*\,(J=2)\rangle$ in the final ASF give a large contribution to the $E1$ transition amplitude. Which means that there is no cancellation at the level of the most significant contribution. The individual contribution from the CSFs $|6s5d*(J=2)\rangle$ and $|6s5d(J=2)\rangle$ in the electronic part are as given below:

$$C_1 \sum_I \frac{\langle 6s5d*\,(J=2)||\vec{D}||\Psi_I(J=1)\rangle\langle\Psi_I(J=1)||\vec{A}||6s^2(^1S_0)\rangle}{E_i - E_I} = -320.6850$$

$$C_2 \sum_I \frac{\langle 6s5d*\,(J=2)||\vec{A}||\Psi_I(J=1)\rangle\langle\Psi_I(J=1)||\vec{D}||6s^2(^1S_0)\rangle}{E_f - E_I} = -3701.5687$$

$$C_2 \sum_I \frac{\langle 6s5d_{5/2}(J=2)||\vec{D}||\Psi_I(J=1)\rangle\langle\Psi_I(J=1)||\vec{A}||6s^2(^1S_0)\rangle}{E_i - E_I} = -58.0524$$

and

$$C_2 \sum_I \frac{\langle 6s5d_{5/2}(J=2)||\vec{A}||\Psi_I(J=1)\rangle\langle\Psi_I(J=1)||\vec{D}||6s^2(^1S_0)\rangle}{E_f - E_I} = 0.0000$$

respectively, where $C_1 = 0.7994$, $C_2 = -0.5981$, E_i is the energy of the initial state and E_f for the final state. Thus the major contribution is from the second term and in this term the most important contribution are:

$$C_1 \left\langle 6s5d* \, (J=2) \middle\| \vec{A} \middle\| 5d* \, 6p* \, (J=1) \right\rangle \left(\frac{\left\langle 6s6p(^1P_1) \middle\| \vec{D} \middle\| 6s^2(^1S_0) \right\rangle}{E_f - E_1} \right) = -4978.7637$$

and

$$C_1 \left\langle 6s5d* \, (J=2) \middle\| \vec{A} \middle\| 5p* \, 5d* \, (J=1) \right\rangle \left(\frac{\left\langle 6s6p(^1P_1) \middle\| \vec{D} \middle\| 6s^2r(^1S_0) \right\rangle}{E_f - E_1} \right) = 1276.0023.$$

These are the two most important cancellations in the computation in the computation for the $E1$ transition amplitude with $5d6s(^3D_2)$ as the final state.

The result discuss so far correspond to the isotope $^{171}\text{Yb}_{70}$ and its natural abundance is 14.31%. The other isotope of Yb which we have chosen for our computation is $^{173}\text{Yb}_{70}$. Its abundance and nuclear spin are 16.13% and 5/2 respectively. We have chosen these two isotopes on account of their abundance, nuclear spin and stability. The result for these two isotopes for different initial and final hyperfine states are as given in following Table:

Table 5.3: Results for different isotopes with different hyperfine states. $T1^{\text{NSD}}$ and $E1^{\text{NSD}}$ are in units of $ea_0\mu_{W'} \times 10^{-11}$.

Isotope	Nuclear	J_f	F_i	F_f	$T1^{\text{NSD}}$	$E1^{\text{NSD}}_{\text{PNC}}$	k
171	1/2	1	1/2	1/2	1.0598	−1.2238	1
,,	,,	,,	,,	3/2	1.0598	0.8654	1
,,	,,	2	,,	3/2	−3.2934	−4.6575	2
173	5/2	1	5/2	3/2	1.0593	−1.2108	1
,,	,,	,,	,,	5/2	1.0593	−0.4237	1
,,	,,	,,	,,	7/2	1.0593	1.2231	1
,,	,,	2	,,	3/2	−3.2195	−1.9079	2
,,	,,	2	,,	5/2	−3.2195	−3.3308	2
,,	,,	2	,,	7/2	−3.2195	−3.9498	2

Among all the isotopes of Yb the most abundant one is $^{174}\text{Yb}_{70}$, this might be suitable for doing a measurement for the nuclear spin-independent $E1$ transition amplitude but not

for the nuclear spin-dependent component. For the nuclear spin-dependent component it needs to couple with the nuclear spin. For better comparison the result of the two isotopes are as given in the table.

5.5.2 The NSI-Parity-Nonconservation

The result doesn't differ qualitatively from those given in [6]. The difference is the larger CSF space used, which induces a change in the shielding parameters. The added CSFs also pick up many forms of correlation but these are not so significant. Yet, in terms of accuracy which is not relative but absolute these are not negligible. The additional CSFs included in this computation are the CSFs with excitations from the core orbitals $5p$ and $4f$.

As in NSD-PNC, here too the major contribution to the intermediate state $|\Psi_I\rangle$ is the $|6s6p(^1P_1)\rangle$ state, given in expression (5.13). The final ASF $|6s5d(^3D_1)\rangle$ has the form

$$
\begin{aligned}
\left|6s5d(^3D_1)\right\rangle &= 0.9983\left|6s5d*\right\rangle + 0.0188\left|4f^76s5d6p*\right\rangle - 0.0139\left|4f^76s5d*5d6p\right\rangle \\
&\quad + 0.0135\left|4f^5*5d*6p*\right\rangle - 0.0131\left|5p^36s5d6p*\right\rangle + \ldots
\end{aligned}
$$

With this set of configuration the value of $E1^{\text{NSI}}_{\text{PNC}}$ is $-0.879 \times 10^{-11}iea_0Q_W$, which is not much different from the result of Das[6] $-0.768 \times 10^{-11}iea_0Q_W$.

References

[1] V. V. Flambaum and I. B. Khriplovich, Zh. Eksp. Teor. Fiz., **79**,1656(1980),[Sov. Phys. JETP, **52**, 835(1980)], I. B. Khriplovich, Comments At. Mol. Phys., **23**,189(1989).

[2] C. S. Wood, S. C. Bennett, D. Cho, B. P. Masterson, J. L. Roberts, C. E. Tanner and C. E. Wieman, Science, **275**, 1759(1997).

[3] David DeMille, Phys. Rev. Lett.,**74**,4165(1995).

[4] I. B. Khriplovich and David DeMille (private communication)

[5] E. H. Boston, D. Phil Thesis, Oxford University. (unpublished).

[6] B. P. Das, Physical Review A,**56**,1635(1997).

[7] P. G. H. Sandars and B. P. Das (unpublished), Swati Malhotra, A. D. singh and B. P. Das,

[8] K.G. Dyall, I. P. Grant, C. T. Johnson, F. A. Parpia and E. P. Plummer, Computer Physics Comm.,**55**, 425(1989).

Chapter 6

Conclusion and Future Directions

6.1 Conclusion

Till date the closed-shell atoms for which EDM computations have been done are Xe and Hg. Atomic Yb has the same advantage like these atoms as a probe for atomic EDM which are nuclear in origin.

Compared to Xe, Yb has the advantage of higher Z and when compared to Hg it has the advantage of an odd parity atomic state which is energetically closer to the ground state. In Hg the ground state configuration is $|4f^{14}5d^{10}6s^2\rangle$ and the most important odd parity configuration is $|4f^{14}5d^{10}6s6p*\rangle$, which is separated from the ground state by 1.7957 hartrees. Whereas in Yb the most important odd parity configuration $|4f^{14}6s6p* \, (J=1)\rangle$ is separated from the ground state by 0.8197 hartrees and is 0.4565 times the value in Hg. Since the atomic EDM is inversely proportional to the energy difference, Yb has an enhancement of 2.12 over Hg but Hg has the advantage of higher Z. The dependence of the TPT atomic EDM on Z scales as Z^2, which makes the enhancement in Hg 1.30 times that of Yb. This is smaller than the enhancement in Yb due to inverse energy dependence. Though in terms of the energy and the Z dependence Yb enjoys an edge over Hg, it is difficult to conclude which is the better of the two as the dipole matrix is not yet included. This is the theoretical estimate, more important is the experimental considerations, for which too it is difficult to arrive at a particular choice.

The unfilled $5d*$ and $5d$ orbitals in Yb contribute significantly to the many-body effects as these are located very close to $6s$ orbital. The orbital $5d*$ and $5d$ are higher than $6s$

by 0.096474 and 0.117699 hartrees respectively. In the even parity CSF-space $|4f^{14}5d*^2\rangle$ and $|4f^{14}5d^2\rangle$ mix strongly with the ground state CSF $|6s^2\rangle$ and within the odd parity CSF space, the two most important doubly excited CSFs that contribute to $|\Psi^0_{\text{corr}}\rangle$ are $|4f^{14}6p5d*\rangle$ and $|4f^{14}6p* 5d\rangle$. Though $5d*$ is closer to $6s$ energetically $|4f^{14}5d^2\rangle$ contribution to $|\Psi_0\rangle$ is larger than the contribution from $|4f^{14}5d*^2\rangle$. As to be expected at the single particle level the most important orbital in the atomic EDM computation is $6p*$. and accounts for 97.747% of the lowest order atomic EDM. In terms of configurations it is the CSF $|4f^{14}6s6p*\rangle$ which has the largest contribution to $\vec{D}_a$ from the odd parity CSF space. The other important configurations are the double excitations from $6s^2$, which is brought out by the plots in Fig4.5.

At the lowest order single particle level the contribution from the continuum orbitals is extremely small. The continuum $p*$ orbitals account for just 0.296%. The computations at the CSF level are without the continuum orbitals, this is because the error accumulation is severe as it requires integrals with the deep core orbitals.

The results from the computations using CI, PCI and matrix based Bloch equation confirms the equivalence of these methods within the restricted active CSF space considered. An important result of the comparison is the importance of contribution from higher order terms to the ground state energy E_0. As E_0 oscillates with the order of perturbation a truncation in the perturbation series while computing E_0 can give inaccurate results. This is also true of $\vec{D}_a$ and is clearly brought out in Table:4.7. In can be clearly stated that for accurate computations inclusion of high order terms is desirable. By comparing the lowest order computation at the single particle level with the result from the matrix based Bloch equation, it is observed that the many-body effect do contribute but they are relatively small–just 10.81%–compared to the lowest order contribution. It is to be noted that the lowest order computation has no many-body effects. Another important result from the computation of atomic EDM with various forms of CEPA method is the small size of the contribution from the size-inconsistent terms. Comparing the results from CEPA-2 and the matrix based Bloch equation, the contribution from the size-inconsistent terms is at the most is 1.206%. From these it can be concluded that for high accuracy computation, one must include higher order terms and avoid size-inconsistent terms. For computations

to estimate atomic EDMs these are not necessary but to do a computation to the accuracy of 1% these are required.

With the successful laser cooling and trapping of atomic Yb, using these techniques with Yb to measure its atomic EDM will be a good contribution to the search of atomic EDMs.

The present calculation of $E1_{PNC}^{NSD}$ includes the most important low lying orbitals and configurations using a shielded potential. Though not complete it incorporates some of the dominant many-body effects and serves as an important guideline for both theoretical and experimental work related to nuclear spin dependent PNC in atomic Yb. From the results of calculations, one can arrive at the following conclusions:

1. The $^3D_1 \rightarrow ^1S_0$ $E1$ transition amplitude in atomic Yb is larger than that of Cs. Hence Yb maybe a very good candidate to look for the nuclear anapole moment.

2. The NSD-PNC $E1$ transition amplitude for $^3D_2 \rightarrow ^1S_0$ as expected is larger than the corresponding transition amplitude for $^3D_1 \rightarrow ^1S_0$. It is worthwhile to explore whether one can do an experiment to observe the nuclear anapole using the former transition.

Though the configuration space considered here is slightly larger than the one used by Das[1], there is no significant change in $E1_{PNC}^{NSI}$, which implies that the configuration space used by Das has all the important configurations.

6.2   Future Directions

The size of the CSF grows significantly when the orbital space becomes large. In addition, inclusion of higher excitation CSFs also increases the size of CSF space enormously. These problems are less formidable if the whole procedure is implemented at the single particle level. An important extension of the present work would be to develop it towards a single particle approach.

The coupled-cluster method has been used by Liu and Kelly[2] to calculate the electron EDM enhancement factor for thallium and Shukla, Das and Mukherjee[3] have recently

proposed a coupled-cluster formalism for the EDM of atoms and molecules based on linear response theory. With these preceding works it is a logical step would be to proceed towards coupled-cluster method. The CEPA-2 is very close to the coupled-cluster method but it requires some more modifications to make it in complete agreement with the latter theory. This requires the inclusion of non-linear terms in cluster amplitude, which can be done with less complications at the single particle level. The computation here is single configuration, making it multi-configuration would make it possible to do computation for open-shell systems.

A good test of different many-body effects and correctness of the various components that goes into the computation would be to compute the excitation energies. In short the present work can be enhanced further in two ways: first make the orbital space larger, which would make the present computation more accurate and second improve the method of computation by including many-body effects that are not included here.

References

[1] B. P. Das, Physical Review A,**56**,1635(1997).

[2] Z. W. Liu and H. P. Kelly, Phys. Rev.**A45**, R4210(1992)

[3] A. Shukla, B. P. Das and D. Mukherjee Phys. Rev. **A 50**,2096(1994).

Appendix:A

Expression for $E1_{PNC}^{NSD}$

The expression for the $E1_{PNC}^{NSI}$ transition amplitude reduced matrix element in terms of the hyperfine states $|\Psi_i\rangle$a and $|\Psi_f\rangle$ is given by:

$$E1_{PNC}^{NSD} = \left\langle \Psi_f \right| \left\{ \left[\vec{I} \left\{ \vec{D} \frac{1}{E_i - H_0} \vec{A} \right\}^k + (-1)^k \left\{ \vec{A} \frac{1}{E_f - H_0} \vec{D} \right\}^k \right] \right\}^1 \left| \Psi_i \right\rangle.$$

After introducing a complete set of intermediate states between the dipole and the spin-dependent PNC, then decoupling the nuclear-spin part from the electron part, the reduced matrix element $(E1^{NSD})_{red}$ assumes the form

$$\left(E1_{PNC}^{NSD} \right)_{red} = -\frac{[1, F_f, F_i]}{I} \left[(2I+1)(I+1)I \right]^{1/2} (2I+1)^{1/2} \begin{Bmatrix} I & I & 1 \\ J_f & J_i & k \\ F_f & F_i & 1 \end{Bmatrix} \times \sum_{\Gamma''J''} (-1)^{J_i+J_f+1} \times$$

$$\begin{Bmatrix} 1 & 1 & k \\ J_i & J_f & J'' \end{Bmatrix} \left[\frac{\left\langle \Psi(\Gamma_f J_f) \left\| \vec{D} \right\| \Psi(\Gamma''J'') \right\rangle \left\langle \Psi(\Gamma''J'') \left\| \vec{A} \right\| \Psi(\Gamma_i J_i) \right\rangle}{E_i - E_{\Gamma''J''}} \right.$$

$$\left. + (-1)^k \frac{\left\langle \Psi(\Gamma_f J_f) \left\| \vec{A} \right\| \Psi(\Gamma''J'') \right\rangle \left\langle \Psi(\Gamma''J'') \left\| \vec{D} \right\| \Psi(\Gamma_i J_i) \right\rangle}{E_f - E_{\Gamma''J''}} \right]$$

From this expression the electronic part $T1^{NSD}$ can be separated out, it is given by:

$$T1_{PNC}^{NSD} = \sum_{\Gamma''J''} (-1)^{J_i+J_f+1} \begin{Bmatrix} 1 & 1 & k \\ J_i & J_f & J'' \end{Bmatrix} \left\langle \Psi(\Gamma_f J_f) \right\| \left(\vec{D} \frac{\left\| \Psi(\Gamma''J'') \right\rangle \left\langle \Psi(\Gamma''J'') \right\|}{E_i - E_{\Gamma''J''}} \vec{A} \right.$$

$$\left. + (-1)^k \vec{A} \frac{\left\| \Psi(\Gamma''J'') \right\rangle \left\langle \Psi(\Gamma''J'') \right\|}{E_f - E_{\Gamma''J''}} \vec{D} \right) \left\| \Psi(\Gamma_i J_i) \right\rangle$$

Appendix:B

Expression for $E1_{\text{PNC}}^{\text{NSI}}$

`he expression for the $E1^{\text{NSI}}$ transition amplitude reduced matrix element in terms of hyperfine states $|\Psi_i\rangle$a and $|\Psi_f\rangle$ is given by:

$$E1_{\text{PNC}}^{\text{NSI}} = \left\langle \Psi_f \right| \left\{ \vec{D} \frac{1}{E_i - H_0} B + B \frac{1}{E_f - H_0} \vec{D} \right\}^1 \left| \Psi_i \right\rangle.$$

r introducing a complete set of intermediate states between the dipole and the spin-ndent PNC, then decoupling the nuclear-spin part from the electron part, the reduced rix element $(E1^{\text{NSI}})_{\text{red}}$ assumes the form

$$1_{\text{PNC}}^{\text{NSI}} = (-1)^{I+J_f+F_i+1} [F_f, F_i]^{1/2} \left\{ \begin{array}{ccc} F'' & 1 & F_i \\ J_i & I & J'' \end{array} \right\} \times \left[\frac{\left\langle \Psi(\Gamma_f J_f) \left\| \vec{D} \right\| \Psi(\Gamma''J'') \right\rangle \left\langle \Psi(\Gamma''J'') \left\| B \right\| \Psi(\right.}{E_i - E_{\Gamma''J''}} \right.$$
$$\left. + \frac{\left\langle \Psi(\Gamma_f J_f) \left\| B \right\| \Psi(\Gamma''J'') \right\rangle \left\langle \Psi(\Gamma''J'') \left\| \vec{D} \right\| \Psi(\Gamma_i J_i) \right\rangle}{E_f - E_{\Gamma''J''}} \right]$$

n this expression the electronic part $T1^{\text{NSI}}$ can be separated out, it is given by:

$$\begin{array}{c} \text{SI} \\ \text{NC} \end{array} = \left\langle \Psi(\Gamma_f J_f) \right\| \left\{ \vec{D} \frac{\left\| \Psi(\Gamma''J'') \right\rangle \left\langle \Psi(\Gamma''J'') \right\|}{E_i - E_{\Gamma''J''}} B + B \frac{\left\| \Psi(\Gamma''J'') \right\rangle \left\langle \Psi(\Gamma''J'') \right\|}{E_f - E_{\Gamma''J''}} \vec{D} \right\} \left\| \Psi(\Gamma_i J_i) \right\rangle$$

134